A CHARACTERISTIC MODE PERTURBATION APPROACH FOR ANTENNA LOADING DESIGN

BY

MATTHEW WILLIAM YOUNG

DISSERTATION

Submitted in partial fulfillment of the requirements
for the degree of Doctor of Philosophy in Electrical and Computer Engineering
in the Graduate College of the
University of Illinois at Urbana-Champaign, 2015

Urbana, Illinois

Doctoral Committee:

Professor Jennifer T. Bernhard, Chair
Professor Steven J. Franke
Professor Jose E. Schutt-Aine
Assistant Professor Songbin Gong

ABSTRACT

Reactive loading is commonly applied to antennas to modify input impedance and radiation pattern properties. However, reactive loading design approaches based on experience, intuition, and modeling are challenged as the demand grows for antennas with increased functionality and performance. New systematic design methods are needed that can manage complicated performance tradeoffs while providing physical insight into the fundamental antenna operation. Characteristic mode theory has shown promise for systematic antenna design, yet significant limitations still exist that restrict its usefulness. The transformations of characteristic modes with respect to frequency or reactive loading are currently understood only qualitatively, and insight into their behavior must be developed through experience. In this thesis, a novel characteristic mode perturbation approach is developed that provides a quantitative description of how mode eigenvalues and eigencurrents transform under reactive loading and frequency variation. Analytical equations are derived using a novel application of eigenvalue perturbation theory to the characteristic mode problem. The equations characterize the effect of impedance loading on the characteristic mode eigenvalues and eigencurrents and reveal the explicit factors governing the mode transformations.

Insight from the perturbation equations suggests a new characteristic mode design paradigm in which loading is used to control the eigencurrent contributions between modes. The new eigencurrent contribution perspective can be used to understand and solve loading problems that traditional characteristic mode theory cannot. The approach is used to design the reactive loading of an Archimedean spiral antenna to produce beam tilt or an endfire radiation pattern while maintaining desirable VSWR properties. Finally, the perturbation approach is used to analyze antenna loss and is applied to the analysis and improvement of antenna radiation efficiency.

ACKNOWLEDGMENTS

This work would not have been possible without the support of a number of individuals. I would first like to thank my advisor and committee chair, Jennifer Bernhard, for her guidance, support, and encouragement throughout my graduate studies. Her mentorship helped me grow not only as a researcher but as an individual. I would also like to thank my committee members Professors Steve Franke, Jose Schutt-Aine, and Songbin Gong. Their constructive comments were valuable for improving this work. Also, I would like to thank my friends and colleagues within the University of Illinois antennas group for the useful technical discussions and camaraderie that helped in the development of this work. Finally, I would like to thank my parents, Bill and Jacquie, and my sister Katie for their unwavering support throughout my studies.

TABLE OF CONTENTS

CHAPTER 1

INTRODUCTION

For over a century, designers have been working to develop new antennas that satisfy ever more challenging performance requirements. Thousands of designs encompassing all different antenna topologies can be found throughout the open literature. Veteran antenna designers have achieved success over the years relying on insight gained from electromagnetic fundamentals and extensive design experience. As a result, many designers assert that antenna design is a well understood area and optimal performance has been achieved with current technologies. Hansen recently wrote "We antenna engineers have done what is possible by rearranging the wires" [1]. The countless antenna designs and reactive loading schemes in the literature certainly validate this argument. However, considering the numerous loaded antenna designs available, a general systematic loading design procedure, in particular, is still not available. Most design models that provide some useful guidelines for reactive loading break down as the complexity of antenna designs increases. As a result, most antennas are currently reactively loaded to achieve novel functionality using trial-and-error methods. A systematic design approach or a deep understanding of the antenna operation is not presented or available. A more systematic design approach that can guide the application of impedance loading to solve specific antenna design challenges while providing a detailed understanding of the fundamental mechanisms of antenna operation is highly desirable and needed.

In this work, a novel loading design methodology based on characteristic mode theory is developed to address both the current limitations of characteristic mode theory and the current challenges associated with designing a useful loading scheme to achieve desired antenna functionality. Eigenvalue perturbation theory is applied to the characteristic mode problem to develop novel equations that describe how loading affects the characteristic modes. The perturbation equations reveal the explicit factors responsible for

characteristic mode transformations along with a new design paradigm that suggests the best load values and positions to achieve desired antenna performance. The new approach provides a unique perspective that allows for the solution of antenna performance problems that cannot be solved using traditional characteristic mode techniques.

1.1 Heuristic and Optimization Design Approaches

The antenna design process has been approached in a number ways with varying degrees of success. Currently heuristic design methods form the foundation for most antenna design. Heuristic methods rely on designer experience and intuition typically developed through years of design experience and trial-and-error. Often a novel antenna idea is first thought of in terms of a simple circuit model to provide general guidance for the electromagnetic design. For instance, models including the transmission line and cavity have proven popular for guiding microstrip antenna design [2, 3]. The models provide insight into the expected input impedance and field distribution behavior. Transmission line models are useful for determining appropriate reactive load values and load positions to affect input impedance behavior for basic microstrip antenna topologies. The models, however, are only valid for the parameters in which they have been specified. As the designs increase in complexity, the assumptions the models are based on are challenged, and the models no longer provide valid design guidance. Increasing the complexity of the models to account for higher order effects may be useful for analysis but typically has limited utility for design purposes. Other antenna topology models such as the lumped component used for electrically small antennas suffer from similar limitations, and antenna performance can quickly deviate substantially from that predicted. As a result, models have limited use for guiding designs that have more complex features necessary to satisfy challenging system requirements. Model based approaches do not scale to complex antenna topologies easily.

Heuristic techniques are often used to assist models when more rigorous antenna specifications are required. Instincts developed through extensive experience or exhaustive parametric studies often compensate for model limitations. Even choosing loading positions to achieve desirable current dis-

tributions for dipole antennas is currently approached mainly through trial-and-error e.g., [4, 5]. No accurate, systematic approach for choosing reactive load positions currently exists in the open literature.

Accurate and efficient full-wave simulation software has allowed parametric simulations and optimization routines to produce useful antenna designs. For instance, genetic algorithm optimization techniques have been used to design optimal loading profiles to maximize low frequency gain from log-spiral antennas, e.g., [6]. Although antennas with desired performance can often be obtained, the nature of optimization algorithms limits the detailed understanding of how the antenna is functioning. Without an understanding of the antenna's fundamental operating principles, rational structure changes cannot be made to obtain small performance modifications. Furthermore, the algorithms often produce designs with unnecessary complexity. Similar performance can often be achieved with far simpler structures or more cost effective loading profiles. The inability of most algorithms to guarantee the optimality of the antenna solution is an additional limitation of the optimization approach.

1.2 The Characteristic Mode Design Approach

Heuristic and optimization design techniques have long been relied upon to develop a wide variety of antenna designs. Recently, however, modal design approaches including characteristic mode theory, in particular, have experienced a resurgence of popularity inspired by the work of Cabedo-Fabres [7]. Characteristic mode theory applied to electromagnetic problems was originally proposed by Garbacz and soon refined by Harrington and Mautz [8, 9]. Although originally developed for perfect electrically conducting structures, the method was soon extended to dielectric and magnetic bodies [10]. Some early applications of characteristic mode theory included work by Newman on antenna placement [11] and work by Garbacz and Pozar on antenna shape synthesis [12]. Some limited interest in characteristic mode methods in the 1990s included an application of characteristic mode theory to vehicle antenna design [13]. However, after the initial investigations by Garbacz and Harrington, characteristic mode theory did not receive significant attention in the literature. In the early 2000s a series of presentations and papers

by Cabedo-Fabres on characteristic mode design culminating in her dissertation and an *Antennas and Propagation Magazine* article renewed interest in the method [7, 14]. More recent work by Ethier used characteristic mode concepts along with optimization algorithms to achieve antenna shape synthesis [15]. Furthermore, Adams and Bernhard used characteristic mode concepts to investigate and design multimode electrically small antennas with enhanced bandwidth [16]. Some recent work by Obeidat looked into the application of characteristic modes to the design of frequency reconfigurable antennas [5]. Characteristic mode theory has even matured beyond the research community, and now the computation of these modes is available using the commercial method of moments simulation software FEKO®.

The application of characteristic modes to antenna design has been met with both enthusiasm and some skepticism from the antenna community. The properties of characteristic modes provide additional information that has proven useful for design purposes. By decomposing the antenna current, modes with desirable properties can often be excited without exciting undesired modes. Because characteristic mode design is a full-wave approach, complex electromagnetic effects are included that are often ignored in simple circuit models. As a result, managing antenna modes provides promise for a topology-independent general systematic design method. However, skeptics argue that solution of the characteristic mode eigenvalue problem is computationally expensive and in many cases the benefits do not warrant the extra expense. Others argue that the application of characteristic modes for design purposes often needlessly complicates the design process and provides little information that is not already understood from experience and fundamental electromagnetics.

The use of characteristic modes as a design tool will become increasingly beneficial as the complexity of antennas begins to challenge heuristic understanding. Most applications of characteristic modes have focused on simple antenna structures that designers already understand well. Therefore, the benefit of complicating the design problem by using characteristic modes is not adequately motivated. Characteristic mode theory allows design procedures to be generalized to antennas with more complex electromagnetic behavior. The modes of simple antennas share the same properties as those of complex structures. Therefore, characteristic mode design approaches for simple structures have the potential to be extended to complex geometries

of various electrical sizes. However, current systematic methods relying on characteristic mode theory have not removed the heuristic aspect from the design process. Extensive experience working with characteristic modes is necessary in order to understand and use them effectively. Although they can be readily computed, understanding how characteristic modes transform with respect to reactive loading or geometry variations is only understood qualitatively through extensive experience. The realization of more complicated designs still requires exhaustive parametric searches now with the added characteristic mode computation cost [17].

In order for characteristic modes to be used systematically for more complicated antenna topologies such as reconfigurable or spiral antennas, a better quantitative understanding of how modes behave is essential. Certainly exhaustive parametric studies can develop qualitative insight into how modes transform. However, the fundamental factors driving the mode transformations and mode behavior are still not adequately understood or quantified from a characteristic mode perspective. Beside feed and antenna placement problems, characteristic modes are still typically used as an analysis tool to guide designs instead of as a predictive method to understand quantitatively how design choices alter the modes. Antenna structure geometries are typically specified fairly precisely before characteristic mode analysis is even performed. As a result, the systematic methods are not independent of designer expectations.

Additionally, for simple antenna loading problems approached using characteristic modes, reactive loads are typically placed in mode current maxima. However, as designs become more complicated this simple approach is no longer satisfactory. For instance, load placements must be chosen heuristically as frequency reconfigurable designs begin to have wider tuning range requirements [5]. The change in mode currents due to reactive loading is not quantified, so extensive parametric studies are necessary to determine the best port locations. A quantitative understanding of how loading affects the modes is necessary. This thesis aims to address these challenges for the design of antenna reactive loading by applying perturbation theory to the characteristic mode problem for the first time. The approach not only advances our understanding of characteristic mode theory, but reveals a new design paradigm for the loading of antennas with complicated electromagnetic behavior.

1.3 Objectives

Characteristic mode theory has shown potential as a systematic design technique and provides a strong foundation on which to develop systematic design approaches. However, the application of characteristic modes as a design tool is still in its infancy. Extensive work is necessary to address the limitations in the application of characteristic modes to antenna design previously discussed. With the limitations addressed, a new systematic design approach can be developed that is more useful for antenna designers. This thesis addresses the limitations in characteristic mode theory for antenna loading applications and develops a new antenna loading design approach based on characteristic mode theory. The methods developed in this thesis are generally applicable to any antenna type. However, the approach is applied to spiral antenna loading for pattern modification to demonstrate the effectiveness of the approach when dealing with antennas with complicated electromagnetic behavior.

Many challenges exist with managing the inevitable tradeoffs that occur in antenna performance as designs become more complex. A better systematic method to manage the tradeoffs and provide more insight into the functioning of the design is necessary. Characteristic mode theory can provide a more systematic approach to manage the design problem. The characteristic current and characteristic field relationship that is obtained from a characteristic mode decomposition is useful for managing the antenna radiation and input impedance properties. However, the change in mode currents as reactive loading is applied is currently not well understood or quantified. Characteristic mode methods currently require a heuristic approach to understand and manage these changing currents and the resulting patterns. The work presented in this thesis quantitatively characterizes the change in mode currents due to reactive loading which allows for more systematic antenna loading design.

This thesis provides new insight into characteristic mode theory for impedance loaded structures. First, the reliance on a qualitative understanding of how modes transform with respect to reactive loading and frequency variation is addressed. Currently, exhaustive parametric studies are used to develop insight into how modes behave and what factors govern the mode transformations. To address this problem, analytical equations that describe the

change in the characteristic modes due to reactive loading are developed. An inspection of these analytical equations provides a clear understanding of the factors governing the mode transformations. The equations not only validate some common design practices but also provide new insight that was not previously available.

The analytical equations are derived using a novel application of eigenvalue perturbation theory to the characteristic mode problem. Inspection of the derived equations reveals the explicit factors behind the transformation of the characteristic mode eigenvalues and eigencurrents when an impedance load is introduced on the antenna. The equations also provide a computationally efficient means to calculate updated eigenvalues and eigencurrents after reactive loading is applied or a variation in the frequency occurs. The equations are validated and new design insight is obtained by first applying them to a basic dipole antenna.

The characteristic mode perturbation equations reveal a new design paradigm in which reactive loading is used to control the eigencurrent contributions between modes. The new paradigm is applied to the design of the loading of an Archimedean spiral antenna. Desirable antenna functionality can be achieved by obtaining higher order mode eigencurrent contributions to the excitable modes. Furthermore, the mode contribution perspective provides a new approach to systematically control antenna input impedance. The approach is used to significantly improve the VSWR performance of the spiral antenna through the use of proper load placement positions revealed by the new equations. It is shown that traditional characteristic mode methods do not reveal the underlying cause of the spiral's high VSWR or a solution.

Furthermore, the perturbation approach is applied to the analysis and improvement of antenna efficiency. The approach provides a more systematic method to control the characteristic mode currents on an antenna. Because antenna efficiency is closely tied to the current through loss elements, a systematic means to manage the currents also provides a method to control the antenna efficiency. The approach is applied to an electrically small dipole antenna to investigate the applicability of the approach. The limitations of this approach for efficiency improvement are also discussed.

Chapter 2 provides an overview of the characteristic mode formulation consistent with the early work of Harrington. The chapter also derives the characteristic mode formulation in the presence of reactive loading, which

forms a foundation for the development of the characteristic mode perturbation approach. Next, Chapter 3 develops the novel characteristic mode perturbation equations and describes, for the first time, the factors governing the mode changes. Insight is discussed concerning potential design opportunities revealed by the analytical equations. In Chapter 4 the derived perturbation equations are applied to a simple dipole antenna. Further design insight provided by the dipole application examples is discussed. The equations are then applied to spiral antenna loading design in Chapter 5. The complex interaction of the spiral antenna arms traditionally makes the topology difficult to model and to modify for alternate functions. The example demonstrates how the perturbation approach can provide signficant insight and guide the loading design to achieve a desirable endfire pattern. Chapter 6 applies the perturbation method to antenna efficiency analysis and suggests a mode contribution design approach for maximizing efficiency. Finally, Chapter 7 discusses the conclusions and contributions of this work along with potential avenues for future research.

CHAPTER 2

REVIEW OF CHARACTERISTIC MODE THEORY

The theory of characteristic modes provides a useful modal expansion for the surface currents of a conducting structure. Although alternative expansions are possible [18], characteristic modes, in particular, have desirable properties that can be used to facilitate antenna design and analysis problems. The theory of characteristic modes applied to electromagnetic problems was originally proposed by Garbacz and Turpin in 1971 [8]. Soon, Harrington and Mautz proposed an alternative formulation derived from the impedance operator relating the surface current to the tangential electric field on the object [9]. Harrington and Mautz showed that characteristic modes can be readily obtained using the impedance matrix from a moment method formulation [19]. Because of the effective computation procedure accompanying the formulation, the approach taken by Harrington and Mautz has seen widespread use in the characteristic mode community. In this chapter, a review of characteristic mode theory based on the Harrington and Mautz formulation is given in order to provide a foundation for later novel developments.

2.1 Derivation of the Characteristic Currents

The electric field outside of a structure composed of a perfect electrical conductor can be expressed as a combination of an incident electric field and a scattered field due to the currents on the structure. On the conducting structure, the boundary condition requires that the total tangential electric field is zero

$$[\mathbf{E}^s + \mathbf{E}^i]_{tan} = 0. \tag{2.1}$$

The operator L gives the scattered electric field due to the surface currents

$$-\mathbf{E}^s_{tan} = L(\mathbf{J})_{tan} = j\omega\mathbf{A}(\mathbf{J}) + \nabla\mathbf{\Phi}(\mathbf{J}). \tag{2.2}$$

The magnetic vector potential is given by

$$\mathbf{A}(\mathbf{J}) = \mu \oiint_S \mathbf{J}(\mathbf{r}')\psi(\mathbf{r},\mathbf{r}')ds', \tag{2.3}$$

the electric scalar potential is given as

$$\mathbf{\Phi}(\mathbf{J}) = \frac{-1}{j\omega\epsilon} \oiint_S \nabla' \cdot \mathbf{J}(\mathbf{r}')\psi(\mathbf{r},\mathbf{r}')ds', \tag{2.4}$$

and the free space Green's function is given as

$$\psi(\mathbf{r},\mathbf{r}') = \frac{e^{-jk|\mathbf{r}-\mathbf{r}'|}}{4\pi|\mathbf{r}-\mathbf{r}'|}. \tag{2.5}$$

The operator $L(\cdot)$ has units of impedance so is often expressed as

$$Z(\mathbf{J}) = [L(\mathbf{J})]_{tan} \tag{2.6}$$

and called the impedance operator. The impedance operator can be expressed as

$$Z = R + jX, \tag{2.7}$$

where R and X are real symmetric operators given by

$$R = \frac{1}{2}\left(Z + Z^*\right) \tag{2.8}$$

and

$$X = \frac{1}{2j}\left(Z - Z^*\right), \tag{2.9}$$

with * denoting the complex conjugate. Harrington and Mautz showed that characteristic modes can be obtained by solving the weighted eigenvalue problem given by

$$Z(J_n) = \nu_n M(J_n), \tag{2.10}$$

where Z is the impedance operator, J_n is an eigencurrent, M is a weight operator, and ν_n is a complex eigenvalue given by

$$\nu_n = 1 + j\lambda_n. \tag{2.11}$$

Any symmetric weight matrix M will diagonalize Z. However, the weight operator M is typically chosen equal to R in order to maintain orthogonality of the mode radiation patterns. With the weight operator chosen equal to R, Eqn. 2.10 becomes

$$X(J_n) = \lambda_n R(J_n). \tag{2.12}$$

Solution of the eigenvalue problem produces a set of eigencurrents J_n with corresponding eigenvalues λ_n. The sign of the eigenvalue denotes the type of net energy stored by the mode. Modes with positive eigenvalues are inductive and store net magnetic energy while modes with negative eigenvalues are capacitive and store net electric energy. A mode with an eigenvalue of 0 is externally resonant and tends to radiate well. The characteristic currents or eigencurrents J_n are real and satisfy the orthogonality relationships

$$\langle J_m, RJ_n \rangle = 0 \tag{2.13}$$

$$\langle J_m, XJ_n \rangle = 0 \tag{2.14}$$

$$\langle J_m, ZJ_n \rangle = 0 \tag{2.15}$$

for $m \neq n$. The inner product is defined as $\langle X, Y \rangle = \oiint_S X \cdot Y ds$ over the structure surface. The real power radiated by a mode eigencurrent is given by

$$P_{real} = \langle J_n, RJ_n \rangle. \tag{2.16}$$

The characteristic currents form a basis for the total current on the antenna structure. As a result, the total current on a structure can be decomposed as a linear superposition of characteristic currents

$$J_{tot} = \sum_n \frac{\langle J_n, E^i \rangle}{1 + j\lambda_n} J_n, \tag{2.17}$$

where E^i is the incident tangential electric field at the surface of the structure and $\langle J_n, E^i \rangle$ is the modal excitation coefficient. The quantity $\frac{\langle J_n, E^i \rangle}{1+j\lambda_n}$ is referred to as the modal weight coefficient. Although the computed eigencurrents are real, a phase is introduced when non-resonant eigencurrents are excited. Because of the $1 + j\lambda_n$ term in the denominator, modes with large eigenvalues are harder to excite and typically have lower contributions to the total current. In order to characterize the significance of a mode's con-

tribution to the total current, the modal significance of mode n is defined as

$$MS_n = \frac{1}{|1 + j\lambda_n|}. \tag{2.18}$$

The eigencurrents have associated characteristic patterns or eigenpatterns that are orthogonal over the sphere at infinity. The relationship between the eigencurrents and eigenpatterns along with the eigenpattern orthogonality allows the total radiated far field pattern to be decomposed as a summation of the eigenpatterns

$$E = \sum_n \frac{\langle J_n, E^i \rangle}{1 + j\lambda_n} E_n, \tag{2.19}$$

where E^i is the excitation electric field and E_n is the mode eigenpattern.

Harrington and Mautz developed a procedure to numerically compute the characteristic modes of a structure [19]. The procedure obtains a discretized impedance matrix using a traditional method of moments formulation. A desired structure is meshed, basis functions such as triangle or Rao-Wilton-Glisson (RWG) are assigned to the mesh elements, and an impedance matrix is generated using the method of moments with Galerkin testing. An impedance matrix is generated which can be used in the numerical solution of the characteristic modes. Therefore, the computed eigenvectors are associated with the geometry via the basis functions. The generation of the impedance matrix can be accomplished using commercial method of moments software. The software package FEKO® is used in a number of ways throughout this work to obtain the characteristic modes. FEKO® contains a convenient built in characteristic mode solver that is sometimes used. However, the impedance matrix is often exported from FEKO®, and the characteristic mode problem solved externally in MATLAB®. This provides more insight into and control over the characteristic mode solution process which is important for characteristic mode research. Both methods are used throughout this work.

2.2 Characteristic Modes of Reactively Loaded Surfaces

Harrington and Mautz performed early investigations into the characteristic modes of reactively loaded surfaces [20]. They showed that any real current can be made a resonant eigencurrent by reactively loading the surface. For a loaded surface the total tangential electric field is related to the surface current $\mathbf{J}$ by the surface impedance Z_L expressed as

$$\mathbf{E}_{tan} = Z_L(\mathbf{J}). \tag{2.20}$$

The total electric field is the sum of the impressed and scattered fields

$$\mathbf{E}_{tan} = \mathbf{E}^i_{tan} + \mathbf{E}^s_{tan}. \tag{2.21}$$

Using Eqns. 2.20, 2.2, and 2.6 in 2.21 results in

$$(Z + Z_L)(\mathbf{J}) = \mathbf{E}^i_{tan}. \tag{2.22}$$

The modal solutions for the loaded structure can be determined from the eigenvalue equation

$$(Z + Z_L)(J_n) = \nu_n M(J_n). \tag{2.23}$$

The surface impedance operator Z_L can be expressed as $Z_L = R_L + jX_L$. Typically lossless reactive loads ($R_L = 0$) are considered. If the loading is not lossless, the weight operator selection will not maintain both real eigencurrents and orthogonality of the radiation pattern. Assuming a choice of weighting $M = R$, Eqn. 2.23 can be simplified to obtain

$$(X + X_L)(J_n) = \lambda_n R(J_n). \tag{2.24}$$

The properties of characteristic modes for a loaded surface are identical to the unloaded surface. The previous unloaded reactance operator X is simply replaced by $X + X_L$.

Harrington and Mautz showed that any real current can be resonated by choosing appropriate surface reactive loading. If a desired real current $\mathbf{J}$ is to be resonated ($\lambda = 0$), Eqn. 2.24 can be used to obtain an expression for

the required loading

$$X_L(\mathbf{J}) = -X(\mathbf{J}). \tag{2.25}$$

The ability to systematically resonate any real current using surface loading is particularly appealing from a design perspective. Characteristic modes provide a systematic approach to determine the required loading. Other authors have applied this approach to antenna design problems [5]. However, any real current can only be resonated if continuous surface loading is available. When a noncontinuous loading scheme is used, only an approximation to the desired current can be obtained.

2.3 Characteristic Modes of a Dipole

Wire dipole antennas are geometrically simple and well understood electrically, which makes them an ideal candidate for a simple characteristic mode analysis. As a result of their simplicity, dipoles can provide significant insight into the behavior of characteristic modes and provides an application to test characteristic mode techniques. A basic characteristic mode analysis of a dipole is presented here to demonstrate basic characteristic mode analysis procedures and to function as a foundation for later work. A characteristic mode analysis performed in FEKO® is shown here for a dipole designed for fundamental operation at 3.5 GHz. The wire antenna is 38.8 mm in length and has a 0.1 mm radius. A mesh with 52 segments is used in order to have about 20 segments per wavelength for the current distribution of the 5^{th} eigenmode. Triangle basis functions are used for expansion and testing resulting in 51 unknowns. The eigenvalues are given in Fig. 2.1 and the eigencurrents are given in Fig. 2.2.

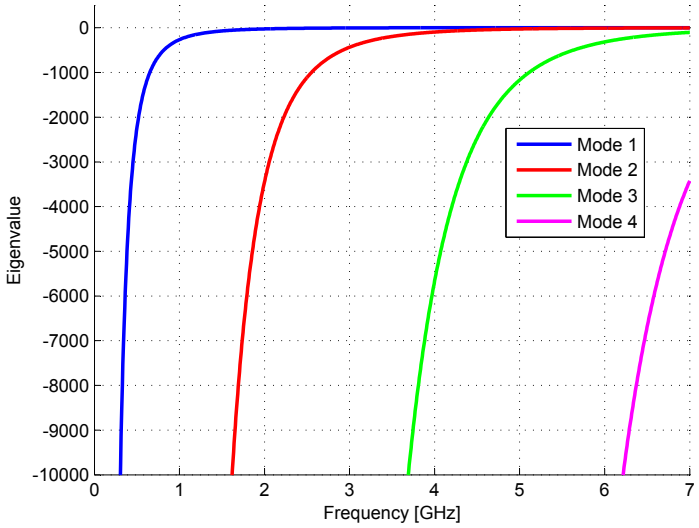

Figure 2.1: Characteristic mode eigenvalues for the dipole.

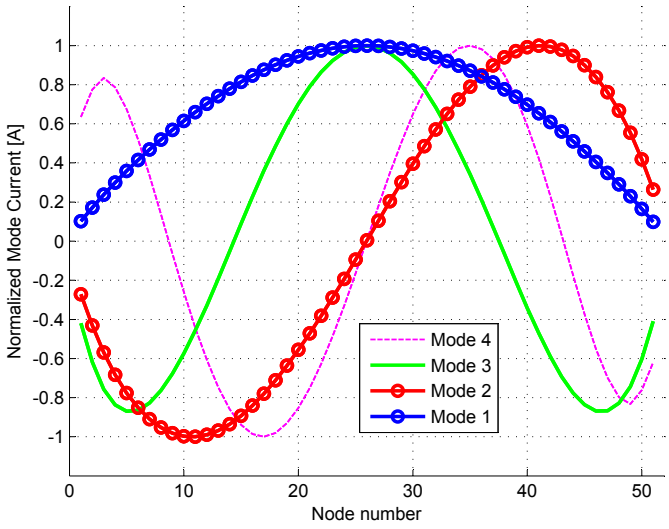

Figure 2.2: Normalized eigencurrents for the dipole at 3.5 GHz.

CHAPTER 3

CHARACTERISTIC MODE PERTURBATION AND SENSITIVITY ANALYSIS

In Chapter 2 the theory of characteristic modes and its extension to reactively loaded structures was reviewed. In the present chapter, a characteristic mode eigenvalue perturbation approach is developed to quantify and provide insight into the effects of reactive loading and frequency variation on antenna characteristic modes. An eigenvalue perturbation approach applied to characteristic modes is presently not available in the open literature. A perturbation approach, however, can provide significant mathematical insight into the development and transformation of antenna characteristic modes over frequency while subject to different loading combinations. Currently, insight into how characteristic modes behave is developed through parametric techniques and designer experience. The perturbation approach developed here establishes a mathematical foundation to explain and complement current characteristic mode heuristic design methods and understanding. The expressions derived here will form the foundation for a new loading design paradigm presented in later chapters.

3.1 Insight for a Characteristic Mode Perturbation Approach

The eigenvalue perturbation approach has traditionally been used to analyze the computational stability of an eigenvalue problem [21]. Small numerical perturbation errors in an eigenvalue system matrix can lead to errors or instabilities in the computed eigenvalues and eigenvectors potentially resulting in significant errors in the calculated values. Using matrix perturbation theory, quantitative error bounds on the computed eigenvalues and eigenvectors can be established to estimate the computation accuracy of an eigenvalue problem.

Careful inspection of the reactively loaded characteristic mode generalized eigenvalue formulation reveals that eigenvalue perturbation theory can be applied to characteristic mode analysis of loaded antennas as well. Instead of characterizing the accuracy of an eigenvalue computation subject to system matrix numerical errors, the sensitivity of the eigenmodes in the presence of reactive loading is now characterized. The characteristic mode generalized eigenvalue equation including reactive loading was given in Section 2.2 as

$$[X + X_L]J_n = \lambda_n R J_n. \tag{3.1}$$

The structure of the equation reveals that load matrix X_L can be viewed as a perturbation to the unloaded reactance matrix X. Therefore, matrix perturbation theory can be applied to characterize the effect of reactive loading on the characteristic modes of the antenna structure described by reactance matrix X. We can assume that the variation in matrix R is negligible as loading is applied.

Furthermore, the sensitivity of an antenna's characteristic modes over frequency can similarly be viewed in terms of matrix perturbation theory. Consider the unloaded characteristic mode generalized eigenvalue equation evaluated at frequency ω_o,

$$[X_{\omega_o}]J_n = \lambda_n R J_n. \tag{3.2}$$

At a second adjacent frequency, the reactance matrix will change consistent with the frequency variation of the electric field integral equation (EFIE) used in the characteristic mode method of moments formulation. The frequency variation of the generalized impedance matrix elements which includes the reactance matrix is given in [19] as

$$Z_{ij} = \oiint_S \oiint_S [j\omega\mu \mathbf{W}_i' \cdot \mathbf{W}_j + \frac{1}{j\omega\epsilon}(\nabla' \cdot \mathbf{W}_i')(\nabla \cdot \mathbf{W}_j)]\psi(\mathbf{r}, \mathbf{r}')ds'ds, \tag{3.3}$$

where $\mathbf{W}$ is a basis function and ψ is the Green's function defined in Section 2.1. The impedance matrix can be readily obtained by commercial full-wave method of moments software packages such as FEKO®. The total system matrix at the second frequency, X_{ω_2}, can be viewed as the original frequency reactance matrix added to a perturbation matrix consisting of the change in

the reactance matrix between the two frequencies $X_{\Delta\omega}$,

$$[X_{\omega_2}]J_n = [X_{\omega_o} + X_{\Delta\omega}]J_n = \lambda_n R J_n. \tag{3.4}$$

Matrix perturbation theory can then be applied to characterize the frequency sensitivity of the eigenmodes. We can assume that the frequency variation in matrix R is negligible.

3.2 Eigenvalue Perturbation Derivation

As described in Section 3.1, the inclusion of reactive loading and frequency variations in the characteristic mode formulation can be viewed as perturbations to the eigenvalue system matrix. As a result, the change in the eigenvalues and eigenvectors for an infinitesimal perturbation can be calculated. A general derivation is given here for the change in the complex eigenvalues and eigenvectors following the approach taken by Faddeev and Faddeeva for a standard unweighted eigenvalue problem [21]. However, their approach must be extended to generalized eigenvalue problems in order to be applicable to the characteristic mode formulation. An extended derivation for the generalized eigenvalue problem is presented here. The general derivation applies to the complex characteristic mode eigenvalue equation given by Eqn. 2.10. It will later be specialized to address the more commonly used reduced eigenvalue equation given by Eqn. 2.12.

Consider the generalized eigenvalue problem given as

$$[Z]J_i = \nu_i R J_i, \tag{3.5}$$

where Z is a complex matrix, R is a complex weight matrix, and J_i is a complex eigenvector with associated complex eigenvalue ν_i. The eigenvalues of matrix Z are assumed to be distinct. If matrix Z undergoes a complex perturbation dZ, the eigenvalue equation can now be expressed as

$$[Z + dZ][J_i + dJ_i] = [\nu_i + d\nu_i]R[J_i + dJ_i], \tag{3.6}$$

where dJ_i is the infinitesimal change in the eigenvector and $d\nu_i$ is the infinitesimal change in the eigenvalue due to the infinitesimal perturbation dZ. For

this derivation, values of second-order smallness are ignored and dZ is considered a differential, not a finite increment. This is, however, an adequate approximation for many practical problems where dZ is a finite increment. The perturbed eigenvalue equation can be expanded and simplified using the expressions $ZJ_i = \nu_i R J_i$ and $dZdJ_i = d\nu_i R dJ_i$ to obtain

$$ZdJ_i + dZJ_i = \nu_i R dJ_i + d\nu_i R J_i. \tag{3.7}$$

Now let $V_1, ...V_n$ be the eigenvectors of the conjugate matrix Z^* with eigenvalues $\bar{\nu}_1, ...\bar{\nu}_n$, where * denotes the conjugate transponse and $^-$ indicates the conjugate. The matrix inner product is defined as $\langle x, y\rangle = x_1\bar{y_1} + ... + x_n\bar{y_n}$, where x and y are vectors. The inner product is then taken between Eqn. 3.7 and the eigenvectors of the conjugate matrix obtaining

$$\langle ZdJ_i, V_j\rangle + \langle dZJ_i, V_j\rangle = \langle \nu_i R dJ_i, V_j\rangle + \langle d\nu_i R J_i, V_j\rangle. \tag{3.8}$$

In order to derive the eigenvalue perturbation, the eigenvector indices are first assumed equal, $i = j$. Additionally, the weight matrix will be assumed to be real and symmetric. In the characteristic mode eigenvalue problem formulation, the weight matrix is typically chosen to be the real part of the generalized impedance matrix in order to produce orthogonality of the mode radiation patterns. With this weight selection R is real and symmetric, so a symmetric weight matrix assumption is appropriate. Therefore, the first term on the right hand side of Eqn. 3.8 can be written as

$$\langle dJ_i, \bar{\nu}_i R V_i\rangle \tag{3.9}$$

by observing the inner product definition. Furthermore, the first term on the left hand side of Eqn. 3.8 can be written as

$$\langle dJ_i, Z^* V_i\rangle. \tag{3.10}$$

The eigenvalues of the conjugate Z matrix are the complex conjugates of the eigenvalues of Z. Therefore, $Z^*V_i = \bar{\nu}_i R V_i$ and the first terms on the left and right hand sides of Eqn. 3.8 cancel. This desired cancellation is why the inner product was taken with the eigenvectors of the conjugate Z matrix. If a different inner product definition is assumed, then the inner product should

be taken with a different quantity. After cancellation Eqn. 3.8 becomes

$$\langle dZJ_i, V_i\rangle = \langle d\nu_i RJ_i, V_i\rangle. \tag{3.11}$$

The scalar value $d\nu$ can be pulled out of the inner product and solved for in order to obtain the desired result,

$$d\nu_i = \frac{\langle dZJ_i, V_i\rangle}{\langle RJ_i, V_i\rangle}. \tag{3.12}$$

Expression 3.12 quantifies the change in the eigenvalue for a given matrix perturbation, dZ. A useful maximum bound can be found for the change in the magnitude of the eigenvalue. The bound is useful in analyzing physical problems, since it can give insight into the maximum obtainable antenna performance under certain conditions. The maximum bound on the change in eigenvalue is given as

$$|d\nu_i| \leq \frac{\|dZ\| \cdot |J_i| \cdot |V_i|}{|\langle RJ_i, V_i\rangle|} = C_i \cdot \|dZ\| \tag{3.13}$$

with

$$C_i = \frac{|J_i| \cdot |V_i|}{|\langle RJ_i, V_i\rangle|}. \tag{3.14}$$

Here, $\|\cdot\|$ represents the matrix norm, and $|\cdot|$ denotes the standard l^2 vector norm. The value $\|dA\|$ provides a bound on the "amplifying power" of the perturbation matrix.

The change in each eigenvector for an infinitesimal matrix perturbation can also be determined from Eqn. 3.8 by assuming that the eigenvector indices of matrices Z and Z^* are not equal, $i \neq j$. Using the same arguments developed above but with different indices, the first term on the left-hand side of Eqn. 3.8 can be expressed as

$$\begin{aligned}\langle ZdJ_i, V_j\rangle &= \langle dJ_i, Z^*V_j\rangle \\ &= \langle dJ_i, \bar{\nu_j} RV_j\rangle \\ &= \langle \nu_j RdJ_i, V_j\rangle \\ &= \nu_j \langle RdJ_i, V_j\rangle. \end{aligned} \tag{3.15}$$

Eqn. 3.8 then becomes

$$\langle dZJ_i, V_j\rangle = (\nu_i - \nu_j)\langle RdJ_i, V_j\rangle + d\nu_i\langle RJ_i, V_j\rangle. \tag{3.16}$$

The eigenvectors of Z and Z^* are R-orthogonal. As a result, for differing eigenvector indices the last term on the right hand side disappears and Eqn. 3.16 can be written as

$$\langle RdJ_i, V_j\rangle = \frac{\langle dZX_i, V_j\rangle}{(\nu_i - \nu_j)}. \tag{3.17}$$

The other eigenvectors can be used as a basis to expand the change in eigenvector i. The expansion is given as

$$dJ_i = \sum_{m=1}^{N} \alpha_{im} J_m \quad m \neq i, \tag{3.18}$$

where α_{im} are the unknown amplitude coefficients. The coefficients can be determined by substituting expansion 3.18 into Eqn. 3.17 to obtain

$$\sum_{m=1}^{N} \alpha_{im}\langle RJ_m, V_j\rangle = \frac{\langle dZJ_i, V_j\rangle}{(\nu_i - \nu_j)}. \tag{3.19}$$

Using the orthogonality property ($\langle RJ_m, V_j\rangle = 0$ for $m \neq j$), the unknown amplitude coefficients are found to be

$$\alpha_{ij} = \frac{\langle dZJ_i, V_j\rangle}{\langle RX_j, V_j\rangle(\nu_i - \nu_j)}. \tag{3.20}$$

The coefficient α_{ii} is undefined and can be assumed to be equal to zero. Substituting the expressions for the coefficients into Eqn. 3.18 results in an expression for the desired change in the eigenvector for a given matrix perturbation dZ

$$dJ_i = \sum_{j=1}^{N} \frac{\langle dZJ_i, V_j\rangle}{\langle RJ_j, V_j\rangle(\nu_i - \nu_j)} J_j \quad i \neq j. \tag{3.21}$$

The derived expression gives the change in the eigenvectors in terms of the contributions from each of the other eigenvectors. A useful maximum bound can be found for the change in the magnitude of an eigenvector. The bound

is useful in analyzing physical problems, since it can give insight into the maximum bound on the change in antenna characteristic mode current under certain conditions. The maximum bound on the change in the eigenvector is given as

$$|dJ_i| \leq \|dZ\| \cdot |J_i| \cdot \sum_{j=1}^{N} \frac{|V_j| \cdot |J_j|}{|\langle RJ_j, V_j \rangle||\nu_i - \nu_j|} \quad i \neq j. \tag{3.22}$$

3.3 Eigenvalue Sensitivity

The perturbation approach provides the change in the eigenvalues and eigenvectors for a given infinitesimal loading perturbation. A similar approach can be taken to find the derivatives of the eigenvalues with respect to a given parameter α. This gives an indication of the sensitivity of the eigenvalues. Eqn. 3.7 can be expressed as

$$Z\left(\frac{\partial J_i}{\partial \alpha}\right) + \left(\frac{\partial Z}{\partial \alpha}\right) J_i = \nu_i R\left(\frac{\partial J_i}{\partial \alpha}\right) + \left(\frac{\partial \nu_i}{\partial \alpha}\right) RJ_i. \tag{3.23}$$

Using the same derivation steps shown in Section 3.2, the derivative of the eigenvalue with respect to the parameter α can be found to be

$$\frac{\partial \nu_i}{\partial \alpha} = \frac{\langle \left(\frac{\partial Z}{\partial \alpha}\right) J_i, V_i \rangle}{\langle RJ_i, V_i \rangle}. \tag{3.24}$$

If the derivatives are approximated using forward differencing, Eqn. 3.24 becomes

$$\frac{\nu_i(\alpha + \Delta\alpha) - \nu_i(\alpha)}{\Delta\alpha} = \frac{\langle \frac{Z(\alpha+\Delta\alpha) - Z(\alpha)}{\Delta\alpha} J_i, V_i \rangle}{\langle RJ_i, V_i \rangle}. \tag{3.25}$$

Multiplying through by $\Delta\alpha$ and letting $\Delta\alpha$ approach zero produces Eqn. 3.12.

3.4 Application of the Perturbation Approach to Characteristic Modes

The expressions derived in section 3.2 give the eigenvalue and eigenvector change due to a complex perturbation dZ. In section 3.1 we saw that for the

characteristic mode problem, the perturbation could represent the loading matrix due to a small impedance introduced on the antenna surface, or it could represent the change in the method of moments impedance matrix as the solution frequency is varied. We will consider the case of impedance loading in more detail here. The perturbation equations were derived generally in order to characterize the effect of complex perturbations on the complex eigenvalues and eigenvectors. The complex formulation will be shown to be useful when analyzing antenna loss and characteristic mode radiation efficiencies. Because the method of moments impedance matrix is symmetric, the eigenvectors of Z^* are the complex conjugates of the eigenvectors of Z. Therefore, $V_j = \bar{J}_j$ and the eigenvalue and eigenvector perturbation equations can be written as

$$d\nu_i = \frac{\langle dZ_L J_i, \bar{J}_i \rangle}{\langle RJ_i, \bar{J}_i \rangle} \tag{3.26}$$

and

$$dJ_i = \sum_{j=1}^{N} \frac{\langle dZ_L J_i, \bar{J}_j \rangle}{\langle RJ_j, \bar{J}_j \rangle (\lambda_i - \lambda_j)} J_j \quad i \neq j, \tag{3.27}$$

where dZ_L is the complex impedance load matrix, J is the eigenmode current, ν is the complex eigenvalue, and R is a chosen symmetric weight matrix.

Although the expressions are useful for including lossy elements in the perturbation analysis, most characteristic mode problems do not need to take into account losses on the antenna structure. As a result, the perturbation equations can be derived starting with Eqn. 2.12. Alternatively, the perturbation equations derived from Eqn. 2.12 can simply be viewed as special cases of Eqns. 3.26 and 3.27. The equations can be specialized for the reactively loaded characteristic mode case given by Eqn. 3.1 to obtain

$$d\lambda_i = \frac{\langle dX_L J_i, J_i \rangle}{\langle RJ_i, J_i \rangle} \tag{3.28}$$

and

$$dJ_i = \sum_{j=1}^{N} \frac{\langle dX_L J_i, J_j \rangle}{\langle RJ_j, J_j \rangle (\lambda_i - \lambda_j)} J_j \quad i \neq j, \tag{3.29}$$

where dX_L is the reactive load perturbation matrix, J is a real eigencurrent, λ is a real eigenvalue, and R is the chosen symmetric weight matrix. The method of moments reactance matrix X is real and symmetric. As a result, X and its conjugate matrix X^* are equivalent and have the same eigenvec-

tors. Therefore, the eigenvectors of the conjugate system matrix previously represented by V have been replaced by the eigenvectors of the system matrix X which in this case is the unloaded eigencurrent J. These simplified expressions will be used throughout most of this work.

Eqns. 3.28 and 3.29 provide insight into how characteristic mode eigenvalues and eigenvectors transform under different loading conditions. The analytical equations reveal interesting properties that can be useful for antenna design. First, consider Eqn. 3.28 governing the eigenvalue change. The equation consists of quadratic numerator and denominator terms. The numerator is a quadratic relationship describing the interaction between reactive loading and the mode eigencurrent. The eigencurrent vector J_i describes the mode current values across the surface of the structure with respect to the basis functions. Since the positions of the loading entries in dX_L are also related to the basis functions and their locations on the structure, the numerator reveals that placing the loads in mode current maxima results in the largest change in eigenvalue. When lumped loading is considered, dX_L is diagonal and has a sifting property that selects the eigencurrent values at the load locations.

Furthermore, the quadratic term in the denominator is the power radiated by the mode as previously given in Eqn. 2.16. Therefore, the change in eigenvalue is inversely proportional to the power radiated by the eigenmode. The change in the eigenvalue becomes unstable when $\langle RJ_i, J_i \rangle = 0$ which corresponds to the interior resonance condition. When the interior resonance condition is satisfied, no power is radiated. If R is positive definite, however, interior resonance cannot be satisfied, so the change in eigenvalue may be large but will always be finite.

Eqn. 3.29 provides insight into how a desired eigencurrent mode, mode i, changes. The equation shows that the change in a particular mode eigencurrent has a contribution from all the other mode eigencurrents. The quantity

$$\alpha_{i,j} = \frac{\langle dX_L J_i, J_j \rangle}{\langle RJ_j, J_j \rangle (\lambda_i - \lambda_j)} \tag{3.30}$$

in Eqn. 3.29 will be referred to as the eigencurrent contribution coefficient since it determines the magnitude of the mode j eigencurrent contribution to the mode i eigencurrent. The numerator of the mode contribution coefficient relates the interaction of the desired mode with the other modes via the

reactive loading matrix. In order to maximize mode j's contribution to the changing mode, mode i, the load should be placed in the current maxima of both modes. If the load is placed in a current null of mode j, mode j will not contribute to the change in mode $i's$ current. Alternatively, if the load is placed in a current null of mode i, mode i will experience no change at all. This shows and quantifies how a designer can control the contribution of each mode to the change in a particular mode's current through proper load placement.

Furthermore, the denominator of the mode contribution coefficient is a product of the power radiated by the contributing mode and the difference in eigenvalues between the contributing and changing mode. In the past, the assumption in characteristic mode design has been that modes with large valued eigenvalues can be ignored. This is generally assumed since large eigenvalues result in low modal significance relative to often desirable resonant modes ($\lambda = 0$). First inspection of the denominator of Eqn. 3.29 may seem to suggest that current modes with eigenvalue magnitudes that differ substantially from that of the desired mode will have negligible contribution to the change in eigencurrent. However, this proves to be an incorrect assumption. Modes with large eigenvalues tend to radiate less power which compensates for the large eigenvalue differences in the denominator product. Therefore, higher order modes, often assumed insignificant, can contribute to the change in resonant mode current. This will be investigated in an example given in Section 4.2.

3.4.1 Eigenvalue Stability

For eigenvalue computation problems, the perturbation method provides a technique to analyze the accuracy of the eigenvalue solution and predict any potential instabilities. Unstable solutions are typically undesirable since they lead to large errors in the computed solution for certain small numerical error perturbations that may be present in the system matrix.

However, in the loaded antenna characteristic mode formulation, the perturbation present in the problem is not from numerical error but from physically introduced reactive loading. Therefore, the perturbation method now quantifies the sensitivity of the characteristic mode eigenvalues to a certain

loading arrangement. Large changes in the eigenvalues for small loading perturbations may now be highly desirable.

Sensitive eigenvalues may be highly desirable for a number of reasons. For instance, variable reactive loading is often applied to frequency reconfigurable antennas using varactor diodes. Varactors are a popular form of loading since they allow the operating frequency of an antenna to be varied electrically using a bias voltage. An important specification of a varactor diode is its tuning ratio, the ratio of the maximum to minimum capacitance value the varactor can achieve. Because of challenges associated with device physics, large varactor tuning ratios are difficult to realize, and as a result, the tuning ratios available from commercial varactors are currently very limited. Additionally, for antenna design purposes, the highest tuning ratio varactors are also often not practical due to cost and availability constraints. As a result of the limitations associated with varactor tuning ratios, it is desirable to design an antenna structure and a loading placement scheme that maximizes the antenna reconfiguration for a limited load reactance range.

A relationship exists between the antenna input impedance and the characteristic mode eigenvalues and eigenvectors [22]. By increasing the sensitivity of certain eigenmodes to a loading perturbation, designers may be able to obtain wider antenna frequency tuning ranges for a given varactor tuning ratio. Theoretically, if an antenna design could be obtained with an unstable eigenvalue solution, a very large change in a mode eigenvalue could be obtainable for a finite load perturbation and could potentially translate into extremely wide tuning ranges.

3.5 Discussion

An eigenvalue perturbation approach has been developed to quantify the effects of reactive loading and frequency variations on antenna characteristic modes. Previously, heuristic methods have been used to understand and predict changes in characteristic modes with respect to design parameters. Extensive experience analyzing various structures and loading combinations was necessary in order to build characteristic mode intuition. A reliance on heuristic techniques reduces the usefulness of characteristic modes as a systematic design tool. The perturbation approach developed here, however,

provides the first quantitative method to describe the transformation of the characteristic modes analytically. The analytical equations not only predict mode changes, but more importantly, they provide an understanding of the factors that cause these changes. By understanding what factors drive mode transformations, designers can make more educated and confident design choices.

An analysis of the derived analytical expressions in Section 3.2 revealed fundamental factors driving mode changes. Salient insight provided by the perturbation method concerning the factors affecting eigenvalue changes with respect to loading are summarized here.

- The change in a mode's eigenvalue depends only on the mode's properties and the applied loading.
- To maximize the change in a mode eigenvalue, loading should be placed in a mode current maxima.
- An instability exists for modes satisfying the interior resonance condition.

The usefulness of the perturbation method becomes even more apparent when trying to understand the factors affecting eigencurrent changes. The factors driving eigencurrent changes are far less intuitive than those for eigenvalue changes. The salient insight gained from the perturbation approach as to the factors driving the change in eigencurrents are given here.

- The change in a mode's eigencurrent is composed of contributions from each of the other modes.
- The extent of a mode's contribution to another mode's current change is governed by the interaction of the applied loading with both mode currents.
- Modes that are insignificant to the antenna's total current can still have considerable contribution to the current transformation of a significant mode.

The factors affecting the change in eigencurrents have previously not been well understood, and as a result, the importance of considering higher order modes has not been realized [5]. By understanding the factors driving the

changes in eigenmodes, designers can create more effective antenna designs with confidence. Furthermore, the perturbation approach provides a solid foundation for a more systematic design approach paradigm as developed in later chapters.

CHAPTER 4

DIPOLE APPLICATION OF THE PERTURBATION METHOD

The characteristic mode eigenvalue perturbation method developed in Chapter 3 quantitatively describes the relationship between the factors driving changes in the eigenvalues and eigencurrents. In this chapter, the characteristic mode perturbation approach is applied to the simple dipole antenna described in Section 2.3 to develop further insight into the perturbation equations and to demonstrate the application and usefulness of the approach.

Dipole antennas are well understood. As a result, they provide an ideal application to explore the utility of the perturbation analytical equations. Here the perturbation equations are used to demonstrate the impact of reactive loading on a dipole's characteristic mode eigenvalues and eigenvectors. The equations are applied to two different dipole case studies each using a different reactive loading arrangement. The effectiveness of the loading schemes in producing eigenvalue change is examined and is generalizable for arbitrary antennas. Following the eigenvalue analysis, the change in dipole eigencurrents due to reactive loading is examined. Chapter 3 showed that the change in a mode eigencurrent contains a contribution from each of the other modes. The analytical eigencurrent perturbation equation provides the insight needed to enhance or suppress certain mode contributions to other modes as loading is applied. This concept is demonstrated for the dipole antenna, and the importance of considering higher order modes that are often ignored in the literature is emphasized.

4.1 Dipole Eigenvalue Perturbation

In this section, the eigenvalue perturbation equation is applied to the characteristic modes for two dipole case studies at 3.5 GHz each focusing on a different reactive loading scheme. The dipole loading examples demonstrate

the factors affecting the change in mode eigenvalues. The eigenvalue perturbation equation applied to characteristic modes was developed in Chapter 3 and is repeated here as

$$d\lambda_i = \frac{\langle dX_L J_i, J_i \rangle}{\langle RJ_i, J_i \rangle}. \tag{4.1}$$

In the first case study, a single inductive load arbitrarily chosen to be +j1 Ω is applied to the dipole at a simulation mesh node using a delta gap load model. After method of moments testing, the load perturbation matrix contains the reactance value in a diagonal entry corresponding to the position of the load on the dipole. The perturbation matrix has a sifting property that selects the eigencurrent values at the particular load location. The load is moved along the dipole to each node position, and the eigenvalue change produced by the loading is calculated using Eqn. 4.1. The second case study analyzes the change in the eigenvalue when two identical loads are applied to the dipole. The loads are symmetrically placed on the mesh nodes starting at the ends of the dipole and are moved toward the center. The change in eigenvalues for the first four modes are reported unnormalized and normalized.

Normalizing the change in eigenvalue provides a useful method to compare loading scheme alternatives. For the dipole case studies, the changes in the dipole eigenvalues are normalized to the maximum bound on the change in eigenvalue. The maximum bound was established in Eqn. 3.13 and is repeated as

$$|d\lambda_{i,max}| = \frac{\|dA\| \cdot |X_i| \cdot |V_i|}{|\langle RX_i, V_i \rangle|}. \tag{4.2}$$

Normalization to the maximum bound provides a useful measure of the loading effectiveness. The normalized results express how well paired the geometry and chosen loading scheme are. The ideal loading scenario to elicit maximum eigenvalue change for a given mode exists when the eigencurrent corresponding to the antenna geometry is also an eigenvector of the load matrix corresponding to the load matrix's largest eigenvalue. The chosen normalization gives an indication of how well the geometry and loading combination satisfies this condition. A loading matrix that has a large maximum eigenvalue that corresponds to an eigenvector that matches the desired antenna eigencurrent will produce a large mode eigenvalue change. For example, when uniform, continuous +j1 Ω mesh node loading is used, the load matrix becomes the identity matrix and any antenna eigencurrent is an

eigenvector of the loading matrix. The actual change in the eigenvalue always equals the maximum bound. As a result, the normalized dipole results can also be viewed as the effectiveness of the loading scheme compared to uniform, continuous loading.

The normalization has an additional benefit. Practically, one method to increase the magnitude of the load matrix eigenvalue is to increase the load component values. However, this does not create a more effective loading scheme since larger loads are generally more costly and difficult to obtain. The $\lambda_{i,max}$ normalization quantity includes the norm of the load matrix which removes the effects of larger load values. This allows only the effectiveness of the loading positions to be analyzed which is useful for comparing alternatives.

Although normalizing by the maximum eigenvalue change bound is useful for cases in which loading appears on the load matrix diagonal, it is not the best choice for comparing alternatives that include the theoretical possibility of mutual loading reactances. Mutual reactances would lead to symmetric, off-diagonal terms in the load matrix. The purpose of considering mutual reactances would be to try to increase the maximum eigenvalue of the load matrix, the matrix norm, for a given constraint on the load value magnitude. This would theoretically produce larger eigenvalue changes for a limited load component value. By including the load matrix norm in the normalization, any desirable increase in the load matrix norm due to an effective loading scheme would be eliminated in the normalized result and a useful metric for comparison would not be obtained. Instead, a constraint should be placed on the load matrix to limit the maximum possible component value and then the change in eigenvalue can be normalized by the quantity $\frac{d\lambda_{i,max}}{\|dX_L\|}$.

4.1.1 Case 1: Single Reactive Load

The first loading arrangement that is considered is a single reactive load applied to the dipole antenna. The load is arbitrarily chosen to be +j1 Ω and is placed at a simulation mesh node. When the loading is converted into a matrix equation by Galerkin testing, the loading appears as a +1 entry on the load perturbation matrix dX_L diagonal. As a result, the loading matrix contains a single entry on the matrix diagonal corresponding to the node's

load position on the dipole. The change in the eigenvalue calculated using Eqn. 4.1 is shown in Fig. 4.1 as the load is moved to different dipole mesh nodes. The eigenvalue change normalized to the maximum bound on the eigenvalue change $d\lambda_{i,max}$ is shown in Fig. 4.2.

A comparison with Fig. 2.2 reveals that the change in a mode's eigenvalue is largest when the load is placed in a maxima of the mode's eigencurrent. On the other hand, when the load is placed in an eigencurrent null, no change in eigenvalue occurs. Inspection of Eqn. 4.1 describes why this behavior occurs. When a single load is placed on a mesh node, the load perturbation matrix in Eqn. 4.1 becomes a projection matrix selecting the eigencurrent value corresponding to the load location. When the largest mode current value is selected, the change in eigencurrent is maximized for a single load. Normalization gives the change in eigenvalue as a percentage of the uniform, continuous loaded case. Therefore, Fig. 4.2 shows that when a single load is used, less than about 4.25% of the potential eigenvalue change is obtained. This quantifies the limited performance a single load can obtain compared to uniform, continuous loading.

For maximum effect, loads should be placed in eigencurrent maxima. This is consistent with previous understanding of characteristic mode loading as well as noncharacteristic mode approaches. For instance, it is well known that a smaller inductive load is needed to resonate a short monopole antenna when the load is placed near the antenna base where the currents are high. Additionally, loading where the eigencurrents are highest is common practice for characteristic mode antenna design [7, 23]. The perturbation approach, however, verifies and quantifies this well known practice.

In addition to quantifying the common loading practice, the perturbation approach example yields further insight for antenna design. Fig. 4.1 shows that the magnitude of the eigenvalue change is much greater for higher order modes. For example, the change in mode 4 is four orders of magnitude larger than the change in mode 1. As described in Section 3.4, the change in eigenvalue is inversely proportional to the power radiated by the mode. The higher order modes that have large eigenvalues do not radiate effectively and, as a result, are much more sensitive to reactive loading. This suggests a potential tradeoff between radiation performance and reconfigurable antenna tunability that can be quantified using the perturbation approach.

Since the eigencurrents are eigenvectors that are not unique, their magni-

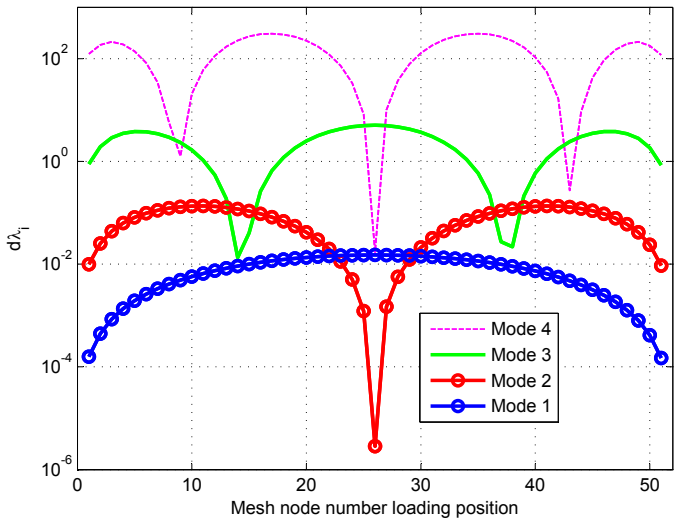

Figure 4.1: Mode eigenvalue change for a single +j1 Ω load applied at different mesh node positions.

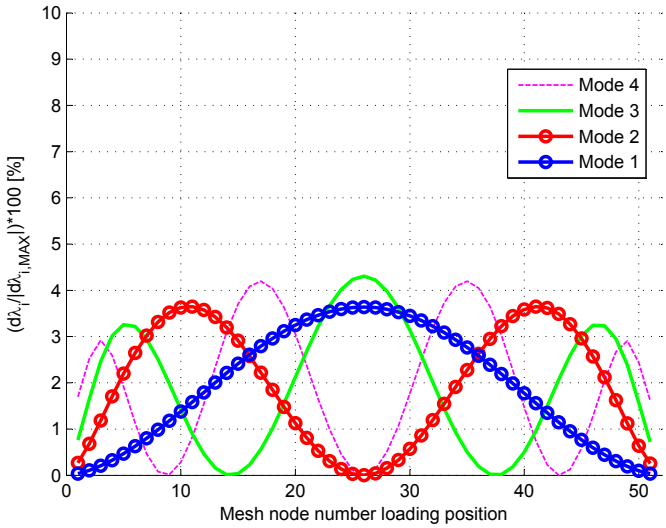

Figure 4.2: Normalized mode eigenvalue change for a single +j1 Ω load applied at different mesh node positions.

tudes can be arbitrarily scaled and still satisfy the eigenvalue problem. The eigencurrents are typically scaled to radiate unit power, which may make the previous inversely proportional to radiated power interpretation suspect. However, higher order modes store large net energies and do not radiate as effectively as lower order modes. As a result, the eigencurrents must be scaled to much larger magnitudes in order to achieve unit power radiation. Therefore, although the denominator of Eqn. 4.1 may always equal one with unit power normalization, the effect is compensated for with much larger eigencurrent magnitudes in the numerator for higher order modes. Therefore, two different viewpoints can be taken to physically interpret the perturbation equations with the same results. The eigencurrents can be assumed normalized to radiate unit power and then higher order modes will have larger eigencurrent magnitudes. Or the eigencurrent magnitudes can be kept constant and the radiated power will decrease with increasing mode order. Regardless of the normalization and physical interpretation chosen, the computed eigenvalue and eigencurrent perturbation values are the same.

4.1.2 Case 2: Two Reactive Loads

The next case that is considered is when two identical loads are placed symmetrically on the antenna. Initially, the loads are placed at both ends of the dipole. The loads are then systematically moved toward the center of the dipole while maintaining symmetry. Similar to the single load case, the change in eigenvalue is calculated using Eqn. 4.1 and the unnormalized and normalized results are shown in Figs. 4.3 and 4.4, respectively. The figures, however, display only half the node positions. Since the loads are applied symmetrically, there are only half the number of loading states before a state is repeated.

As expected, the results show that an additional load that experiences the same eigencurrent magnitude as the original doubles the change in eigenvalue. Up to about 8.5% of the potential eigenvalue change is now obtained. Additionally, the results indicate that the higher order modes with large eigenvalues continue to be more sensitive to the loading than the nearly resonant modes.

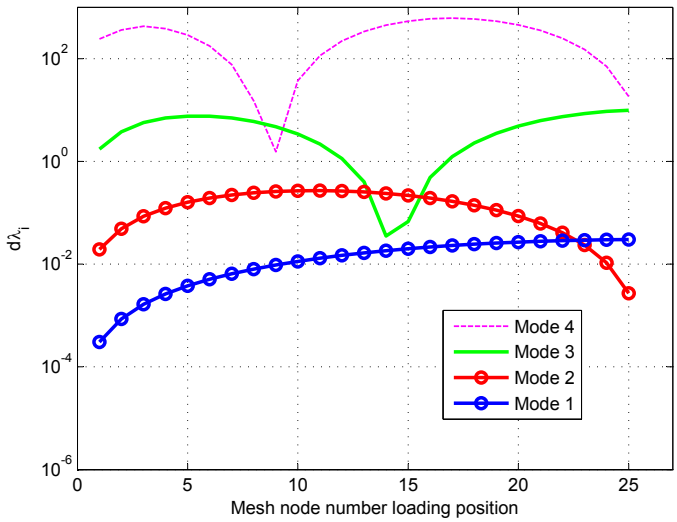

Figure 4.3: Mode eigenvalue change for two +j1 Ω load applied at symmetric mesh node positions.

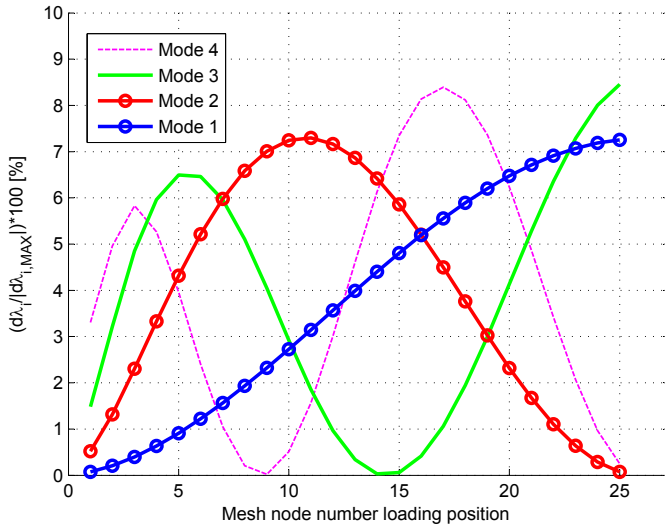

Figure 4.4: Normalized mode eigenvalue change for two +j1 Ω load applied at symmetric mesh node positions.

4.2 Dipole Eigencurrent Perturbation

Quantitatively characterizing how eigencurrents change with respect to loading is an essential part of understanding the behavior of characteristic modes. The perturbation approach provides a quantitative description of how these eigencurrents transform. The equation governing the change in eigencurrents was developed in Section 3.29 and is repeated here as

$$dJ_i = \sum_{j=1}^{N} \frac{\langle dX_L J_i, J_j \rangle}{\langle RJ_j, J_j \rangle (\lambda_i - \lambda_j)} J_j \quad i \neq j. \tag{4.3}$$

In this section, the transformations of a dipole's eigencurrents are investigated using Eqn. 4.3. The perturbation equation shows that the change in mode eigencurrent is composed of a contribution from each of the other modes. The dipole example demonstrates the importance of considering the effect of higher order modes in the characteristic mode analysis. First, Eqn. 4.3 is applied to a continuously loaded dipole and the changes in the mode eigencurrents are examined. After analyzing the continuously loaded case, a case involving application of only a single load will be studied. In both case studies, useful insight obtained from the perturbation approach is highlighted.

4.2.1 Uniform, Continuous Loading

The first case that is considered is the eigencurrent change when a uniform, continuous loading of +j1 Ω is applied to each mesh node. After testing, dX_L is simply the identity matrix. The continuous loading is used in Eqn. 4.3 and the eigencurrent changes are calculated. Fig. 4.5 shows the changes in the mode current when the contribution from all 51 eigenmodes are included. Notice that the change in the mode current is smooth and there are no sharp spatial variations in the current around any particular load. This is a typical characteristic of continuous loading. Recall from Section 2.2 that continuous loading allows any desired current distribution to be resonated. In general, as the number of loads is decreased, only an approximation to a desired current distribution can be obtained. An entirely smooth spatial variation in the eigencurrent change as seen here will not be possible.

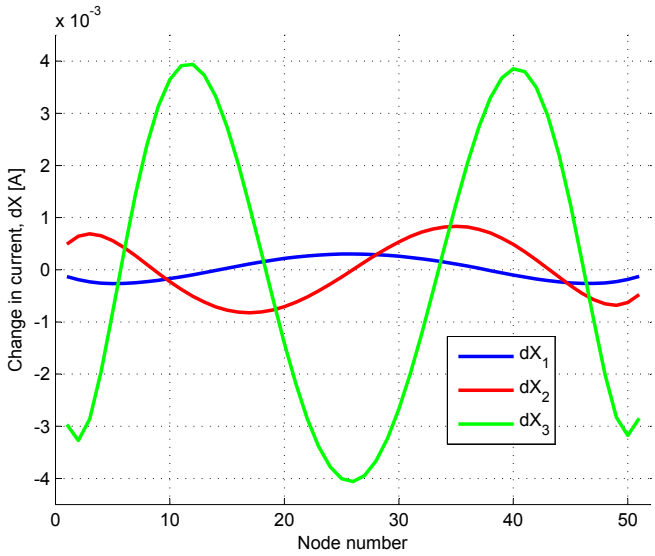

Figure 4.5: Change in mode currents considering contribution from all 51 calculated modes with uniform, continuous loading.

Furthermore, closer inspection of the eigencurrent changes reveals further details about the transformation of the modes. A comparison to the dipole eigencurrents given in Fig. 2.2 shows that the change in mode 1 is dominated by the contribution from mode 3 while the change in mode 2 is dominated by the contribution from mode 4. Therefore, as the reactive load values increase, mode 1 will begin to look increasingly like mode 3 while mode 2 will begin to look more like mode 4. Eqn. 4.3 reveals the factors governing the contribution of each mode to the eigencurrent change. The three factors include the difference in eigenvalues between the modes, the power radiated by the contributing mode, and the interaction of the loading with the changing and contributing eigencurrents. Although mode 1 and mode 2 have the closest eigenvalues, when the same loading is applied at each node of the dipole, the mode 2 contributions to mode 1 cancel. Inspection of the numerator of Eqn. 4.3 reveals the cause of this cancellation. As seen in Fig. 2.2, the mode 1 current on each dipole arm is in phase while the mode 2 current is out of phase. Therefore, when the same load value is used symmetrically on the antenna, the mode 2 contributions to mode 1 from symmetric loads cancel

$$\langle dX_L J_1, J_2 \rangle = (+|X_L|)(+|J_1|)(-|J_2|) + (+|X_L|)(+|J_1|)(+|J_2|) = 0. \quad (4.4)$$

Because mode 2 is suppressed, mode 3 tends to dominate the mode 1 eigen-

current change as seen in Fig. 4.5. This insight forms the foundation for a useful technique for enhancing or suppressing mode contributions. The technique is developed and applied in the spiral loading design example in Chapter 5.

4.2.2 Single Reactive Load

Another case considered is the eigencurrent change when only a single load of +j1 is applied to the antenna. For each position as the load is moved across the dipole, Eqn. 4.3 is calculated and reported. Fig. 4.6 shows the change in mode 1 when the contribution from all 51 eigencurrents are included in the calculation. The figure provides the mode 1 eigencurrent change when the load is initially placed at node 1 near the end of the dipole and for subsequent positions as the load is moved across the antenna. Additionally, Figs. 4.7 and 4.8 show the changes in the eigencurrents for modes 2 and 3, respectively.

The results for a single load situation provide insight into how each particular load affects the mode currents. Inspection of Eqn. 4.3 shows that the change in eigencurrent is dependent on the interaction of the load with both the changing and the contributing modes. As expected, Fig. 4.6 shows that no eigencurrent change occurs when the load is placed near the end of the dipole. The load is in a current null of mode 1 so there can be no contribution from any of the modes regardless of their distributions. Fig. 4.7 shows a similar situation for the change in mode 2. When the load is placed in the center of the antenna, a mode 2 null, there are no contributions from any of the modes regardless of their current distributions. When the load is moved to node 11, however, the load is near a mode 2 current maxima. Therefore, the change in mode 1 current in Fig 4.6 is dominated by the contribution from mode 2 evidenced by the two half-sine variations. However, when the load is moved to the center of the dipole, the load is in the mode 2 null and the contribution from mode 3 begins to dominate the current change.

First inspection of Eqn. 4.3 suggests that the difference in eigenvalue between the changing and contributing modes has a significant impact on a mode's contribution to the current change. Modes with similar eigenvalues to the changing mode will have more impact since the denominator of the mode contribution coefficient will be smaller. Therefore, one might expect

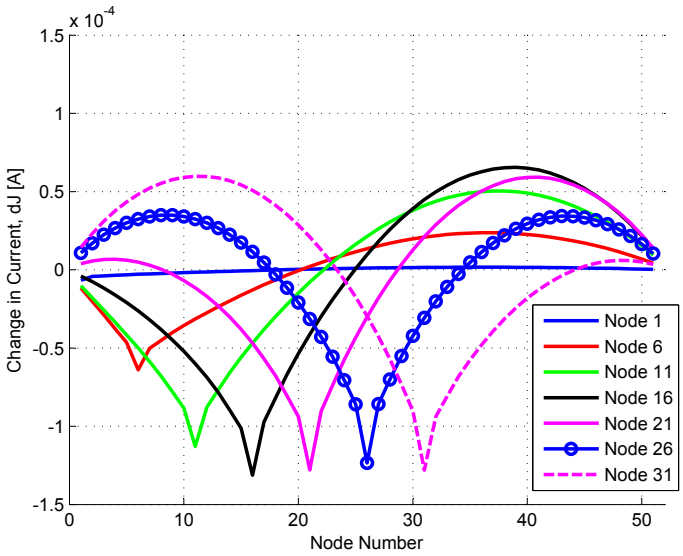

Figure 4.6: Change in mode 1 current considering contribution from all 51 calculated modes for a single load placed at different nodes along the dipole.

that the significant modes with respect to the total structure current will only be affected by other modes that have similar eigenvalues near resonance. If this was true, modes with large eigenvalues could once again be ignored as they are when considering the total current on the structure. However, Fig. 4.8 shows that modes having large eigenvalues that are insignificant to the total structure current can have a substantial impact on the current change of a small eigenvalue mode. The figure shows that when a load is placed at the center of the antenna, the fifth order mode having five half-sine variations has the most significant contribution to the current change. However, the fifth order mode also has the largest eigenvalue magnitude of all 51 modes. Therefore, this demonstrates that the relationship between a changing and contributing mode's current distribution is the most critical factor determining the mode's contribution to another mode's eigencurrent change. Large eigenvalue modes have low radiated power, which tends to compensate for the large eigenvalue difference in the denominator.

It is also interesting to note that the modes with large eigenvalues, which are insignificant to the total structure current, have the ability to experience the largest eigencurrent changes. Consider the eigencurrent contribution between two higher order modes that have small eigenvalue differences. The two factors in the denominator of Eqn. 4.3, the radiated power and the

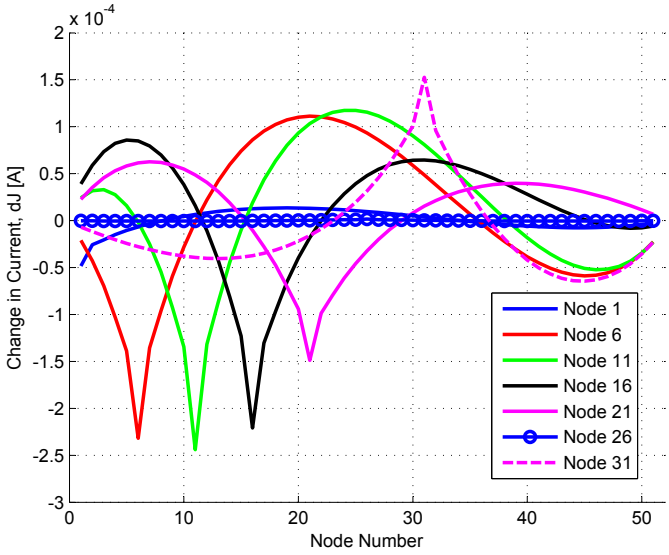

Figure 4.7: Change in mode 2 current considering contribution from all 51 calculated modes for a single load placed at different nodes along the dipole.

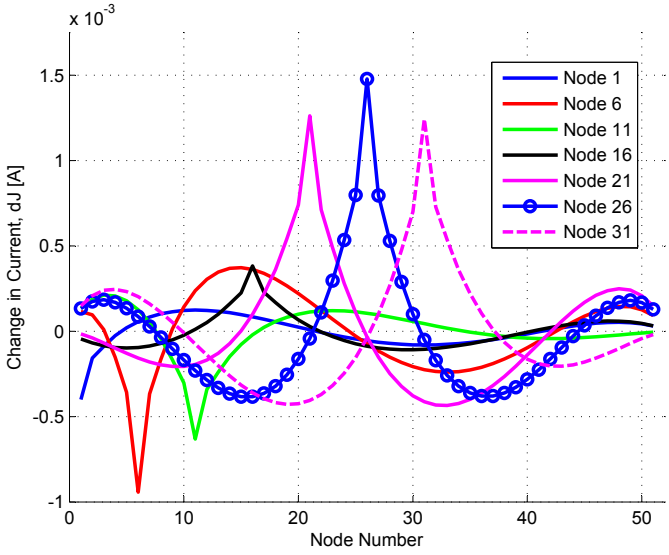

Figure 4.8: Change in mode 3 current considering contribution from all 51 calculated modes for a single load placed at different nodes along the dipole.

eigenvalue difference, are now both smaller, which results in a larger mode contribution and an overall larger eigencurrent change than that for a similar lower order mode case. This is consistent with the result described in Section 4.1 where the modes with larger eigenvalues experienced larger eigenvalue changes. This result is expected because the eigenvalues and eigencurrents are related and are not independent quantities.

Although the change in current tends to be dominated by the contribution of a few modes, the figures clearly show a sharp change in current around where the load is positioned. The sharp peak is formed from higher order mode contributions. In order to capture the more rapid variation in the current with respect to position on the dipole, higher order modes must be considered. Therefore, it is important to consider the contribution of all the modes in order to accurately predict all features of the change in mode current. An analogy to the Fourier decomposition of a pulse can provide a better understanding of this phenomenon. The rapidly varying edges of a pulse are captured by high frequency components of the Fourier decomposition just as the rapidly varying spatial changes in current are captured by the high order characteristic modes.

The dipole example demonstrates how insight from the eigencurrent perturbation equation can be used for reactive loading design. The example shows how certain mode contributions can be enhanced or suppressed through proper load positioning. If a reactive load is placed in a mode's eigencurrent null, no other modes can contribute to the mode's current change. As a result, no change in that particular eigencurrent results. However, if a change in the mode eigencurrent is desired, the load can be moved away from the eigencurrent's null position. The perturbation equation quantifies how certain contributions from other modes to the changing mode can be enhanced or suppressed through proper load placement. A contributing mode can be suppressed by placing the load in its null. That particular mode can no longer contribute to a change in any of the other modes. Therefore, a particular mode can be suppressed if it is producing an undesirable eigencurrent contribution to another mode. Furthermore, a mode contribution can be enhanced by trying to place the load in a position that maximizes the mode contribution coefficient numerator. Maximum contribution occurs when the load is placed in the current maxima of both the changing and contributing modes. Using the perturbation equations to guide antenna loading by work-

ing to enhance or suppress the contribution of various modes to other modes will form the foundation of a new loading design paradigm in later chapters.

4.3 Accuracy of the Perturbation Method

The perturbation equations were derived in Chapter 3 assuming an infinitesimal loading perturbation. Up to this point, however, the equations have been explored using a noninfinitesimal arbitrarily chosen load value of +j1 Ω. As a result, a comment on the accuracy of the equations with respect to different magnitudes of loading is warranted. An arbitrary load value is appropriate for obtaining design insight from the approach. Choosing a larger perturbation simply scales the contribution from each mode equally and does not alter the distribution of the eigencurrent change. Therefore, the insight gained from the perturbation equation does not depend on the applied load size. However, the size of the load perturbation is important when calculating the actual transformation of an eigencurrent. The equations are first order accurate. As a result, the accuracy will decrease for nonlinear changes in the eigenvalues and eigencurrents with respect to loading. Smaller loading steps must be chosen in order to achieve a desired accuracy. For large applied loads, however, the load values can always be arbitrarily broken down into smaller load increments that can be successively applied. The changes in eigenvalue and eigencurrent due to the first load increment can be calculated, and the new eigenvalue and eigencurrent values can be used for the next calculation. The portions of the load can be stepped through until the change due to the final total load value has been reached.

Fig. 4.9 provides experimental insight into the accuracy of the perturbation equations. To test the accuracy, the mode 1 and 2 eigencurrent changes for a +j1 Ω load placed at dipole node 6 were calculated using the perturbation method as previously shown in Figs. 4.6 and 4.7. The actual change in the mode currents were then determined using a full-wave characteristic mode simulation for the same load application. The figure shows the difference between the calculated and simulated change in eigencurrent for both mode 1 and 2. The results verify that the perturbation calculation is quite accurate for this situation. Therefore, the perturbation equations can be useful not only to elucidate the fundamental factors governing mode transformations

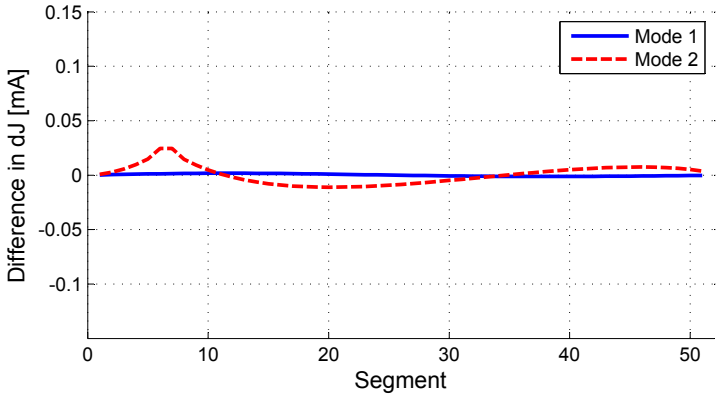

Figure 4.9: The difference between the simulated and calculated change in eigencurrent for a +j1 Ω load at node 6.

but for efficiently calculating the characteristic modes after reactive loading is applied or after frequency variations have occurred.

4.4 Discussion

The application of the characteristic mode perturbation equations to the dipole example reveals further insight concerning the factors governing characteristic mode transformations. Although the dipole is a simple example, the insight gained can be generalized to more complicated geometries where heuristic understanding is challenged. The examples show that the change in eigenvalue is related to the magnitude of the mode current at the location of the load. The results also show that modes with larger eigenvalues are more sensitive to loading since the eigenvalue change is inversely related to the power radiated by the mode. Large eigenvalue modes do not radiate as effectively so tend to be more sensitive to loading.

The relationship of the eigenvalue sensitivity to the power radiated has similarities to the modal quality factor Q mentioned by Harrington [20]. Modal Q gives a measure of the frequency sensitivity of a mode current and is defined as

$$Q = \omega \frac{[\tilde{I}^*][X'][I]}{[\tilde{I}^*][R][I]} \approx \omega \frac{\partial \lambda}{\partial \omega}, \tag{4.5}$$

where I is the mode current, $[X]$ is the reactance matrix, and $X' = \frac{dX}{d\omega}$. When the perturbation method is applied with a perturbed reactance ma-

trix due to frequency variation, the derived result is the modal Q divided by the radian frequency. The mode Q is large when the reactance matrix perturbation interacts with the largest eigencurrent magnitude and when the power radiated by the mode is smallest. In this case the energy stored by the mode is large and the radiation loss is small. As a result, the Q is large and the frequency sensitivity of the mode is high.

When a load perturbation is considered, however, the frequency is held constant and the change in the eigenmode properties with respect to a loading perturbation is now determined. When the load is placed in a current maxima, the energy stored by the loaded mode is maximized which leads to a more sensitive eigenvalue. Furthermore, modes with large eigenvalues radiate poorly and so have low radiation loss, which also contributes to a more sensitive eigenvalue. Due to these factors, the mode eigenvalue and eigencurrent will be very sensitive to a change in the load value.

The relationship to modal Q is useful in understanding the change in eigenvalue. A simple modal Q quantity, however, provides little insight into the factors governing eigencurrent changes and the interaction with the other modes. The perturbation method provides an avenue to derive a quantitative relationship describing the contribution of each mode to a particular mode's eigencurrent change. The perturbation method reveals that the change in a mode's eigencurrent can be viewed as having a contribution from each of the other modes. The modes are interacting with each other via the reactive load. The placement of the load simply determines the degree of interaction. Of course, other factors such as the power radiated by the mode and the difference in eigenvalues further scale the contribution of each mode. This relationship established through the application of perturbation theory has not been established in the characteristic mode literature. By understanding these relationships, designers will be able to design load placement schemes much more systematically.

In many ways the perturbation equations reveal a parallel between reactive loading and source excitations. After all, a reactive load can often be viewed as a dependent source in the method of moments. Therefore, when a reactive load is placed on the antenna, the change in the eigencurrents can be viewed as the eigencurrents that a source at the load position would excite. When viewed from this perspective, the characteristic mode perturbation approach shares similarities with the compensation theorem used in network analy-

sis and boundary value electromagnetic problems. Looking at eigencurrent changes from the compensation theorem approach provides useful insight and an alternative view to better understand the meaning of the perturbation expressions. Appendix A for the first time applies the compensation theorem to the characteristic mode problem and establishes its relationship with the characteristic mode perturbation approach. Useful insight can be gained by viewing the eigencurrent changes from the compensation theorem perspective.

The characteristic mode perturbation equations reveal that eigencurrent contributions can be enhanced or suppressed through careful load placement. This insight suggests a new design paradigm in which loading is used to obtain desirable contributions or suppress undesirable contributions to other modes. In the later chapters, we will show how the new design approach can guide antenna loading in a systematic fashion in order to achieve desirable antenna performance.

CHAPTER 5

SPIRAL ANTENNA LOADING DESIGN USING THE PERTURBATION APPROACH

The characteristic mode perturbation approach offers direct insight for the antenna loading design problem. Characteristic mode theory has historically been most useful as an analysis tool. Design insight is typically gained by working extensively with the modes and developing a heuristic understanding of how they behave. In this chapter, a novel antenna design paradigm is explored based on the new characteristic mode perturbation equations. The perturbation equations suggest that the properties of unexcitable yet highly desirable modes can be realized by using loading to obtain a contribution of the unexcited modes to those that are significant and excitable. In this chapter, the approach is specifically applied to the design of spiral antenna loading in order to synthesize a desirable antenna pattern at a target frequency. Insight from the equations is used to guide the spiral loading design process and to reveal a useful loading scheme. The design example is intended to demonstrate the new design methodology and will not address the practical issues associated with implementing a practical antenna design.

The wire spiral topology is a logical progression from the previous dipole example in Chapter 4. Because both antennas are wire, the mechanics of applying the perturbation equations to the spiral are identical to that of the dipole. However, the spiral has much more complex electromagnetic behavior and serves to better reveal the benefits of the new systematic perturbation loading design approach. Although the spiral is often selected because of its broadband properties, here we focus on applying the new approach at a single frequency. Because eigencurrents in general tend to vary slowly over frequency, in many cases the narrowband design approach can provide useful insight that holds true over a wider bandwidth.

5.1 Introduction

Spiral antennas exhibit consistent input impedance and radiation properties over very wide frequency ranges. The broadband nature of the topology along with its inherent circularly polarized radiation pattern has made it a desirable choice for various direction finding and electronic intelligence applications. The first broadband spiral antenna was developed by Edwin Turner at the Wright Air Development Center in 1955 [24]. As a result of the widespread uses for the antenna, significant research was performed to better understand the operation of these structures and to better control their electrical properties.

In order to understand spiral antenna operation and to provide an analytical framework for the design of these structures, significant mathematical analysis and modeling of these antennas was performed. A mathematical description of antenna frequency independence was proposed by Rumsey [25]. Furthermore, a specific mode theory for equiangular infinite arm antennas was developed by Cheo, Rumsey, and Welch [26]. The mode theory was then explored experimentally for finite arm antennas by Sivan-Sussman [27]. Although insightful, current analytical models are extremely limited for practical spiral design applications. Their significant complexity along with the many necessary practical approximations significantly limits their use for practical spiral design problems.

The Archimedean spiral, an alternative to the equiangular spiral and the topology used in this work, is a class of spiral antenna in which the expansion of the spiral is linear with respect to the angle. Early investigation of the Archimedean spiral was performed by Kaiser [28] and later by Bawer and Wolfe [29]. The operation of these antennas is often described by the band theory in which the radiation from the structure occurs from the antenna arms when they are approximately one wavelength in circumference. When the arms are near one wavelength in circumference, the currents on neighboring arms are in phase leading to an active region in which strong radiation occurs. Inside the active region the currents on neighboring arms are out of phase forming a transmission line mode that does not radiate effectively.

Variations on the Archimedean design have been proposed in the open literature. Filipovic developed a cavity backed Archimedean slot spiral antenna for dual-band operation [30]. Furthermore, lumped reactive loading schemes

have been investigated to reduce spiral size while maintaining low frequency performance [31, 32]. Modern research initiatives are working to add additional capability to spiral antennas beyond the broadband impedance behavior and circularly polarized radiation properties. For instance, investigations focusing on adding pattern and frequency reconfiguration capabilities to spiral antenna designs are becoming more prevalent. Recent work by Gong et al. has explored using microelectromechanical systems (MEMS) switches to obtain pattern reconfigurability from an Archimedean spiral [33]. Mookiah et al. have also proposed spiral pattern reconfiguration using PIN diodes [34]. A frequency reconfigurable design using PIN diodes has also been proposed [35].

As spiral requirements increase beyond wideband performance, better spiral design methodology is becoming essential. In this chapter, the characteristic mode perturbation approach is applied to the Archimedean spiral antenna topology to provide insight and a guided design approach for advanced antenna performance. The perturbation approach is based on full-wave characteristic mode analysis, so unlike most analytical spiral models, it does not rely on geometry approximations when designing practical spiral antennas. The method provides insight needed to systematically load the spiral in order to obtain a desirable radiation pattern at a target frequency of 3 GHz.

5.2 Using the Perturbation Approach for Design

The characteristic mode perturbation equations offer a new approach to design antenna loading schemes to achieve desirable antenna electrical performance. As introduced in Chapter 2, the eigencurrent perturbation equation is given as

$$dJ_i = \sum_{j=1}^{N} dJ_{i,j} = \sum_{j=1}^{N} \frac{\langle dX_L J_i, J_j \rangle}{\langle RJ_j, J_j \rangle (\lambda_i - \lambda_j)} J_j \quad i \neq j, \tag{5.1}$$

where dJ_i is the total change in mode eigencurrent i and $dJ_{i,j}$ is the particular contribution of eigencurrent j to the change in eigencurrent i. The modified mode i eigencurrent following a load perturbation is then the sum of the

original unloaded mode eigencurrent and the eigencurrent change

$$J_{i,loaded} = J_i + \sum_{j=1}^{N} dJ_{i,j}. \tag{5.2}$$

The expressions suggest that the change in a particular eigencurrent due to a load perturbation has a contribution from each of the other modes. Therefore, the expressions reveal a new design paradigm in which the designer thinks in terms of using loading to enhance or suppress mode contributions. Through the proper choice of load type and placement, the properties of desirable modes that are not originally significant or excited by the feed can be made to contribute to an excited significant mode on the antenna. As a result, the properties of the desirable contributing modes eventually manifest themselves in the excitable modes, which allows desirable higher order mode properties to be realized. Furthermore, contributions from higher order modes can be used to modify the current at the feed position to control the input impedance and resulting VSWR. The characteristic mode perturbation equations describe where to place the loads and the type of loads needed to obtain these desired mode contributions. The perturbation expressions, for the first time, quantify characteristic mode contributions and provide insight into how the contributions can be controlled.

5.3 Spiral Design using the Perturbation Approach

The perturbation approach is a general method based on characteristic modes that can be applied to any antenna topology. In this section, we investigate the application of the method to the loading of an Archimedean spiral antenna. The spiral antenna is an interesting case study. Although the mechanics of applying the method share many similarities with the previous dipole examples, the spiral is much more complex electromagnetically. Traditionally the complex interaction of the spiral arms makes it difficult to determine loading positions to achieve a target performance goal without heavily relying on trial-and-error techniques. In this section, the perturbation approach design process is applied to systematically guide the reactive loading necessary to transform a spiral's pattern from broadside to endfire. First, an

Archimedean spiral antenna geometry that provides the foundation for loading is presented. The unloaded characteristic modes are examined and then the perturbation approach is used to investigate how loading transforms the characteristic modes. The approach is then used to design a reactive loading scheme that achieves an endfire radiation pattern while maintaining desirable input impedance properties.

5.3.1 Spiral Geometry

An arm of an Archimedean spiral antenna is described by the equation

$$r = a\theta + r_o, \tag{5.3}$$

where r is the arm radius, a is the growth rate, θ is the angle, and r_o is the radius when $\theta = 0$. An additional arm is governed by the same equation with an offset angle. A two-arm, two-turn Archimedean spiral antenna was designed to provide a foundation for reactive loading. The spiral was designed to achieve a 3 GHz active region after one turn of the spiral. To accomplish this specification, the spiral parameters were chosen as $a = 2.38$ mm and $r_o = 1$ mm. Using these parameters, the spiral radius after one turn would form a circle with one wavelength circumference at 3 GHz, approximately forming an active region at this frequency. The spiral was meshed using 1 mm segments, which results in 100 segments per wavelength at 3 GHz. The wire radius was chosen as 0.1 mm in order to approximate a current filament and to provide an acceptable length to radius ratio for the relatively short 1 mm mesh segment length. Characteristic mode analysis requires a finer mesh than total current solutions in order to adequately resolve the higher order mode eigencurrents. The two-turn spiral design is shown in Fig. 5.1. The spiral radiates a broadside pattern at 3 GHz when excited in the center at node 217.

5.3.2 Spiral Characteristic Modes

The first step in applying the perturbation approach for antenna loading design is to find the characteristic modes of the underlying antenna structure. These modes form a foundation on which to apply the new loading design

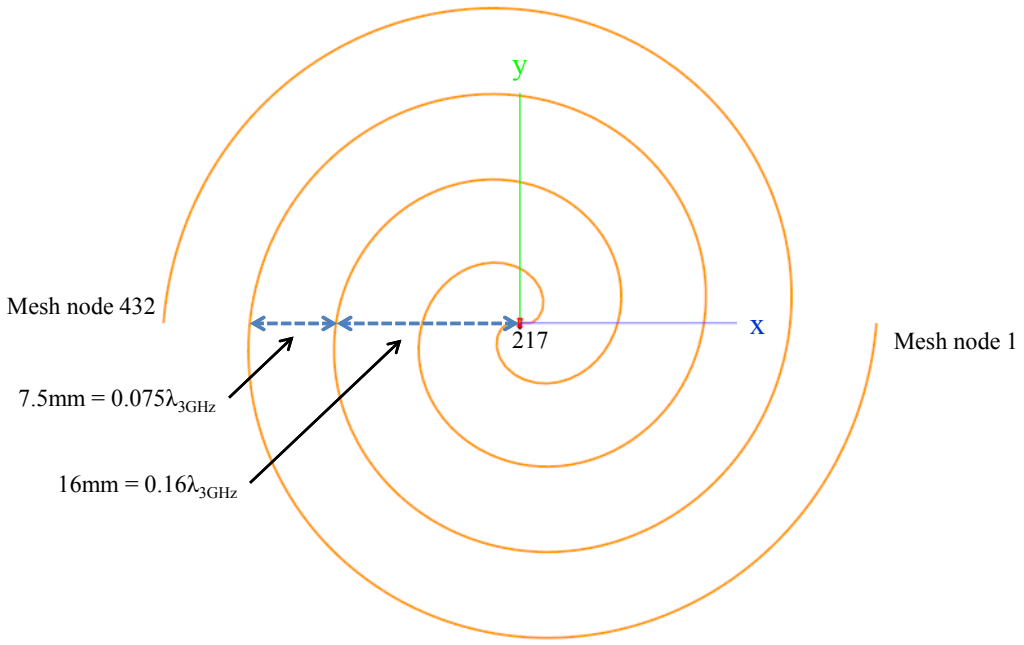

Figure 5.1: Archimedean spiral geometry with two turns.

approach. The characteristic modes of the spiral are found by solving the generalized eigenvalue problem given by Eqn. 2.12. Characteristic modes are feed independent, so a feed location is not specified for the solution of the modes. The modes presented here are found by solving the characteristic mode eigenvalue problem and are different than the modes often referred to in spiral antenna literature [27, 36]. The first six eigencurrents of the unloaded perfect electrically conducting wire spiral at 3 GHz are illustrated in Fig. 5.2 and the corresponding eigenvalues are given in Table 5.1. The figure shows the eigencurrents along the spiral corresponding to each mesh node. Because the mesh segments are equally spaced and the nodes are numbered consecutively, the plots can be interpreted as the eigencurrent along the spiral wire. Node 217 corresponding to the center of the spiral is indicated by a black circle along the graph's abscissa. Additionally, colored triangles are present along the plot axis to indicate each 90 degree progression of the wire. The positions of the triangles on the spiral geometry are shown below the eigencurrent plot for reference. The triangles point in the direction of the side of the spiral they are located on. For instance, a green upward pointing triangle appears every time the geometry wire passes through the positive y-axis. The triangles allow the plotted current values to be related to their

Table 5.1: Eigenvalues of the first six modes at 3 GHz.

Mode Number	Eigenvalue
1	0.66457
2	0.78522
3	-2.57716
4	4.55718
5	-8.23537
6	16.82017

physical position on the spiral geometry.

The eigencurrents exhibit quasi-sinusoidal behavior along the spiral. The modes can be classified based on their symmetry. The current distributions with even symmetry about the spiral center are plotted in blue in Fig. 5.2 and will be referred to as even modes. The other distributions with odd symmetry about the spiral center are plotted in red and will be referred to as odd modes. The electric field magnitudes for the eigenpattern distributions of the first six modes are shown in Fig. 5.3. Modes 1 and 3 are even modes that exhibit a broadside pattern. Modes 2 and 4 are odd modes that have an endfire pattern.

Fig. 5.4 gives the time averaged power radiated by the first 25 characteristic modes when the spiral is center fed (node 217) using a one volt delta-gap feed model. When the spiral is center fed, the even modes are not excited because they have no current present at the center feed location. Instead, the radiation from the spiral is dominated by modes 1 and 3 which radiate comparable power. Some power is radiated by mode 6, but it is significantly less than the power radiated by the two lower order even modes. Since modes 1, 3, and 6 each have a broadside pattern, the total pattern of the center fed excited antenna also has a broadside pattern at 3 GHz when the modes combine.

Although only a few modes radiate power when center fed, some higher order modes have current magnitudes on the same order of magnitude as the lower order modes that radiate most of the power. Fig. 5.4 also shows the eigencurrent magnitude of the first 25 modes at the center feed location. Although only modes 1, 3, and 6 radiate significant power, many other higher order modes have significant excited current magnitudes on the antenna structure. These are reactive modes that store net energy but do not

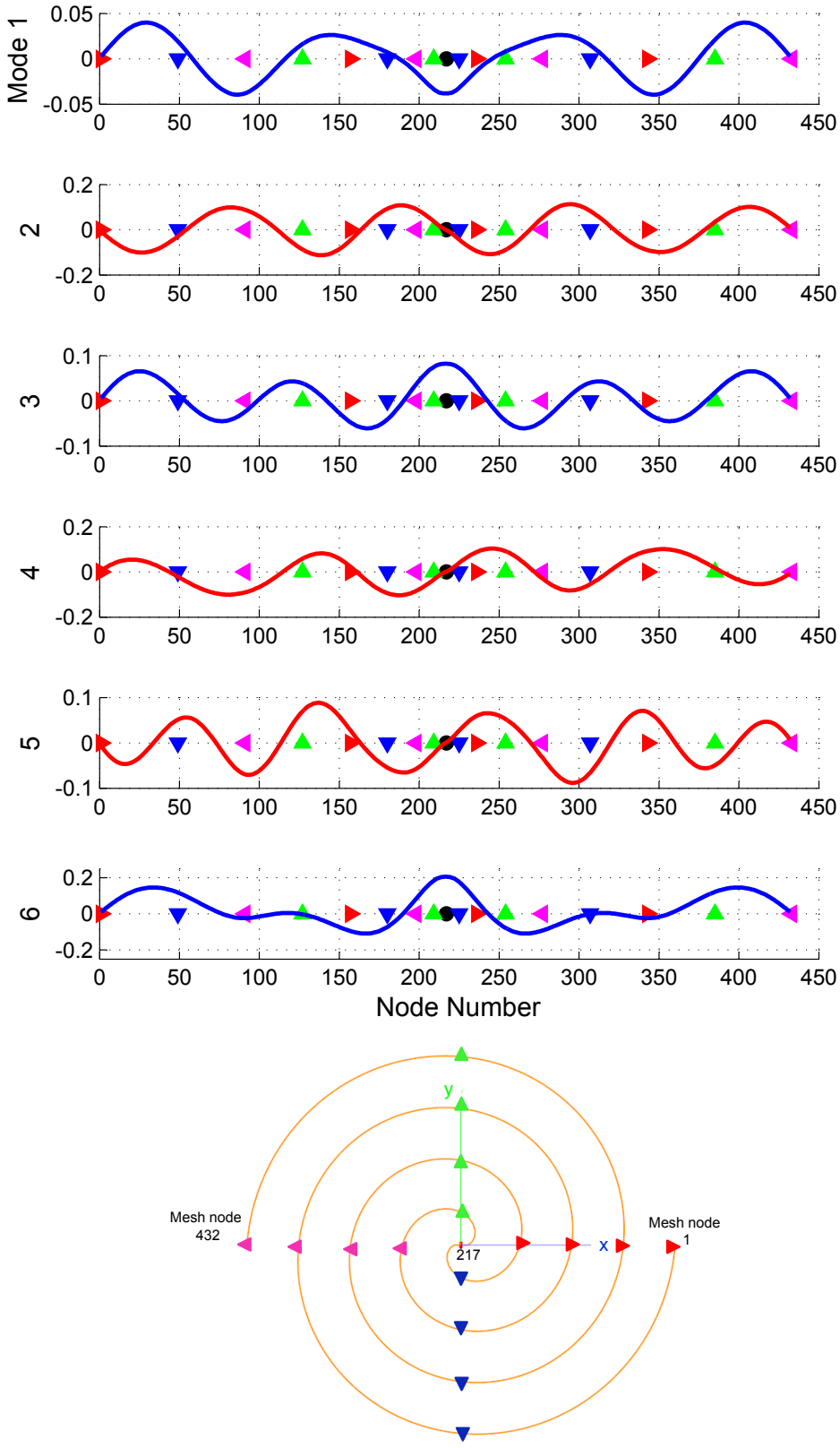

Figure 5.2: Eigencurrents of the unloaded two-turn spiral at 3 GHz.

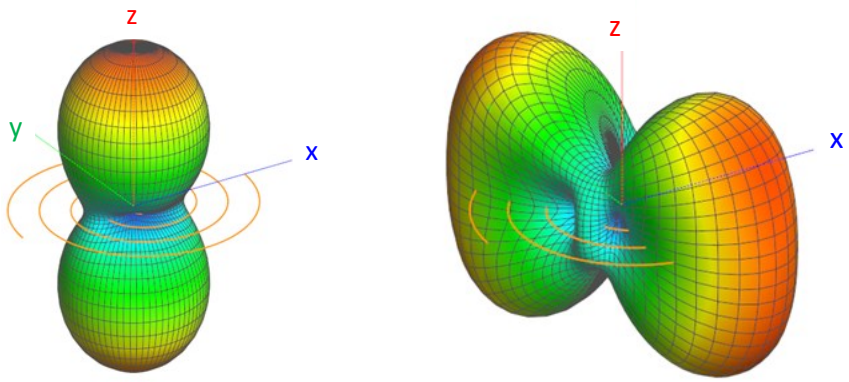

(a) Mode 1

(b) Mode 2

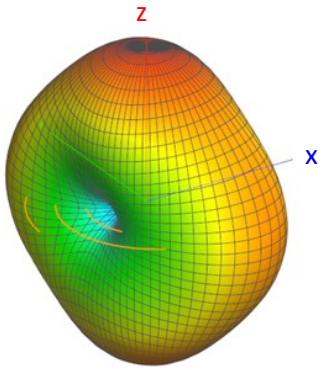

(c) Mode 3

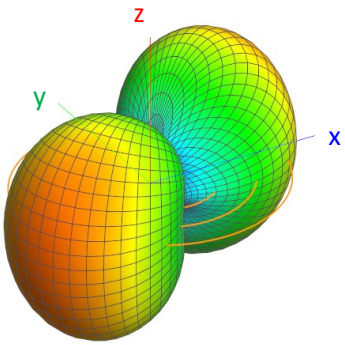

(d) Mode 4

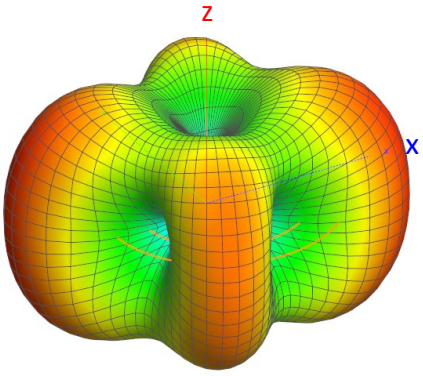

(e) Mode 5

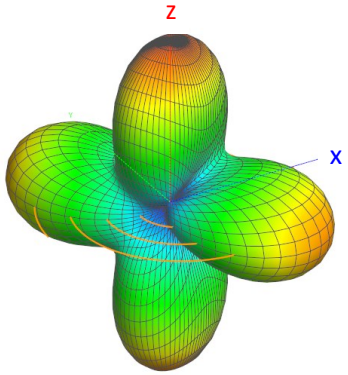

(f) Mode 6

Figure 5.3: Total electric field eigenpatterns of the unloaded two-turn spiral at 3 GHz. E-Field magnitudes range from blue to red, 0 to (a) 11.25 V (b) 10 V (c) 8 V (d) 10 V (e) 8 V and (f) 11.25 V.

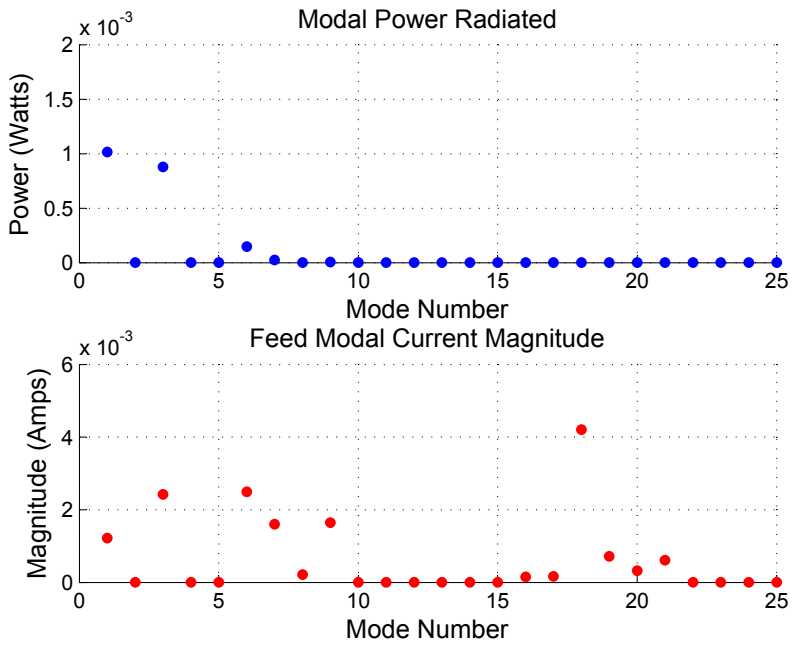

Figure 5.4: Time average power radiated by the first 25 characteristic modes, and the mode eigencurrent magnitudes at the feed (node 217) for the center fed unloaded, two-turn spiral.

radiate effectively. The high current modes are important contributors to the input impedance of the antenna. Fig. 5.5 gives the real and imaginary input impedance values for the center fed unloaded spiral as the contribution from each additional mode is added to the antenna impedance. We can see that although the low order radiating modes are most significant to the impedance, other higher order modes also modify the input impedance considerably. For the unloaded spiral, about 21 modes must be included before the input impedance is accurate.

5.3.3 Endfire Radiation Pattern Goal

For many applications, a broadside pattern is desirable from a spiral antenna. However, in many contested environments the ability to alter the radiation pattern of the antenna is very useful. Reception of a desirable signal may be maintained in a hostile environment by placing a null in the direction of an interfering source or by tilting the mainbeam off broadside. The ability to reconfigure between a broadside and endfire antenna pattern can provide

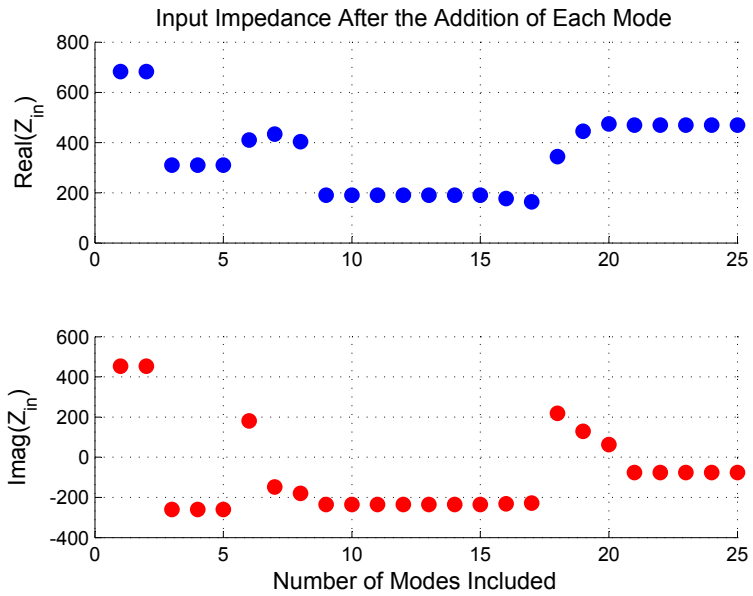

Figure 5.5: Input impedance of the center fed (node 217) unloaded spiral at 3 GHz as each additional mode is included in the impedance value.

signficant system performance improvement in many current and future environments.

Designing a reactive loading scheme to obtain a particular desirable radiation pattern is a challenging problem. Current spiral antenna models that accurately take into account the complex interaction of the spiral arms are limited leading to cut-and-try design approaches. The characteristic mode perturbation approach provides a new framework for a systematic reactive loading design method for spiral antennas that can achieve a particular desirable radiation pattern. To demonstrate the application of the perturbation equations, the expressions will be used to provide the insight necessary to systematically load the spiral to change the unloaded broadside pattern into an endfire radiation pattern.

The center fed unloaded spiral produces a broadside radiation pattern. However, consider the case where an endfire pattern is desired from the same center fed spiral geometry. After considering the characteristic mode radiation patterns given in Fig. 5.3, a mode 2 endfire pattern would be desirable. Using a single center feed, the mode 2 pattern along with other odd modes is not excited because the odd mode eigencurrents have a null at the feed location. Although the feed could potentially be moved away from the cen-

ter or an additional feed introduced, the cost and complexity of the design would increase and the balanced nature of the spiral would be altered. Additionally, when using only a single feed, mode 2 is difficult to excite without even mode contamination. The use of reactive loading to obtain an endfire pattern is more advantageous. Reactive loading is usually more cost effective than introducing an additional feed and provides many opportunities for reconfigurability using electrically controlled components such a varactor diodes.

5.3.4 Choosing Load Positions

Although the odd modes cannot be excited directly using a center feed, the perturbation expressions suggest that the even mode behavior can be excited as part of an excitable odd mode. For instance, reactive loading can be placed to obtain a strong contribution from mode 2 to excitable modes 1 and 3. Consider mode 1 after a small load perturbation is placed on the antenna structure. As shown by Eqns. 5.1 and 5.2, the perturbation expression indicates that the new loaded mode 1 eigencurrent will be a composite current composed of the particular unloaded mode current J_1 plus the summation of the contributions from the other modes scaled by the magnitude of their individual mode contribution coefficients. The magnitude of the mode contribution coefficient for a particular mode depends on the factors described in Section 3.5. A factor controllable by the designer is the position of the load with respect to both the changing and contributing modes. In the present design example, the significant changing modes to consider are modes 1 and 3 and the desirable contributing mode is mode 2. Therefore, the load should be placed on the structure in a position that maximizes the mode 2 contribution to modes 1 and 3.

The load position that creates a maximum contribution from contributing mode 2 to changing modes 1 and 3 is then considered. The load position for maximum mode 2 contribution can be determined by considering the numerator of the mode 2 to mode i contribution coefficient from Eqn. 5.1 for every possible load position. Because the denominator of the mode contribution coefficient is constant with respect to load position, only the numerator of the mode contribution coefficient must be considered. Furthermore, since the

load perturbation magnitude will be kept the same for each load position, only the product of the changing and contributing eigencurrent magnitudes must be considered as a metric for determining the best load position. The position with the largest eigencurrent product is the best position to obtain the largest mode contribution to the particular changing mode for a given small load perturbation.

Because the test for maximum contribution for each potential load location is simply a vector multiplication, the computation is inexpensive compared to the large matrix inversion required in conventional full-wave parametric simulations. Therefore, the load position for maximum contribution can be computationally determined quickly by simply analyzing each possible load position. However, because the maximum mode contribution occurs when the product of the eigencurrent magnitudes of the changing and contributing modes at the load location is largest, a close estimate of the best load position can be obtained simply through visual inspection of the eigencurrents. Fig. 5.6 gives the calculated multiplication of mode eigencurrent 2 with both modes 1 and 3 at each position along the spiral. We will first choose nodes 203 and 230 for the load positions. These are the contribution local maxima closest to the spiral center. The use of the contribution global maxima positions near the spiral ends will be considered in a later section.

Although the largest contribution of a contributing mode occurs when the load is positioned on the spiral where the changing and contributing mode eigencurrent product is maximized, this highest contribution position is only guaranteed for a small load perturbation. The eigencurrent distributions will change as loading is applied. Therefore, it may be necessary to modify the position of the next load perturbation as the antenna loading increases and the best load application positions continue to change. The change in the eigencurrents can be accounted for by continually reexamining the mode properties and considering the best load position after each load perturbation is applied.

Although the load application position can be continually modified as further perturbations are considered, the design process can be simplified as needed by trading off design accuracy for design process simplicity. For instance, the design example described here will be initially limited to only a single load on each spiral arm. Although the loading limitations will not always allow the largest desirable mode contributions, limiting the number

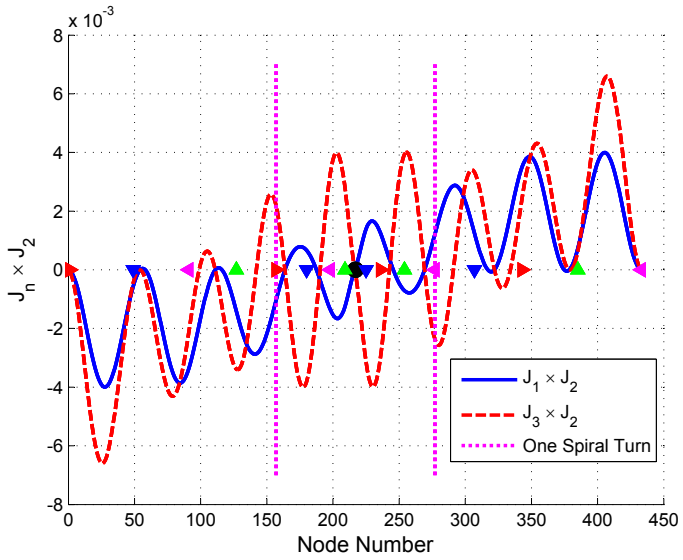

Figure 5.6: Eigencurrent interaction metric for maximizing the mode 2 contribution to modes 1 and 3.

of loads is the most cost effective and practical for implementation which makes it a desirable scenario to consider. Furthermore, this case will be considered first to best demonstrate the insight obtainable from the perturbation expressions. The example will show how a basic application of the perturbation expressions can guide a design to achieve desirable antenna performance and provide insight into the performance limitations inherent in a particular antenna geometry.

5.3.5 Choosing Load Types

In order to achieve desirable antenna functionality, we would like to obtain contributions from certain unexcitable modes with desirable properties to the significant excitable modes. If loading is applied correctly, a desirable property of an unexcitable mode may eventually manifest itself in the excitable modes providing the necessary antenna functionality. As seen in the dipole investigation in Section 4.2, load position is one variable that can be used to enhance or suppress the contribution of certain modes. However, a challenge becomes immediately apparent when one tries to obtain a particular desirable mode contribution using load position alone. A contribution from a particular desirable mode is often impossible to achieve without also ob-

taining a contribution from other undesired modes. Certain unwanted mode contributions can overwhelm the desirable contribution leading to the realization of an undesired current distribution. To help overcome this problem, additional insight from the perturbation expressions reveals techniques that rely on multiple loads and different load types to help enhance or suppress the contributions from various modes. Here we consider a technique developed to obtain the desired endfire spiral radiation pattern.

The contributions of each particular mode to the changing mode will be analyzed in terms of the mode radiated power contribution. The mode radiated power contribution is the power radiated by the eigencurrent contribution to another mode. Analyzing the power contribution from each mode gives the best indication of each mode's contribution to the change in another mode's far field pattern. A large magnitude eigencurrent contribution does not necessarily imply a large real radiated power contribution. Therefore, analyzing the radiated power contributed by each mode provides a better indication of the effect of the particular eigencurrent contribution on the far field pattern than analyzing the eigencurrent contribution coefficient. Appendix B provides quantitative derivations detailing the effects of the mode radiated power contributions on a particular mode.

Consider the case when two inductive +j1 Ω load perturbations are placed on the spiral at nodes 203 and 230. As seen from Fig. 5.6, the load positions correspond to the first mode 2 to mode 1 contribution maxima from the spiral center. Fig. 5.7 shows the radiated power contribution to the first three modes from the first 25 modes. Even though only a mode 2 contribution to mode 1 is desired, contributions from modes 3 and 6 are present that dominate the total contribution. As a result, loading in this fashion will maintain the broadside radiation pattern. Now consider the case when a +j1 Ω inductive load and a −j1 Ω capacitive load are placed at nodes 203 and 230, respectively. Fig. 5.8 shows the radiated power contribution to the first three modes for this loading combination. Only a strong mode 2 to mode 1 contribution is now present.

To understand what is happening, consider the load positions with respect to the first three eigencurrent distributions as shown in Fig. 5.9. The eigencurrent perturbation equation quantitatively describes how each eigencurrent contributes to a particular changing eigencurrent. The numerator

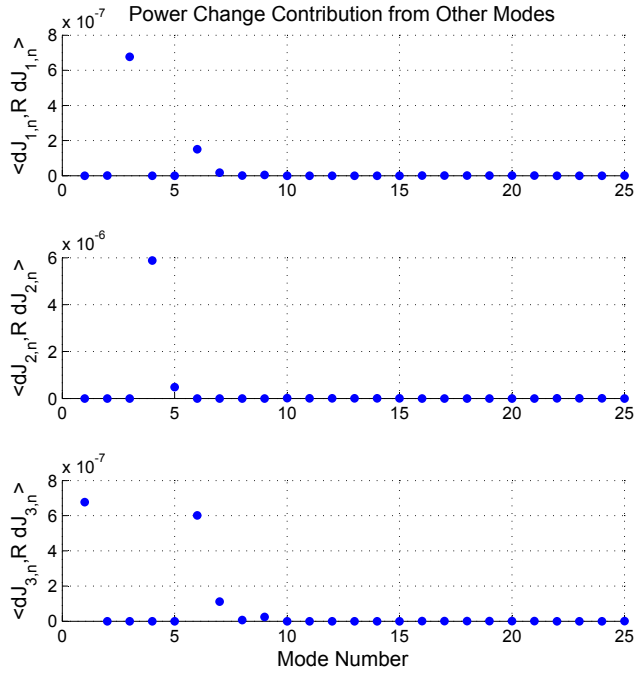

Figure 5.7: The radiated power contribution to the first three modes when two +j1 loads are placed on the spiral at nodes 203 and 230.

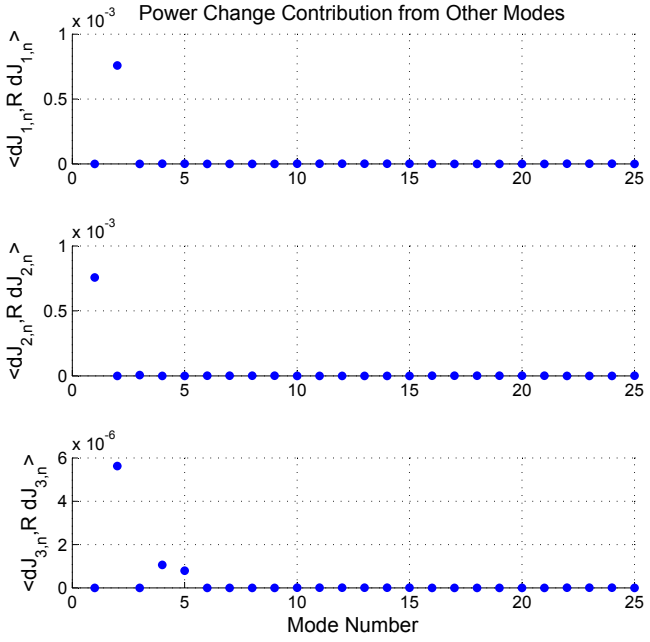

Figure 5.8: The radiated power contribution to the first three modes when +j1 and −j1 loads are applied at spiral nodes 203 and 230, respectively.

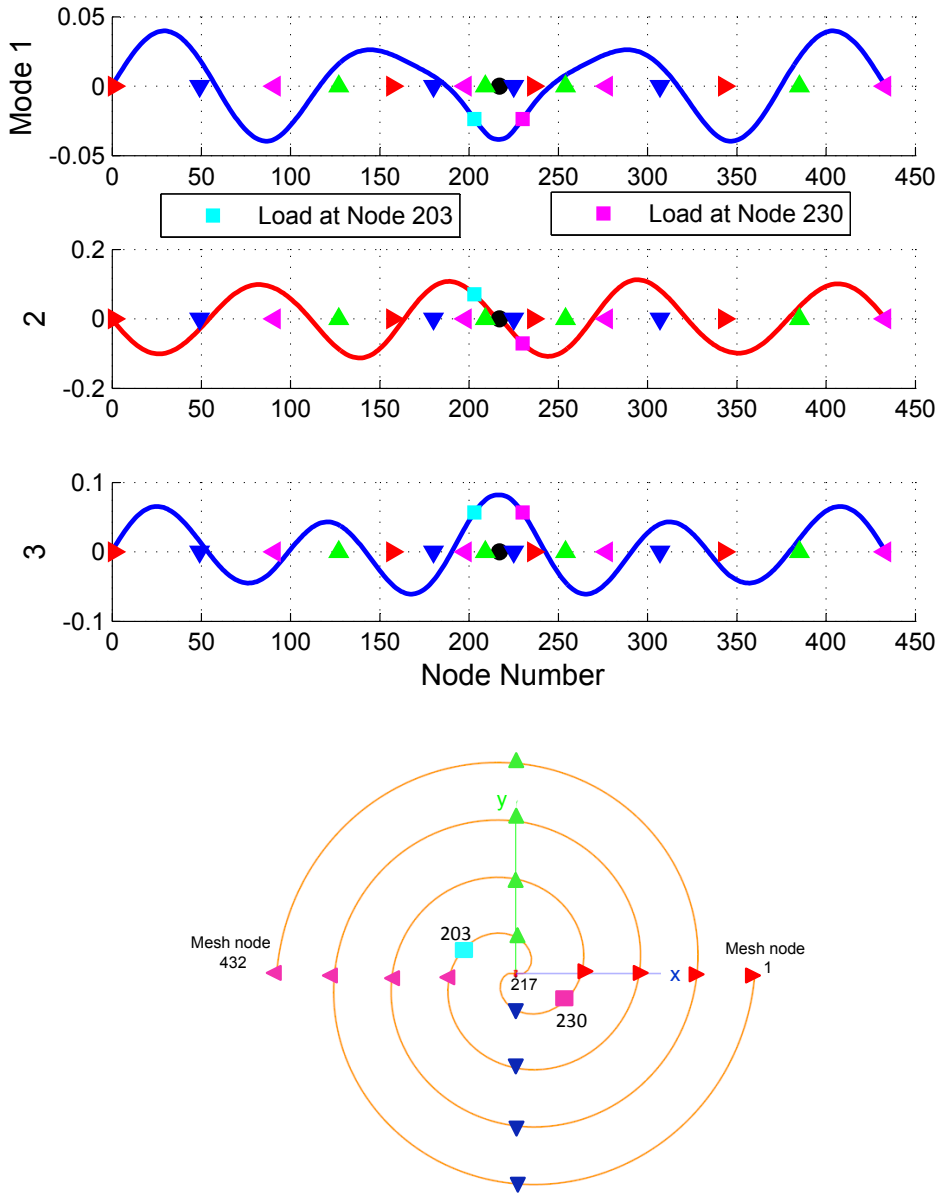

Figure 5.9: Load positions with respect to the first three unloaded modes at 3 GHz.

inner product of the mode contribution coefficient is expanded as

$$\langle dX_L J_i, J_j \rangle = X_L^{203} J_i^{203} J_j^{203} + X_L^{230} J_i^{230} J_j^{230}, \tag{5.4}$$

where the subscript indicates the eigencurrent mode number and the superscript indicates the node at which the eigencurrent value is considered. If two small inductive loads of the same value are placed symmetrically on the antenna, the expanded numerator inner product of the mode contribution coefficient becomes

$$\langle dX_L J_1, J_2 \rangle = (+|X_L^{203}|)(-|J_1^{203}|)(+|J_2^{203}|) + (+|X_L^{230}|)(-|J_1^{230}|)(-|J_2^{230}|) = 0 \tag{5.5}$$

for the contribution of mode 2 to mode 1 and

$$\langle dX_L J_1, J_3 \rangle = (+|X_L^{203}|)(-|J_1^{203}|)(+|J_3^{203}|) + (+|X_L^{230}|)(-|J_1^{230}|)(+|J_3^{230}|) \neq 0 \tag{5.6}$$

for the contribution of mode 3 to mode 1. The inner product expands into two terms each corresponding to a different load. Although the magnitude of the mode 2 eigencurrent is the same on both sides of the spiral, mode 2 is an odd mode resulting in out-of-phase currents at the load positions. The mode 1 eigencurrent, however, is even and so has the same magnitude and phase on both spiral arms. When two inductive loads are used, the resulting reactances have the same sign. Therefore, the numerator of the mode 2 to 1 contribution coefficient evaluates to zero resulting in no mode 2 contribution. Instead, the mode 3 to 1 numerator inner product is nonzero resulting in a large contribution from mode 3. The mode 3 contribution occurs because mode 3 is also an even mode like mode 1.

Alternatively, further inspection of the mode contribution coefficient numerator shows that the mode 2 contribution can be enhanced while suppressing the mode 3 contribution by using opposite sign reactances on opposing spiral arms. Using inductor and capacitor loading cancels the mode 3 contribution allowing the desirable mode 2 to 1 contribution to dominate as seen by expansions

$$\langle dX_L J_1, J_2 \rangle = (+|X_L^{203}|)(-|J_1^{203}|)(+|J_2^{203}|) + (-|X_L^{230}|)(-|J_1^{230}|)(-|J_2^{230}|) \neq 0 \tag{5.7}$$

and

$$\langle dX_L J_1, J_3 \rangle = (+|X_L^{203}|)(-|J_1^{203}|)(+|J_3^{203}|)+(-|X_L^{230}|)(-|J_1^{230}|)(+|J_3^{230}|) = 0. \tag{5.8}$$

The eigencurrent perturbation expression provides the loading insight needed to obtain the desirable endfire pattern. It suggests that different load types, inductors and capacitors, should be used at nodes 203 and 230 to obtain the desired mode 2 endfire pattern contributions to modes 1 and 3. The perturbation expressions show that inductor/capacitor loading results in odd to even mode contributions while suppressing the even to even mode contributions. This is seen by the mode power contribution plot for the inductor/capacitor loading at nodes 203 and 230 given in Fig. 5.8. Furthermore, loading of the same type produces even to even mode contributions while suppressing odd to even mode contributions.

The eigencurrents do not always possess even or odd mode symmetry about the spiral center, however. For instance, an inductor/capacitor loading perturbation will soon upset the eigencurrent symmetry to some extent as the load magnitudes are increased. Insight from the perturbation expression can still be employed if the eigencurrent magnitudes are not symmetric about the spiral center. However, now the positions of each load perturbation should be manipulated to select the mode eigencurrent magnitudes needed to obtain perfect numerator cancellation from undesirable modes. In general, even when the eigencurrents become unsymmetric, opposite loading will still tend to enhance or suppress the altered odd or even modes even though exact cancellation of the undesired modes is not occurring. The perturbation equations provide a quantitative guide to not only choose the load position but to also choose the type of loads necessary to obtain the mode contributions needed to realize desirable antenna performance.

5.4 Mode Transformation as Loading Increases

The perturbation equations were derived to provide design insight for antenna loading problems. As seen in previous sections, the equations provide insight into the best load location and load type to realize a desirable antenna functionality. The perturbation equations describe how the characteristic mode

eigenvalues and eigencurrents change for small reactive load perturbations. However, in order to realize useful antenna functionality, larger loads must typically be used that can no longer be accurately considered perturbations. The perturbation approach is very applicable to these larger magnitude loading design problems as well. In the spiral antenna example, the perturbation expressions provide insight for placing inductor and capacitor loading at nodes 203 and 230 to realize an endfire radiation pattern. The initial load locations and types were chosen to obtain a strong mode 2 contribution to the excitable modes 1 and 3. Although a small load perturbation will produce a mode 2 contribution to modes 1 and 3, the resulting composite eigencurrent will still be dominated by the unloaded mode 1 and 3 current distributions. In order to get the mode 2 current contributions to dominate, the loading magnitude must be increased beyond small perturbations. In this section, the perturbation equations will be used to investigate how the eigencurrents transform as loading is increased. The analysis shows how some simple perturbation insight from the initial unloaded antenna problem results in a desirable design even as the loading magnitudes are increased.

In order to realize useful antenna functionality, larger reactances that do not satisfy the small perturbation requirement must often be applied to the antenna. Methods must be developed to allow the perturbation approach to handle the larger reactance values in the design process. Two approaches can be taken to investigate the application of large magnitude loads using the characteristic mode perturbation approach. First, a large reactance value can be divided into arbitrarily small chunks and then the effect of each load chunk on the antenna characteristic modes can be progressively determined using the perturbation equations. Alternatively, a hybrid approach can be taken in which a large load is partially applied by solving the loaded characteristic mode eigenvalue problem. The perturbation approach can then be applied to the loaded eigencurrents and eigenvalues in order to analyze how the mode is changing for each remaining load increment.

When analyzing the effect of a large reactance on the antenna characteristic modes using the perturbation approach, the total large load value can be broken into small reactance chunks that can each be considered a perturbation. The effect of each chunk on the characteristic modes can be accurately determined by applying the perturbation equations. For each load increment the change in the eigenvalues and eigencurrents can be found, and

the modes can be updated with the calculated changes. This process can be repeated until the entire reactance value is applied. The transformation of the modes can be monitored as each load increment is applied. This process is illustrated in Fig. 5.10. As with any finite difference technique, the error in the eigenvalues and eigencurrents will increase with the application of each increment since the perturbation equations are fundamentally first order accurate. The error can be reduced by decreasing the size of the load increment. As the size of the increment is reduced, however, the number of computations will increase leading to longer computation times.

An alternative approach can be viewed as a hybrid approach that uses both the perturbation equations and the solution of the loaded eigenvalue problem. Part of the large reactance value can be applied by solving the loaded characteristic mode eigenvalue problem instead of the unloaded eigenvalue problem. The calculated modes then reflect the effects of a portion of the total desired load value. The perturbation approach can then be applied to the loaded modes to analyze how the modes are changing when the antenna is partially loaded. This hybrid approach allows the designer to gain insight from the perturbation equations without having to manage each load increment and the associated error up to the desired large load value. The hybrid approach is often more efficient during the design process and is used in the following analysis.

Viewing the antenna loading design process as independently applying small load increments to the antenna is a new paradigm in antenna loading design. The new perspective can significantly aid the design process. Each individual small load increment can be independently positioned at desirable locations on the antenna in order to properly modify the characteristic modes to achieve desirable antenna performance. After all the load increments have been positioned to suitably modify the characteristic modes, the sum of the small load increments at each position on the antenna translates into the total value of the reactive loads that must be applied along the antenna.

The spiral characteristic modes transform as loading is increased on the antenna, and eventually the desired endfire radiation pattern is achieved. The spiral characteristic modes will be analyzed using the hybrid approach for two loads placed on the antenna at nodes 203 and 230. A few loading iterations will be analyzed to understand how the increased loading affects the characteristic modes and resulting antenna performance. Initially the un-

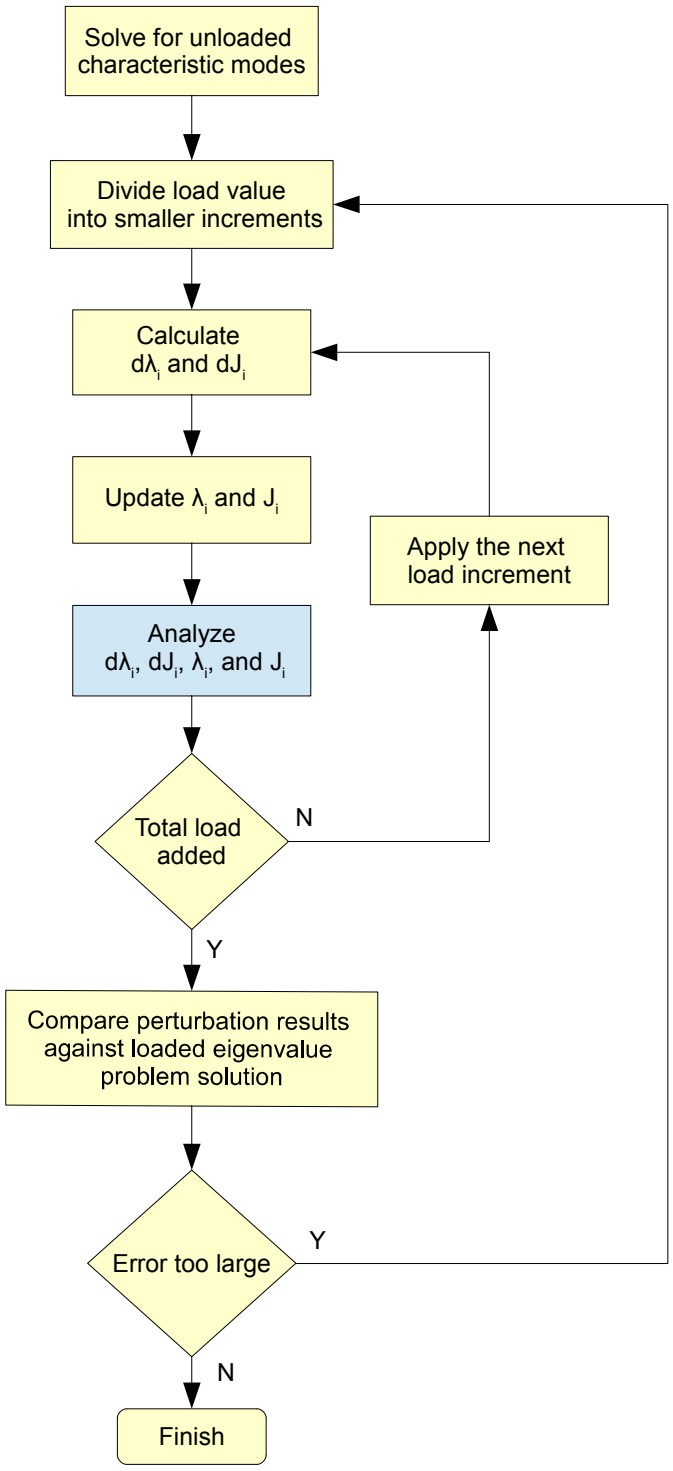

Figure 5.10: Flowchart illustrating how loading is applied and how the effects are analyzed using the perturbation approach.

loaded antenna properties are analyzed along with small load perturbations from the unloaded state. Next, the spiral is analyzed with +j100 Ω and −j100 Ω loads applied at nodes 203 and 230 (±j100 Ω), respectively, and again the effects of small load perturbations around these load values are examined. Finally, loading is increased to ±j1500 Ω and the excited endfire pattern is analyzed. For each load increment case, the perturbation approach is used to understand how the loading is transforming the characteristic modes.

5.4.1 Case 1: Unloaded Spiral

First, the unloaded spiral is considered along with the effects of small load perturbations from the unloaded state. Some of the plots are repeated here from section 5.3.2 for convenient comparison against the other cases with increased antenna loading. Fig. 5.11 and Table 5.2 give the characteristic currents and eigenvalues for the unloaded spiral described in Section 5.3.1. Fig. 5.12 gives the total electric field eigenpatterns of the first three characteristic modes. Inspection of the mode patterns suggests that the mode 2 pattern would provide a desirable endfire pattern. As described in Section 5.3.5, a +j1 Ω inductive load and a −j1 Ω capacitive load are placed at nodes 203 and 230, respectively, in order to enhance the even mode 2 contribution to the excitable modes 1 and 3. The resulting mode power contribution to the first three modes is shown in Fig. 5.13. The plot shows that essentially only mode 2 has a radiated power contribution to the change in modes 1 and 3 as desired. The plot also shows that the power contribution to mode 1 is orders of magnitude greater than the contribution to mode 3. As a result, due to the reaction property described in Appendix B, mode 1 has a large power contribution back to mode 2. Therefore, as loading increases both mode 1 and 2 eigencurrents will become composite modes consisting of the combination of unloaded mode 1 and 2 eigencurrent distributions.

Fig. 5.12 gives the electric field magnitude for the first three eigenmodes. These are total magnitudes that can be further decomposed in terms of electric field E_ϕ and E_θ real and imaginary components. When loading is applied to the antenna, each mode becomes a composite mode having a contribution from the other characteristic modes. In order to gain insight into the formation of the composite eigenpattern, the patterns must be added

in terms of their real and imaginary vector components. Fig. 5.14 gives the real and imaginary E_ϕ and E_θ components for the unloaded spiral for the $\phi = 292$ degree cutplane which is the plane in which the mode 2 endfire pattern maxima occur.

Figs. 5.15 through 5.17 characterize the total excited antenna performance for comparison to later cases when loading is increased. Fig. 5.15 confirms that the unloaded spiral has a broadside total gain pattern. Furthermore, the spiral obtains minimal VSWR variation for frequencies over 2 GHz as shown in Fig. 5.16. Finally, Fig. 5.17 gives the amount of power each characteristic mode contributes to the total excited antenna radiated power. The plot shows that the spiral's broadside pattern is composed of power radiated mostly by modes 1 and 3. Inspection of Fig. 5.12 shows that both modes 1 and 3 have broadside patterns and therefore produce the broadside total excited gain pattern.

5.4.2 Case 2: ±j100 Ω at Nodes 203 and 230

Changes to the spiral radiation performance occur as the reactance values on the spiral arms at nodes 203 and 230 are increased to +j100 and −j100 Ω, respectively. For comparison, Figs. 5.18 through 5.24 give the identical plots for the ±j100 Ω loaded spiral as Figs. 5.2 through 5.17 gave for the unloaded spiral. The initial loading perturbations to the unloaded spiral produced strong mode 2 eigencurrent contributions to mode 1. As a result of the reaction property described in Appendix B, mode 1 also had a large power contribution back to mode 2. As perturbations continue to be applied, the mode 1 and 2 current distributions become similar as seen in Fig. 5.18. The eigenvalues shown in Table 5.3 stayed relatively constant as loading was increased due to the application of the equal and opposite loading discussed in Appendix B. Because the mode 1 and 2 eigenpatterns are directly related to the eigencurrent distributions, the mode eigenpatterns also become similar as seen in Fig. 5.19. The loaded modes 1 and 2 can now be considered composite modes consisting of the previous unloaded mode 1 and mode 2 eigencurrent distributions. When mode 1 is excited by a center feed, it radiates a corresponding composite pattern consisting of both the previous unloaded mode 1 and mode 2 patterns.

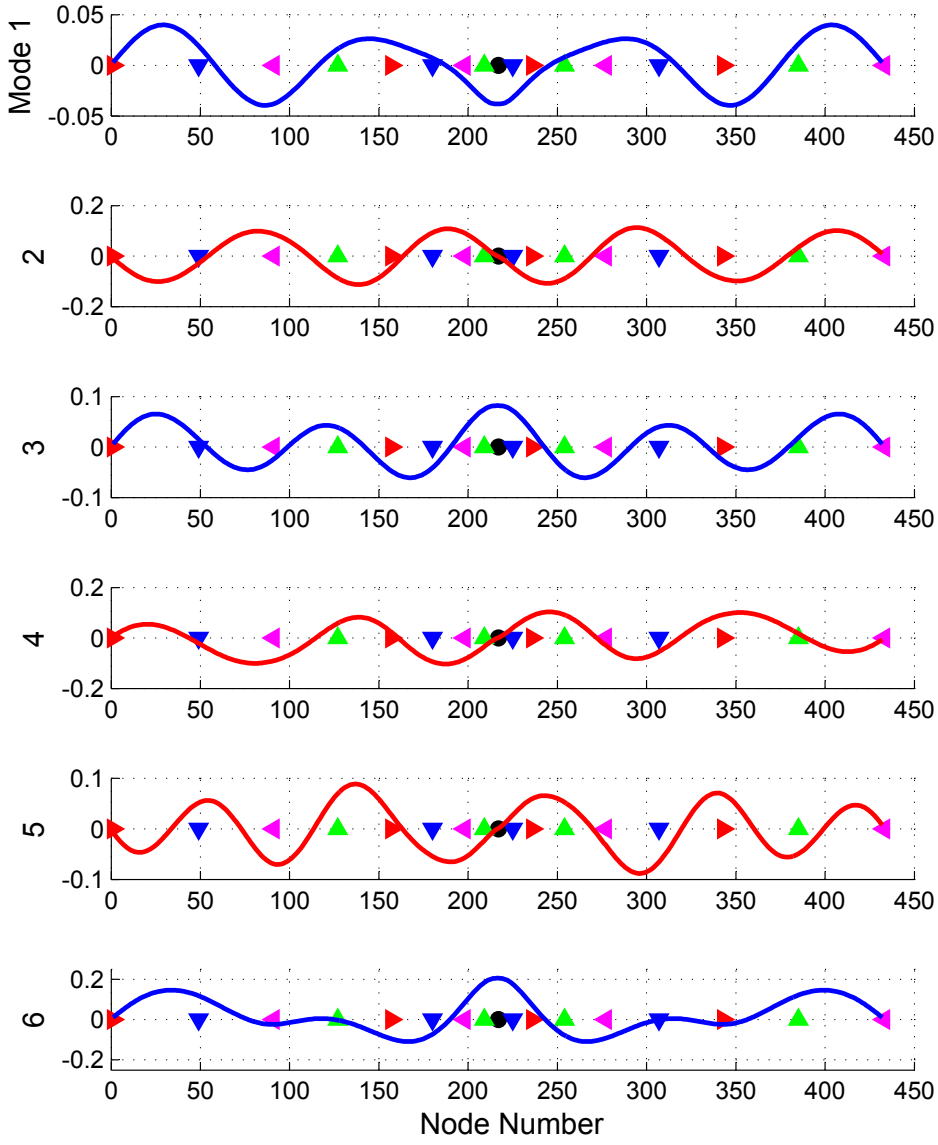

Figure 5.11: Eigencurrents of the unloaded two-turn spiral at 3 GHz.

Table 5.2: Mode eigenvalues of the unloaded two-turn spiral at 3 GHz.

Mode Number	Eigenvalue
1	0.66457
2	0.78522
3	-2.57716
4	4.55718
5	-8.23537
6	16.82017

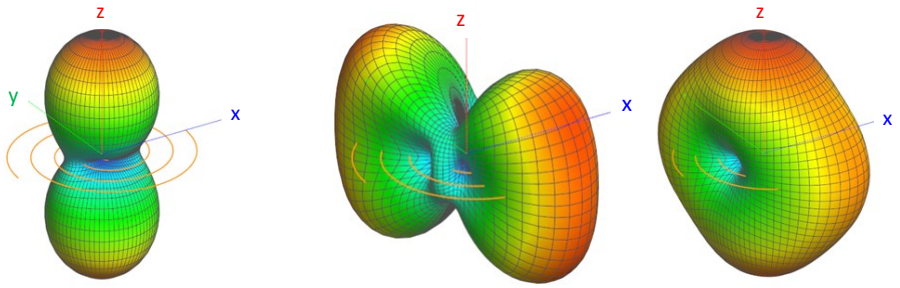

(a) Mode 1 (b) Mode 2 (c) Mode 3

Figure 5.12: Total electric field eigenpatterns of the unloaded two-turn spiral at 3 GHz. E-Field magnitudes range from blue to red, 0 to (a) 11.25 V (b) 10 V and (c) 8 V.

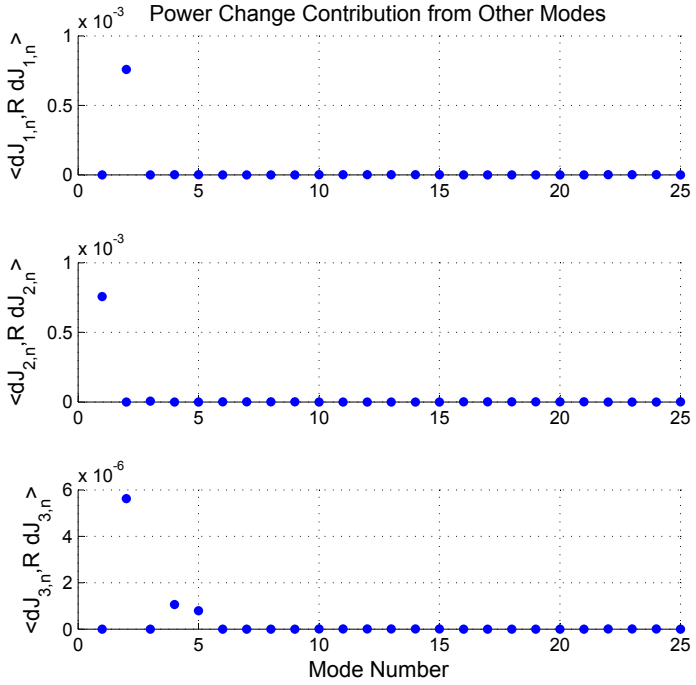

Figure 5.13: The radiated power contribution to the first three unloaded modes when +j1 and −j1 loads are applied at spiral nodes 203 and 230, respectively.

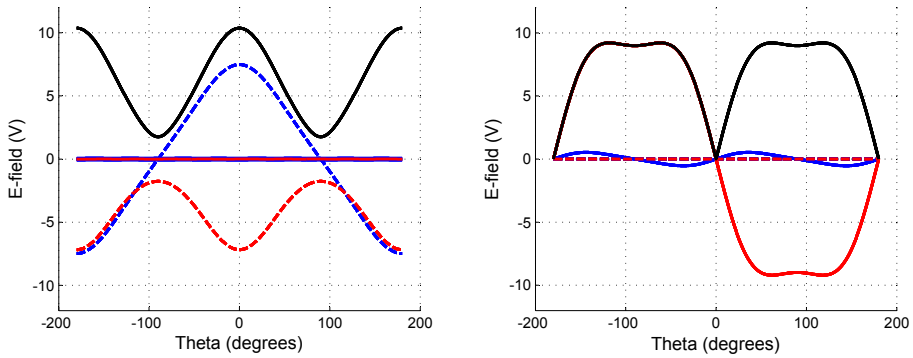

(a) Mode 1

(b) Mode 2

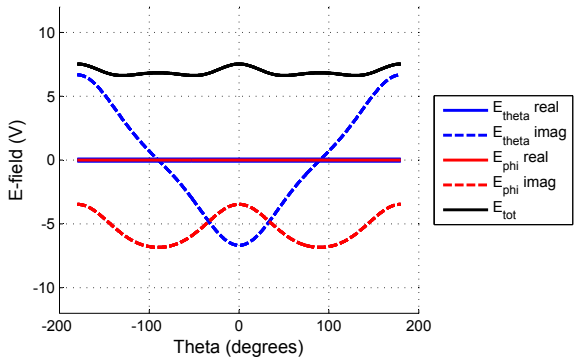

(c) Mode 3

Figure 5.14: Real and imaginary components of the $\phi = 292$ degree cutplane eigenpattern E-field components at 3 GHz for the two-turn unloaded spiral.

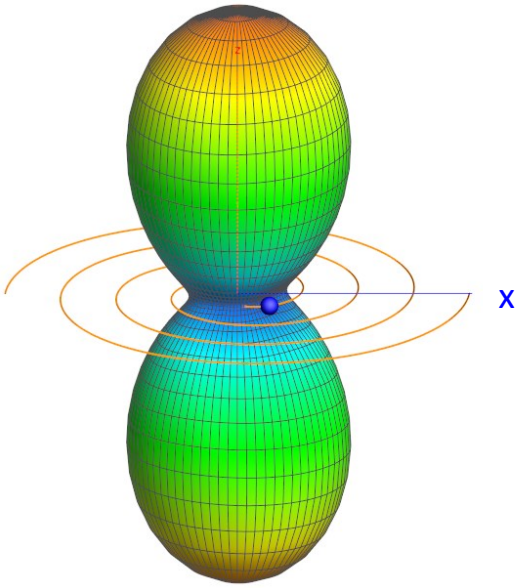

Figure 5.15: Total gain pattern of the center fed unloaded two-turn spiral antenna at 3 GHz. Magnitude ranges from 0 (Blue) to 3 (Red).

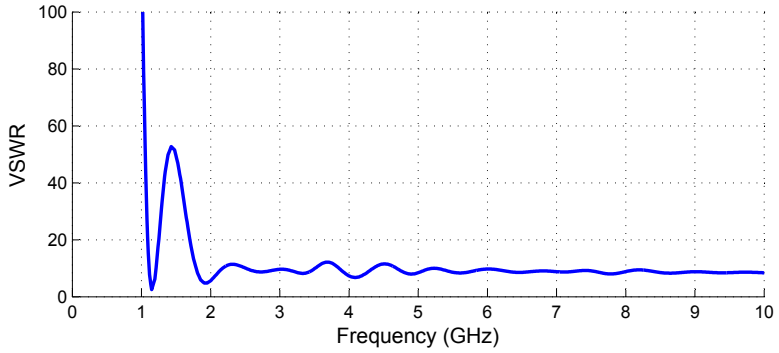

Figure 5.16: VSWR of the center fed unloaded two-turn spiral antenna over frequency.

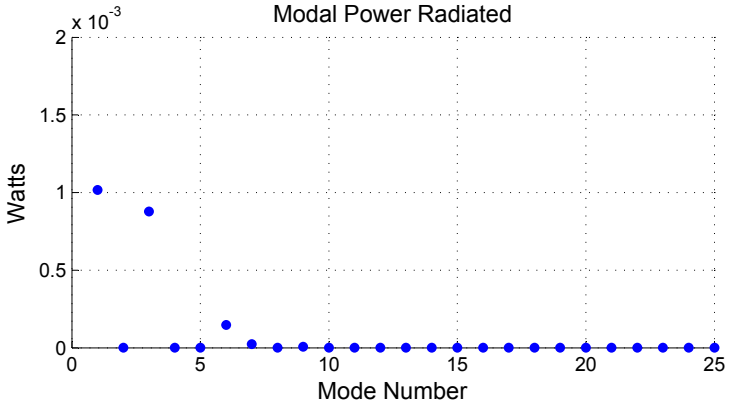

Figure 5.17: Radiated power by each characteristic mode of the center fed unloaded two-turn spiral antenna at 3 GHz.

After the loading is increased to ±j100 Ω, modes 1 and 2 have very similar distributions and eigenpatterns. The first three modes have a broadside total electric field pattern as seen in Fig. 5.19. Fig. 5.20 shows that mode 3 obtains comparable power contributions from both modes 1 and 2 when ±j1 Ω perturbations are further added to the antenna. Closer inspection of the electric field components shows how mode 3 will eventually transition toward an endfire pattern as loading continues to increase. Fig. 5.21 gives the electric field E_ϕ and E_θ real and imaginary components for the first three characteristic modes for currents scaled to radiate unit power. The plots are for the $\phi = 292$ degree cutplane which is the plane in which the endfire pattern maxima occur. Qualitatively, we see that the real E_ϕ component from both modes 1 and 2 will add constructively with the real E_ϕ component of mode 3. The real E_ϕ component is the desirable endfire pattern. The imaginary E_ϕ component contribution from mode 1 will tend to cancel with that from mode 2 resulting in minimal contribution to mode 3. Furthermore, the real E_θ component in modes 1 and 2 is negligible and will not contribute significantly to mode 3. Also, the imaginary E_θ component contributions from mode 1 and 2 will tend to cancel since the mode 1 and 2 components have similar distribution but opposite sign.

The contributions to mode 3 are governed by the perturbation equations and are excitation independent. Therefore, the contributions from modes 1 and 2 do not have to be modified by a complex weight coefficient. The mode contribution coefficients which determine the contribution amount from modes 1 and 2 are always real and so do not modify the phases of the contributing currents. Therefore, it is appropriate to add the real and imaginary components when considering the contributions to mode 3. We can expect the endfire pattern to manifest itself in the mode 3 total E-field pattern as loading increases.

Similar to those given for the unloaded spiral, plots 5.22 through 5.24 characterize the excited spiral loaded with ±j100 Ω. Fig. 5.22 shows that the total excited pattern is still broadside in nature but is now tilted slightly. Furthermore, the VSWR with loading in Fig. 5.23 is still relatively constant above 2 GHz. Finally, Fig. 5.24 shows that the total excited radiated power is still dominated by modes 1 and 3. However, mode 1 radiates slightly more power while mode 3 radiates slightly less.

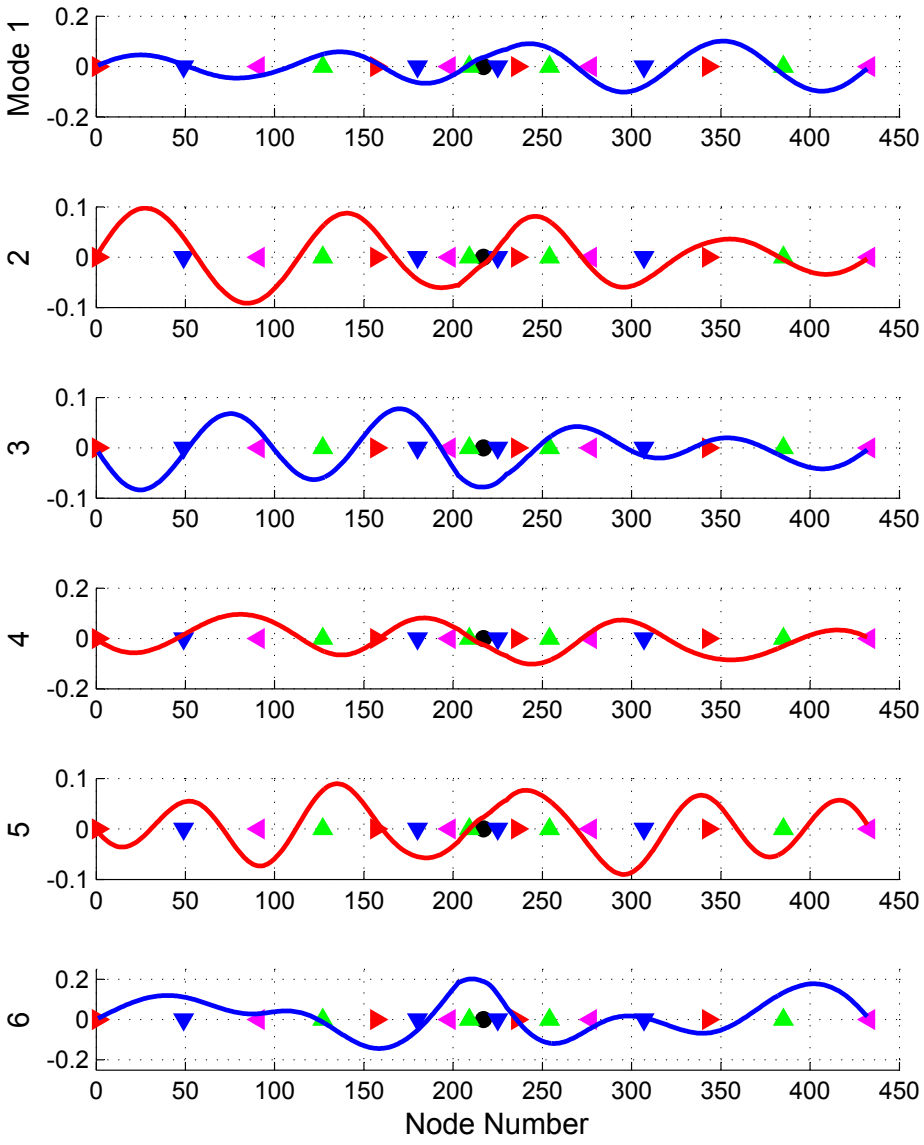

Figure 5.18: Eigencurrents at 3 GHz of the two-turn spiral with ±j100 Ω loading at nodes 203 and 230.

Table 5.3: Mode eigenvalues at 3 GHz of the two-turn spiral with ±j100 Ω loading at nodes 203 and 230.

Mode Number	Eigenvalue
1	0.34694
2	0.96793
3	-2.55648
4	4.34035
5	-8.37695
6	30.62152

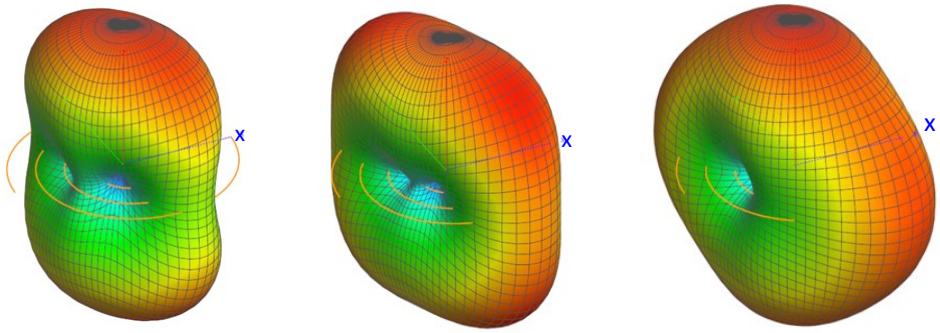

(a) Mode 1 (b) Mode 2 (c) Mode 3

Figure 5.19: Total electric field eigenpatterns at 3 GHz of the two-turn spiral with ±j100 Ω loading at nodes 203 and 230. E-Field magnitudes range from blue to red, 0 to (a) 8.25V (b) 8V and (c) 7.5V.

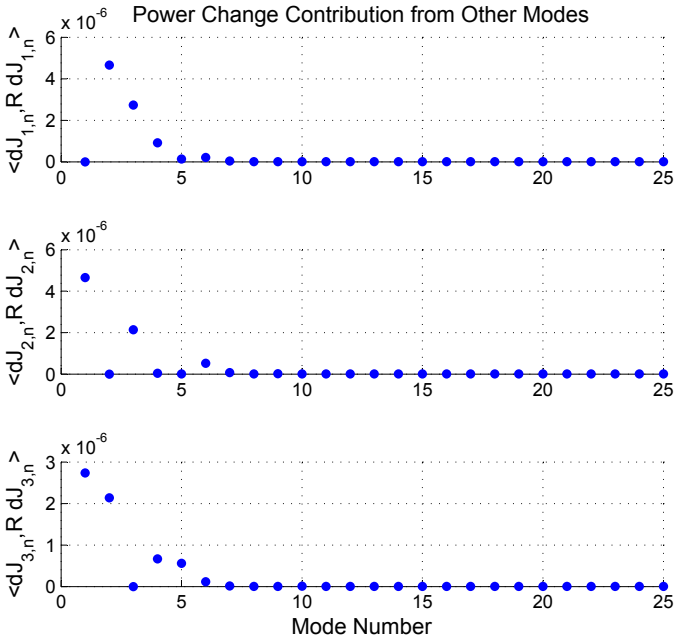

Figure 5.20: The radiated power contribution to the first three modes when additional perturbations of +j1 and −j1 Ω loads are applied at spiral nodes 203 and 230, respectively, on top of the ±j100 Ω loads already present.

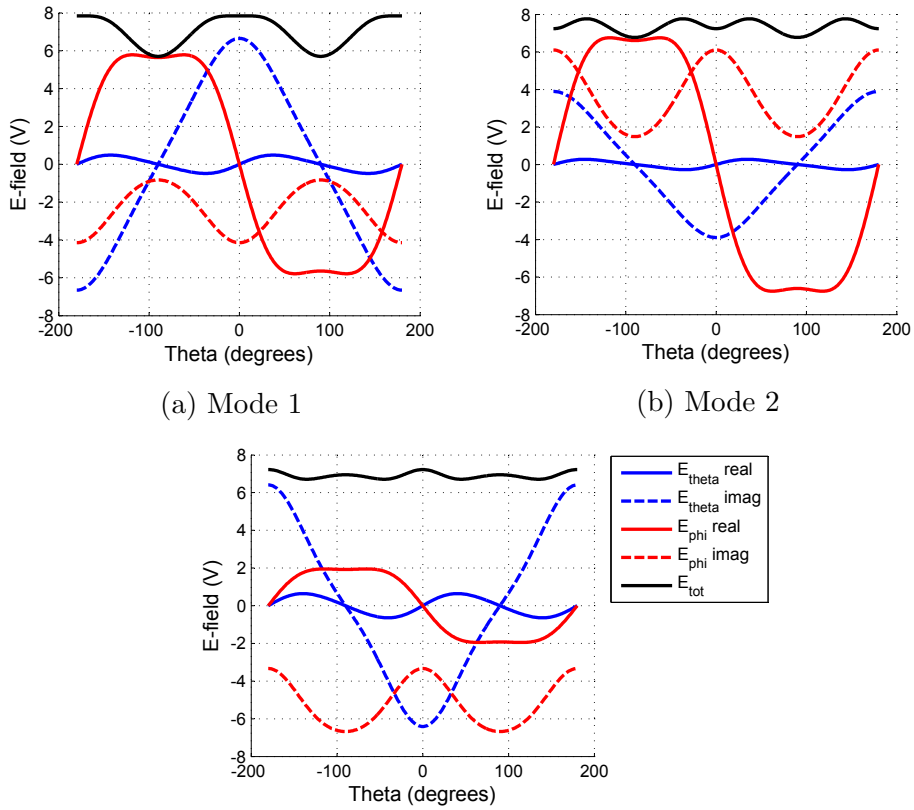

(a) Mode 1

(b) Mode 2

(c) Mode 3

Figure 5.21: Real and imaginary components of the $\phi = 292$ degree cutplane eigenpattern E-field components at 3 GHz for the two-turn spiral with $\pm$j100 Ω loading at nodes 203 and 230.

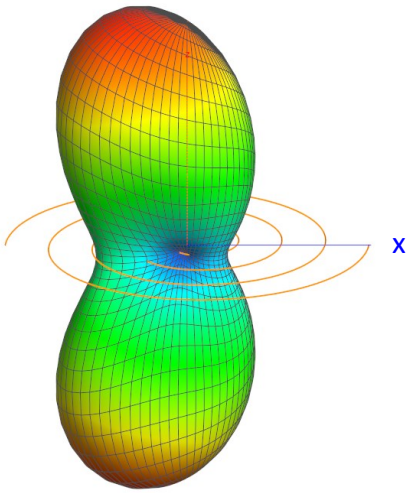

Figure 5.22: Total gain pattern at 3 GHz of the two-turn spiral with ±j100 Ω loading at nodes 203 and 230. Magnitude ranges from 0 (Blue) to 2.5 (Red).

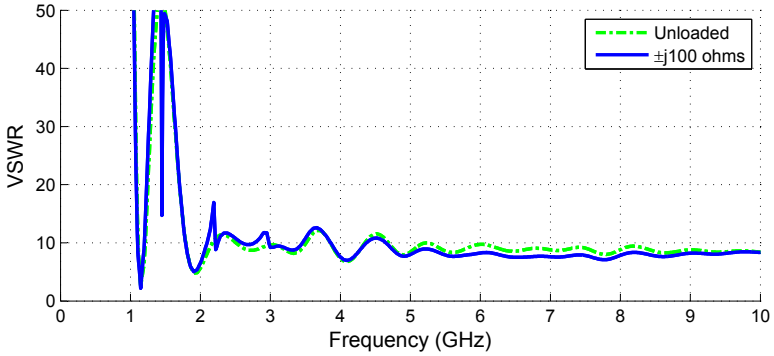

Figure 5.23: VSWR over frequency of the two-turn spiral with ±j100 Ω loading at nodes 203 and 230.

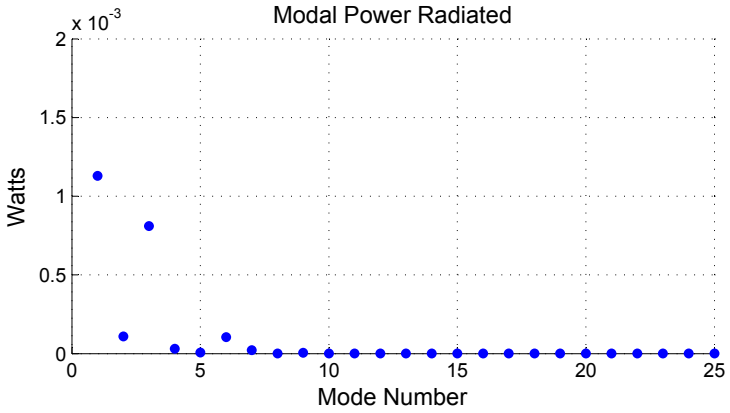

Figure 5.24: Radiated power by each characteristic mode of the two-turn spiral with ±j100 Ω loading at nodes 203 and 230.

5.4.3 Case 3: ±j1500 Ω at Nodes 203 and 230

Next, the loading is increased to relatively large load values to further analyze the mode transformations. Figs. 5.25 through 5.33 characterize the spiral when loaded to ±j1500 Ω. Fig. 5.25 shows the loaded eigencurrents while Table 5.4 gives the corresponding eigenvalues. Inspection of the eigenvalues shows that they have not changed significantly from the unloaded case because of the application of equal and opposite reactive loading values. However, the eigenvalues have changed a small amount because of increased asymmetry in eigencurrent magnitude on the spiral arms. Fig. 5.26 shows that, as expected, the mode 3 total electric field pattern is endfire in nature and is similar to the previous unloaded mode 2 pattern from Fig. 5.12. As loading was increased, the mode 3 eigencurrent received contributions from modes 1 and 2 eventually transitioning toward a current distribution with an endfire pattern. Although the mode 3 pattern looks similar to the unloaded mode 5 pattern from Fig. 5.3, the lobes actually point in different ϕ directions. Therefore, we can tell that mode 3 did not obtain its most significant contributions from mode 5.

Fig. 5.27 gives the radiated power contributions to the first three modes when additional perturbations of +j1 and −j1 Ω loads are applied at spiral nodes 203 and 230, respectively, on top of the ±j1500 Ω loads already present. The power change contribution magnitudes are very small compared to the changes that occurred at lower loading values. Therefore, increasing the loading magnitude beyond the ±j1500 Ω load values will result in negligible changes to the excited pattern.

In the previous section we looked at how the mode contributions transform the mode 3 eigencurrents and resulting eigenpattern. Because only the unexcited eigenpatterns were considered, the complex weight coefficient did not have to be considered. However, here we would like to consider how the modes contribute to the total excited pattern. To better understand how the modes combine to form the total excited endfire pattern, the total excited pattern is broken down in terms of its characteristic mode components. Because the total excited pattern is being considered, the eigenpattern components must be modified by their complex weight coefficients before they

can be combined. The eigenpattern decomposition is given by

$$E = \sum_n \frac{\langle J_n, E^i \rangle}{1 + j\lambda_n} E_n, \tag{5.9}$$

where E^i is the excitation electric field and E_n is the mode eigenpattern that corresponds to the eigencurrent scaled to radiate unit power. Fig. 5.28 shows the unexcited mode 1 and 3 eigenpattern distribution θ and ϕ vector components along the $\phi = 292$ degree cutplane. Because the modes are not resonant ($\lambda \neq 0$), the complex weight coefficient modifies both the magnitude and phase of each field component which alters the real and imaginary component distributions when excited. Fig. 5.29 shows the mode 1 and 3 eigenpattern distributions modified by each complex weight coefficient. Finally, Fig. 5.30 shows the combined total excitation pattern components. The total excited antenna gain pattern as shown in Fig. 5.31 comes from a combination of modes. However, the excitation of mode 3 is primarily responsible for the endfire pattern. More specifically, the plots demonstrate that the endfire pattern is primarily from the mode 3 E_ϕ component, and the finite magnitude pattern at broadside comes from the E_θ field component. However, although the total excited pattern is dominated by mode 3, other modes do help shape the total pattern.

Fig. 5.31 shows the total gain pattern for the excited spiral alongside the unloaded mode 2 endfire pattern. The figure shows close agreement between the loaded excited pattern and the unloaded mode 2 pattern. Originally, the mode 2 pattern was desirable but could not be excited using a single center feed. However, after loading the antenna using insight from the perturbation approach, the desirable endfire pattern is achieved. The endfire pattern is achieved by using loading to obtain contributions from the unexcitable mode 2 eigencurrent to the excitable modes. As loading was increased, the mode 2 pattern eventually was excited within mode 3.

Figs. 5.32 and 5.33 show the VSWR and modal radiated power, respectively. Although the desirable pattern was achieved using the loading scheme, the input VSWR increased significantly below 4 GHz. The high VSWR is also apparent when considering the mode radiated power. Although mode 3 radiates the most power, the amount of power radiated by each mode is significantly less when compared to the unloaded case. Instead of being ra-

diated, the power is reflected, resulting in a higher VSWR. The high VSWR will be addressed in Section 5.6.

5.5 A New Design with Larger Mode Contributions

In the previous example, basic insight from the perturbation approach was used to determine the load positions and load types to obtain an endfire pattern. However, many different load position choices can be made to arrive at various loading combinations that achieve the same target goal. In the previous example, opportunities were available to obtain larger mode contributions but required the tradeoff of more reactive loads to achieve the goal. For instance, the eigencurrent interaction plot in Fig. 5.6 suggests that load positions near the spiral ends are the best locations to initially receive the strongest eigencurrent contribution from mode 2 to modes 1 and 3. In this section, the perturbation design approach will be more rigorously applied in order to arrive at an alternative loading scheme. The alternative design will help demonstrate the sensitivity of the spiral to load position, load type, and load value. The example will show how larger mode contributions can be obtained, but multiple loads will be needed on the structure to maintain large contributions as loading is increased. Multiple loads can give the designer more control over mode contributions and may allow smaller reactance values to achieve a desired goal. However, we will show that obtaining larger contributions themselves will not solve the spiral VSWR issue at 3 GHz. An understanding of why the VSWR degrades and a solution to the problem will be presented following this section.

As previously mentioned, mode 2 contains the desired endfire pattern but cannot be excited using a center feed. The mode 2 behavior can be excited as part of modes 1 or 3 or if mode 2 receives an eigencurrent contribution that gives it finite current magnitude at the feed. In order to obtain the mode 2 behavior from the spiral using the smallest reactances possible, the designer should place the loads in positions that obtain the largest mode 2 contributions to modes 1 and 3. Fig. 5.6 shows that the largest mode 2 to 1 contribution will occur for loads placed at nodes 26 and 407 near the ends of the spiral. Inspection of Fig. 5.11 shows that opposite load types must be used on opposing arms to keep the contributions from each load

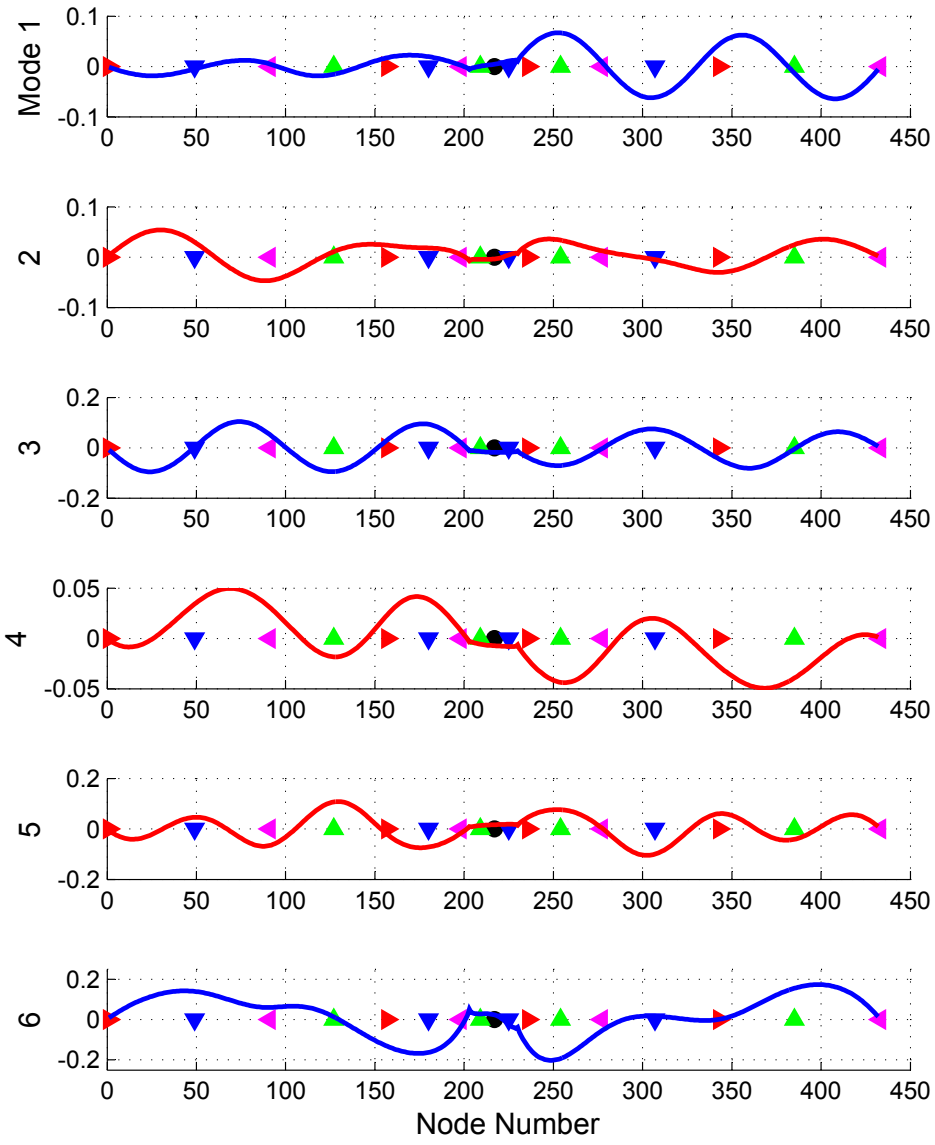

Figure 5.25: Eigenpatterns at 3 GHz of the two-turn spiral with ±j1500 Ω loading at nodes 203 and 230.

Table 5.4: Mode eigenvalues at 3 GHz of the two-turn spiral with ±j1500 Ω loading at nodes 203 and 230.

Mode Number	Eigenvalue
1	-0.95316
2	1.20587
3	-2.31235
4	3.49615
5	-9.87317
6	30.62152

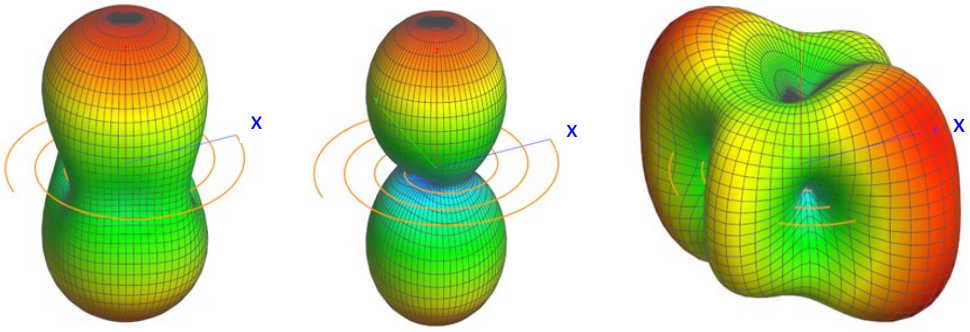

(a) Mode 1 (b) Mode 2 (c) Mode 3

Figure 5.26: Eigenpatterns at 3 GHz of the two-turn spiral with ±j1500 Ω loading at nodes 203 and 230. E-Field magnitudes range from blue to red, 0 to (a) 9 V (b) 11.25 V and (c) 8 V.

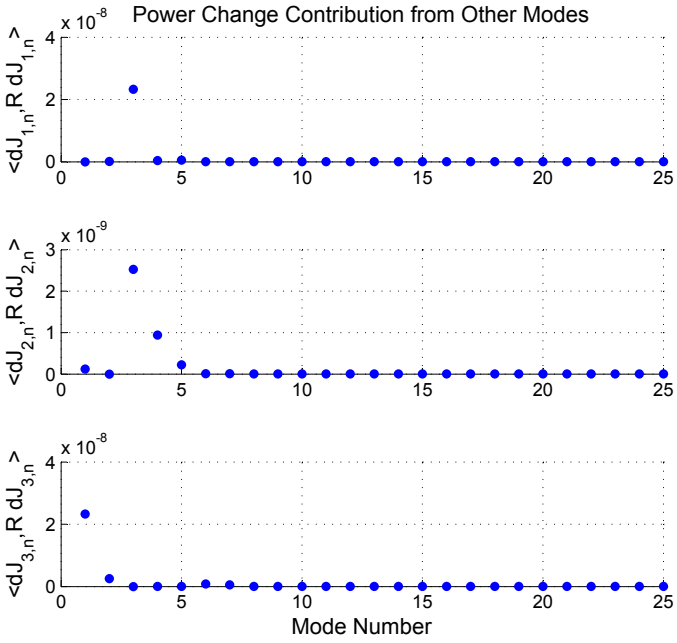

Figure 5.27: The radiated power contribution to the first three modes when additional perturbations of +j1 and −j1 Ω loads are applied at spiral nodes 203 and 230, respectively, on top of the ±j1500 Ω loads already present.

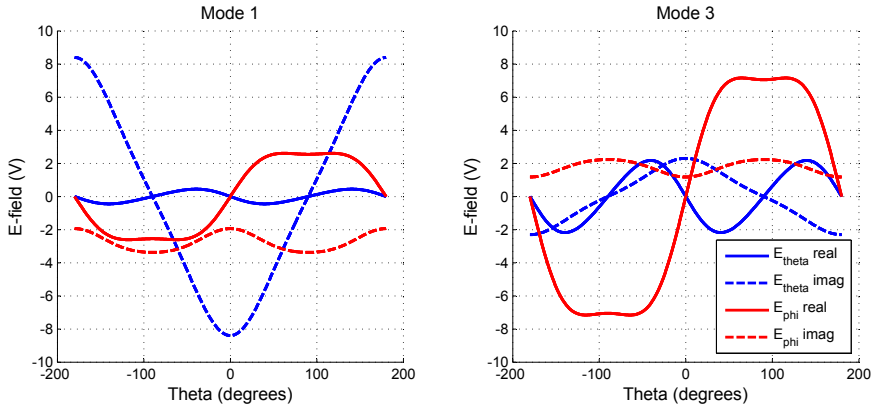

Figure 5.28: Eigenpattern real and imaginary components of the $\phi = 292$ degree cutplane eigenpattern E-field components at 3 GHz of the two-turn spiral with ±j1500 Ω loading at nodes 203 and 230.

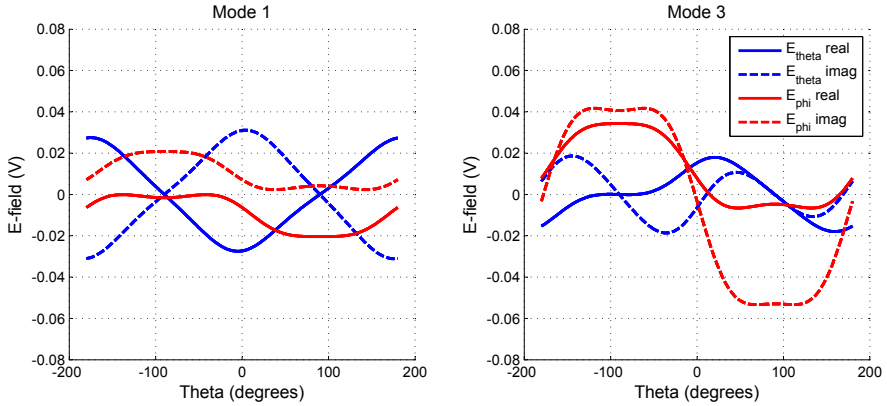

Figure 5.29: Excited real and imaginary components of the $\phi = 292$ degree cutplane eigenpattern E-field components at 3 GHz of the two-turn spiral with ±j1500 Ω loading at nodes 203 and 230.

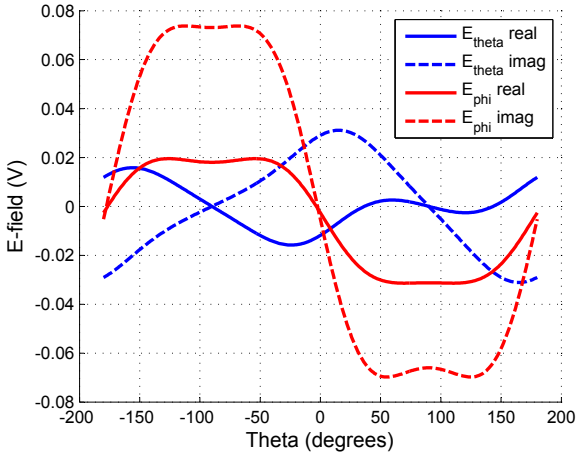

Figure 5.30: Total excited pattern real and imaginary components of the $\phi = 292$ degree cutplane E-field at 3 GHz of the two-turn spiral with ±j1500 Ω loading at nodes 203 and 230.

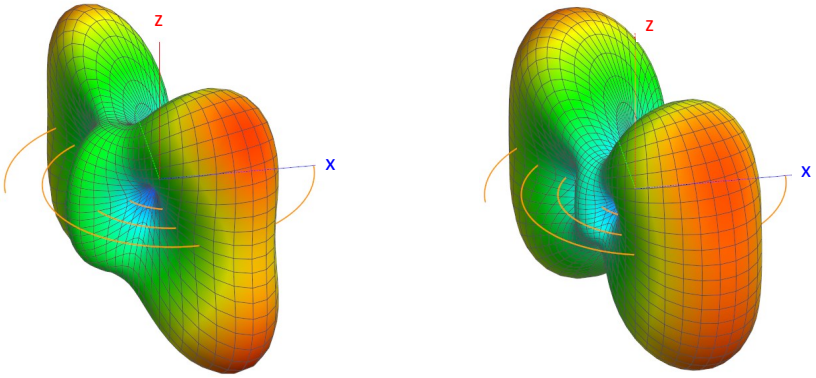

(a) (b)

Figure 5.31: (a) Total gain pattern at 3 GHz of the two-turn spiral with ±j1500 Ω loading at nodes 203 and 230. Magnitude ranges from 0 (Blue) to 2.5 (Red). (b) Unloaded mode 2 E-Field pattern for comparison. Magnitude ranges from 0 (blue) to 10V (red).

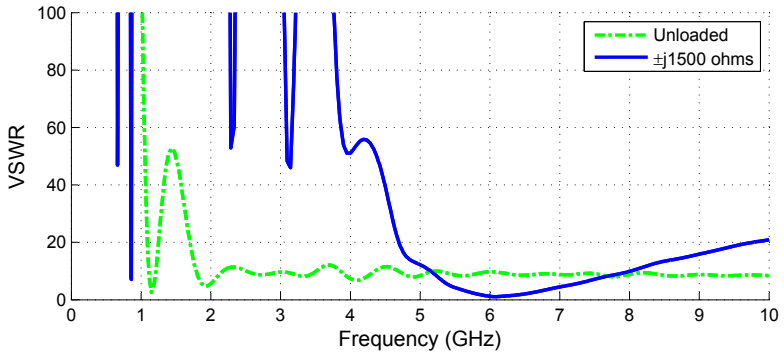

Figure 5.32: VSWR over frequency of the two-turn spiral with ±j1500 Ω loading at nodes 203 and 230.

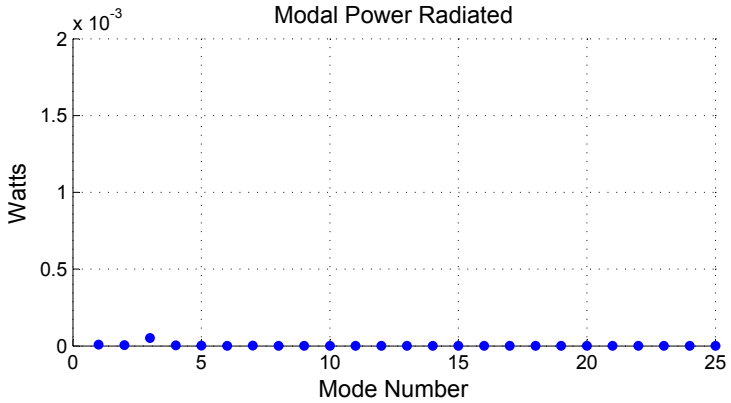

Figure 5.33: Radiated power by each characteristic mode of the two-turn spiral with ±j1500 Ω loading at nodes 203 and 230.

from canceling each other. As the loading is increased at these locations, the mode 2 contributions decrease the magnitude of the mode 1 eigencurrent at node 26. When the loading increases beyond $\pm$j7 Ω, mode 1 current at node 26 becomes negative so is out of phase with the current at node 407. Therefore, the mode 2 contributions from opposite loads begin to cancel each other and the additional loading at these locations is no longer effective. Further increasing the inductive and capacitive reactances at these locations is counterproductive and will not eventually produce the desired endfire pattern. Therefore, additional loading should be applied at new loading positions to further enhance the mode 2 to 1 contributions.

To determine the best locations to apply the next set of loading, we look at the eigencurrent interaction plot given in Fig. 5.34 when the spiral is loaded with the $\pm$j7 Ω loads at nodes 26 and 407. We would like to focus on obtaining the contribution of mode 2 to mode 1. From the plot, we see that applying the next set of loads at nodes 186 and 241 allows a sizeable mode 2 to 1 contribution while suppressing all contributions from modes 1 and 2 to mode 3. No contributions to mode 3 result because both loads are in mode 3 eigencurrent nulls at these locations. The type of load to place at these new locations is chosen to obtain the desired mode 2 to 1 contribution coefficient sign. The desired contribution coefficient sign is selected so the next set of mode 2 to 1 eigencurrent contributions add in phase with those from the last set of loads. The contribution coefficient sign is determined by the load type, the mode 1 and 2 eigencurrent phase signs at the load locations, and the sign of the eigenvalue difference between the changing and contributing modes. In this case, the same sign reactance must be used on each arm since the eigencurrents of modes 1 and 2 are in phase at the load positions. The desired mode 2 eigencurrent contribution phase is obtained using capacitive loads at both nodes 186 and 241. Both load values are increased to $-$j6 Ω. At these load values, mode 1 has received enough contribution from mode 2 and vice versa such that both modes radiate the same amount of power when center fed as seen in Fig. 5.35. The mode 1 and 2 eigenpatterns are very similar, displaying the desirable E_ϕ endfire pattern component, while mode 3 is still dominated by the broadside pattern.

The spiral antenna radiation pattern is dominated by power radiated by the broadside mode 3 pattern. Now that modes 1 and 2 display the desirable endfire pattern component, loading can be placed to try to obtain a

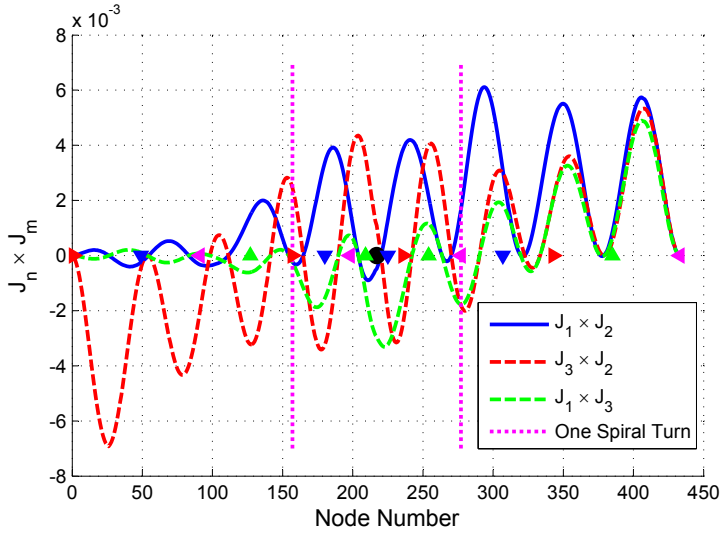

Figure 5.34: Eigencurrent interaction metric when the spiral is loaded with ±j7 Ω at nodes 26 and 407.

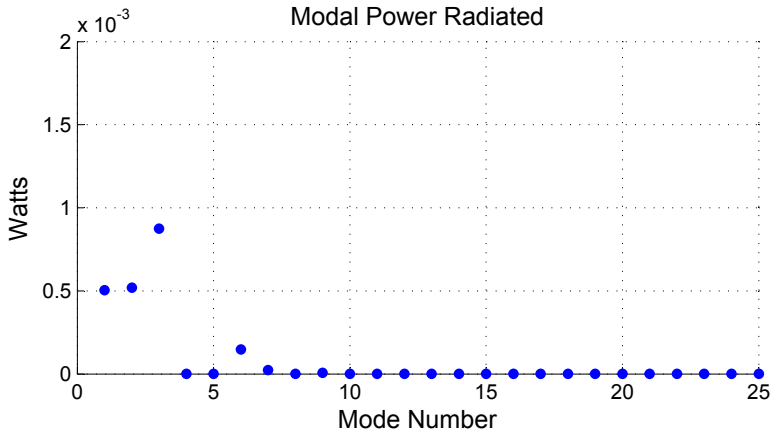

Figure 5.35: Radiated power by each characteristic mode of the two-turn spiral with ±j7 Ω loading at nodes 26 and 407 and −j6 Ω loading at nodes 186 and 241.

contribution from modes 1 and 2 to mode 3. Modes 1 and 2 have very small eigenvalue differences. As a result, the denominator of the mode 2 to 1 contribution coefficient is small producing large mode 2 to 1 contributions for relatively small load values. Mode 1 received large contributions from mode 2 and transitioned rapidly toward the mode 2 current distribution. However, the eigenvalue difference between mode 3 and modes 1 or 2 is much larger. Therefore, the eigencurrent contribution coefficients for contributions to mode 3 are much smaller, and as a result, it is more difficult to obtain contributions to mode 3 from modes 1 and 2. Much larger load values will be necessary to obtain the desired contributions to mode 3.

To determine the best locations to apply the next set of loads to obtain contributions to mode 3, the updated eigencurrent interaction plot given in Fig. 5.36 is examined. The plot reflects the spiral loaded with $\pm$j7 Ω loads at nodes 26 and 407 and $-$j6 Ω loads at nodes 186 and 241. The mode 1 eigencurrent has a null at node 210. Therefore, Fig. 5.36 shows that when a load is placed at this location, only mode 2 can contribute to mode 3. There are no contributions between modes 1 and 3 or between modes 1 and 2. The position is also close to a mode 2 to 3 contribution maximum. Loading at this position is useful since it allows strong contributions to mode 3 from mode 2 without affecting mode 1. The symmetric load position on the opposite arm is node 224. In contrast to node 210, node 224 has a mode 2 eigencurrent null at the node location and is near a mode 1 to 3 contribution maximum. Loading at node 224 allows mode 1 to contribute to mode 3 without affecting or receiving a contribution from mode 2. The loading positions are desirable since they allow strong independent contributions from modes 1 and 2 to mode 3. Using these load positions, the size of the mode 1 and 2 contributions to mode 3 can be independently controlled through each separate load value.

Consider a +j1 Ω load placed at node 210 to obtain a strong mode 2 contribution to mode 3. Fig. 5.37 shows the power contribution between the first three modes. The figure shows that mode 3 only obtains a contribution from mode 2. Mode 1 is completely unaffected by the load. However, the power change contribution from mode 2 is only 1.2 μW while mode 3 radiates on the order of a milliwatt of power when excited with a center feed. Therefore, in order to get a mode 2 contribution that will significantly impact the mode 3 excited radiation pattern, we will need to apply loading upwards of +j500

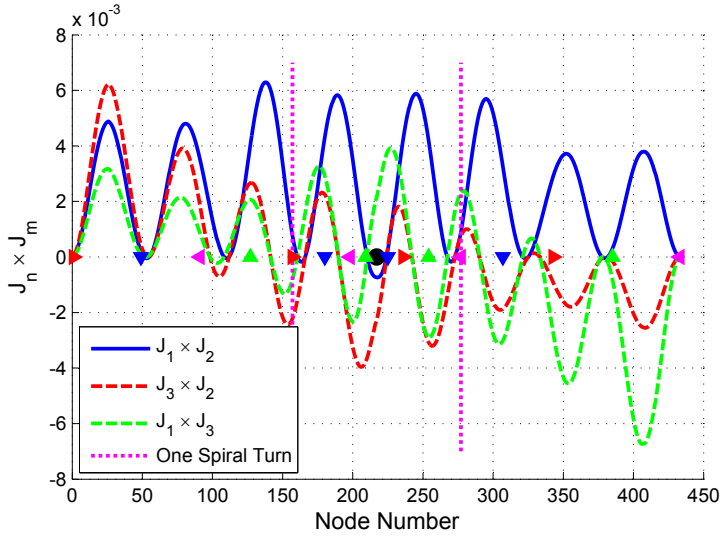

Figure 5.36: Eigencurrent interaction metric when the spiral is loaded with ±j7 Ω at nodes 26 and 407 and −j6 Ω at nodes 186 and 241.

Ω. Therefore, the perturbation approach shows that this loading scheme requires relatively large loads if the endfire radiation pattern is to be obtained using series loading. Figs. 5.38 and 5.39 show the final total gain pattern and VSWR when ±j500 Ω loading is applied at nodes 210 and 224.

Because the unloaded spiral mode 1 and 2 eigenvalues are similar in value, we get strong contributions between these modes regardless of whether the load is placed at the outside of the spiral (node 26/407) or near the inside (node 203/230). Therefore, for the particular endfire pattern goal there is no significant benefit to using multiple loads and complicating the design. Modes 1 and 2 contribute significantly to each other regardless of the load locations assuming the loads are not placed in eigencurrent nulls, and it is still difficult to get sizeable contributions to mode 3 from modes 1 or 2 largely due to the larger eigenvalue difference in the contribution coefficient denominator. Although stronger contributions were shown to be obtainable, more loads were required to continually load in the best locations on the spiral. In this particular case the extra expense associated with using more loads is probably not warranted since large reactance values are still required to achieve the endfire pattern design goal. The benefit of separating the loads in order to apply them in the most optimal contribution locations will be more advantageous for other various antenna design applications where the desired design goal does not require such large loads.

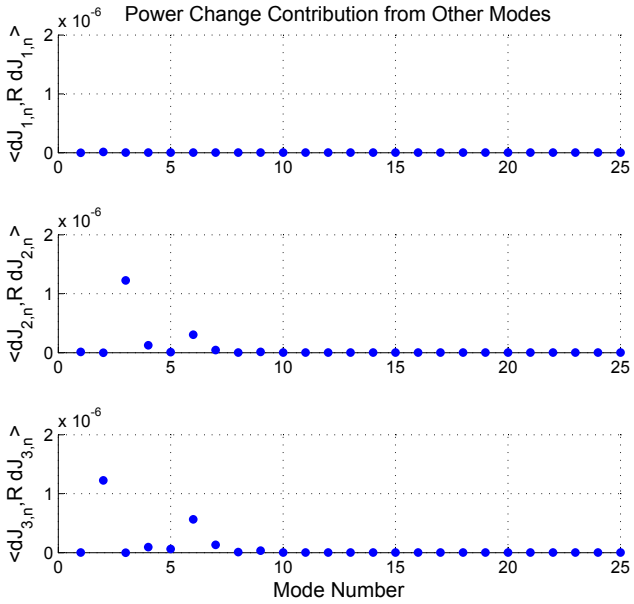

Figure 5.37: Power change contribution for the first three modes when a +j1 Ω load is introduced at node 210. The spiral is loaded with ±j7 Ω at nodes 26 and 407 and −j6 Ω at both nodes 186 and 241.

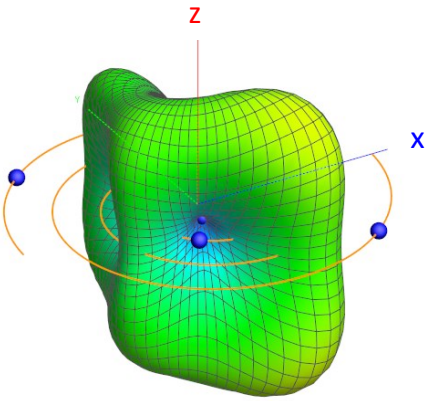

Figure 5.38: Total gain pattern at 3 GHz of the two-turn spiral with ±j7 Ω loading applied at nodes 26 and 407, −j6 Ω loading applied at nodes 186 and 241, and ±j500 Ω loading applied at nodes 210 and 224. Magnitude ranges from 0 (Blue) to 3 (Red).

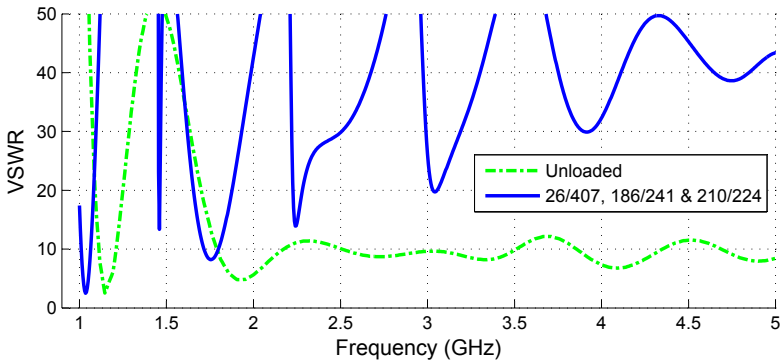

Figure 5.39: VSWR over frequency of the two-turn spiral with ±j7 Ω loading applied at nodes 26 and 407, −j6 Ω loading applied at nodes 186 and 241, and ±j500 Ω loading applied at nodes 210 and 224.

The perturbation approach showed that relatively large load values are required to obtain the desired endfire pattern. The large load values were placed at nodes 203 and 230 in the first example and at nodes 210 and 224 in the present example. The examples show that the design approach in which the endfire pattern is obtained through mode 2 contributions to modes 1 and 3 has limitations. The attempts to transition the mode 3 current toward that of mode 2 produced loading schemes that required large reactance values to achieve the target endfire pattern goal. Furthermore, the loading schemes resulted in very high VSWR values at 3 GHz. In the next section we use the perturbation approach to understand why large VSWRs result and suggest a new variation on the design approach that produces designs with desirable VSWRs at the target frequency.

5.6 Improving the VSWR at 3 GHz

Although endfire patterns were achieved in the previous examples, the designs required very large reactance values and suffered from very high VSWR at 3 GHz. The high VSWR is a result of an impedance mismatch at the antenna feedpoint. Because the input impedance of the antenna is related to the voltage and current relationship at the feed, the mode current at the feed must be investigated to understand why the VSWR increases. Inspection of how the eigencurrent values at the feed change as loading increases provides insight that can be used to manipulate how the modes are excited by a fixed

location feed. In this section we use the perturbation approach to understand why the VSWR for the previous spiral designs increase dramatically with loading. The results suggest a new approach using the perturbation method to not only improve the VSWR but to accomplish the endfire design objective using smaller reactance values.

The excitation of a mode is highly dependent on the magnitude of the eigencurrent at the excitation location. As a result, analyzing the eigencurrent magnitudes at the feed as the loading is increased provides significant insight into how the loading is affecting the excitation of each mode. The first design presented in section 5.4 in which inductive and capacitive loading is used at nodes 203 and 230, respectively, will be analyzed. Fig. 5.40 shows the unexcited and excited eigencurrent magnitude at the center feed location (node 217) for the first three eigencurrents as the loading is increased to $\pm$j1500 Ω. Again, the positions of the loads correspond to local maxima for obtaining the largest contribution of mode eigencurrent 2 to modes 1 and 3. Initially we see the magnitude of eigencurrent 2 increase as small loading is placed on the antenna. This results from contributions to mode 2 from the odd modes that have finite current magnitude at the feed. As a result, these previously unexcitable modes can be excited to a small extent. However, the excitation of these modes still tends to be negligible compared to the excitation of modes 1 and 3. As the loading continues to increase, the eigencurrent magnitudes stop increasing and begin to decrease. The eigencurrent magnitudes of modes 1 and 3 decrease significantly as the loading continues to increase. Mode 3 is strongly excited for all loading situations and influences the total radiation pattern extensively. Therefore, in order to obtain a total endfire pattern from the antenna, large load values have to be used to transition mode 3 toward a current distribution that radiates an endfire pattern. However, as the loading is increased to transition mode 3, all of the eigencurrent feed magnitudes are decreasing. Therefore, the modes become more difficult to excite, and the total powers radiated by these modes decrease as seen in Fig. 5.33. The smaller current at the feed increases the spiral's impedance at 3 GHz producing the large undesirable VSWR.

The perturbation approach can be used to understand why the eigencurrent magnitudes are decreasing and how the design can be modified to solve this issue. The characteristic mode eigencurrent perturbation equation given by Eqn. 5.1 describes how a particular eigencurrent changes due to scaled

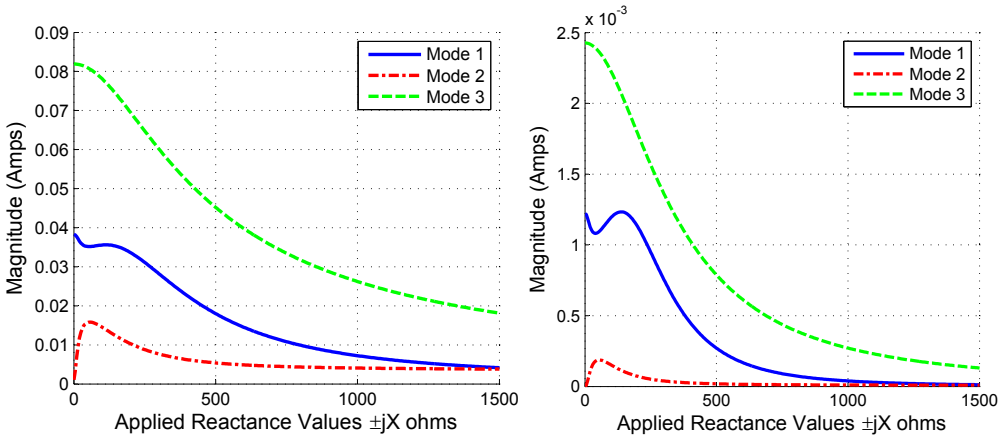

(a) Unexcited (b) Excited

Figure 5.40: Spiral eigencurrent feed magnitude (Node 217) as the inductive and capacitive reactance values at nodes 203 and 230, respectively, are increased. (a) Unexcited magnitude (b) excited magnitude.

contributions from each of the other mode eigencurrents. The equation can be used to clearly identify which modes act to increase or decrease a particular eigencurrent feed value. After the undesirable eigencurrent contributions have been established, load positions can be altered to suppress the undesired contributions. Consider the spiral loaded with ±j500 Ω loads at nodes 203 and 230. Fig. 5.41 gives the first 25 eigencurrent contributions to the first three modes when additional ±j1 Ω reactance perturbations are applied at nodes 203 and 230. Table 5.5 gives the eigencurrent values at the feed for the first three modes. In contrast to the values provided in Fig. 5.40, the values listed here include the eigencurrent's phase which is necessary for contribution analysis. Considering the contributions to mode 1 in Fig. 5.41, the largest in phase current contribution is -16.9 μA from mode 18. The contribution is in phase and will tend to increase the mode 1 feed current magnitude. Interestingly, mode 18 is not a significant radiating mode, yet it has a significant impact on the change in the mode 1 eigencurrent near the feed. Therefore, we see that higher order modes that are often ignored must be considered. Unlike the contribution from mode 18, the mode 3 contribution is the largest contribution out of phase with the mode 1 current at the feed and has a relatively large value of 36.7 μA. The mode 3 contribution acts to reduce the magnitude of the mode 1 current at the feed location. Checking the mode contributions at other loading values verified that the mode 3

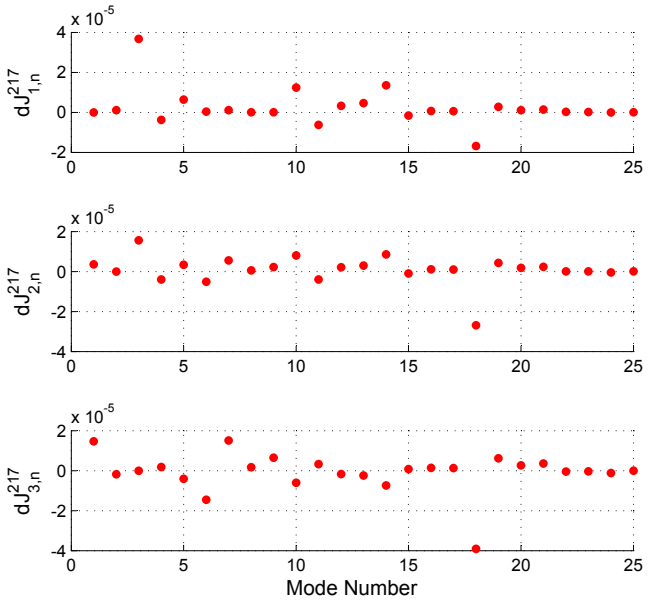

Figure 5.41: Eigencurrent change contribution to the first three mode feed currents when a ±j1 Ω load is introduced at nodes 203 and 230. The spiral is originally loaded with ±j500 Ω at nodes 203 and 230.

Table 5.5: Eigencurrent value of the first three modes at the feed.

Mode Number	Eigencurrent Value (mA)
1	-18.0
2	5.4
3	45.2
4	19.5

contributions to mode 1 are primarily responsible for the decrease in mode 1 feed current magnitude as loading is increased. If mode 3 contributions can be suppressed, the mode 1 feed eigencurrent magnitude will increase as load perturbations continue to be added to the antenna.

A larger mode 1 eigencurrent magnitude at the feed will increase its excitation. Therefore, the endfire pattern that is present in mode 1 from mode 2 contributions may be excited much more strongly. The contributions to mode 3 that are difficult to obtain will not be required. Furthermore, a larger feed current magnitude will bring the input impedance of the antenna closer to 50 Ω improving the VSWR at 3 GHz. We showed that contributions from mode 3 to mode 1 are primarily responsible for reducing the mode 1 eigen-

current feed magnitude. If mode 3 contributions can be eliminated over the loading range, other mode contributions that add in phase with the mode 1 feed current will dominate increasing the mode 1 eigencurrent magnitude at the feed. As mentioned in Section 3.4, the eigencurrent perturbation equations reveal how to suppress the contribution of certain modes. This can be accomplished by moving the load positions into the nulls of the eigencurrent whose contributions should be suppressed. Therefore, the inductive and capacitive loading was moved to nodes 190 and 243, respectively, which correspond to mode 3 eigencurrent nulls. Fig. 5.42 shows the unexcited and excited mode eigencurrent magnitude at the feed as loading in the new load positions is increased. The plot reveals that when loaded in the mode 3 nulls, the mode 1 eigencurrent magnitude no longer decreases with the application of increasing reactance. Instead, the mode 1 eigencurrent at the feed grows. Soon mode 1 begins to be more strongly excited than mode 3, and the mode 1 pattern begins to dominate the spiral's total excited radiation pattern. Radiation from mode 3 becomes negligible. The endfire pattern is achieved with much smaller load values because the current contributions from modes 1 and 2 with endfire patterns must no longer transform mode 3. Instead, significant contributions from mode 2 to mode 1 must be obtained, and then the mode 1 feed current magnitude must be increased so that mode 1 radiates significantly more power than mode 3. These requirements can be achieved with much lower reactance values than were necessary to transform the mode 3 current distribution. Fig. 5.43a shows the spiral pattern performance when loaded with $\pm$j500 Ω at nodes 190 and 243. The small asymmetry in the endfire pattern exists since loaded mode 1 is a composite pattern of the original mode 1 broadside pattern and the contributions from mode 2. Further increasing the loading improves the symmetry of the endfire pattern since mode 2 continues to contribute to mode 1.

Theoretically, according to the eigencurrent perturbation equation, the mode 3 eigencurrent should not change if the loads are placed in mode 3 eigencurrent nulls. Therefore, the change in the mode 3 current magnitude at the feed shown in Fig. 5.42 warrants additional discussion. Fig. 5.42 shows that the mode 3 eigencurrent at the feed does begin to change substantially as loading increases. This is because the loads cannot be placed in perfect nulls due to the finite resolution of the simulation mesh. The mesh nodes do not occur exactly at the null locations and as a result, very small contributions to

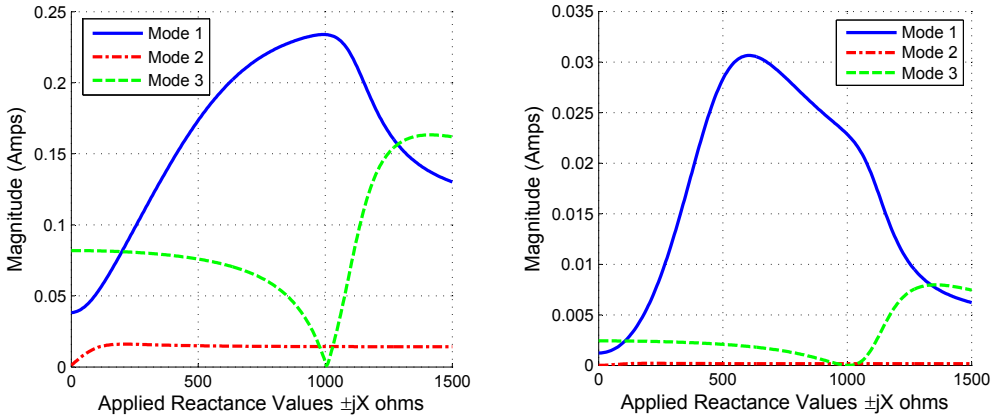

(a) Unexcited (b) Excited

Figure 5.42: Spiral eigencurrent feed magnitude (Node 217) as the inductive and capacitive reactance values at nodes 190 and 243, respectively, are increased; (a) Unexcited magnitude (b) excited magnitude.

mode 3 do occur in the practical simulation. As expected, we see very little mode 3 change for initial loading values. However, mode 3 does gradually begin to change as load values become large. This effect can be reduced by decreasing the simulation mesh size so that loads can be placed closer to the mode 3 nulls. This effect further demonstrates that the antenna performance can be very sensitive to load position, especially as the load sizes increase.

The VSWR is significantly improved at 3 GHz by modifying the load application positions from nodes 203 and 230 to nodes 190 and 243. The spiral antenna performance is compared here for both loading position cases when ±j500 Ω is applied to the antenna. The ±j500 Ω load values were chosen since Fig. 5.42 shows that these values are close to maximizing the mode 1 eigencurrent magnitude at the feed for the node 190 and 243 loading case. The same loading is then used at nodes 203 and 230 for fair comparison purposes. The performance comparison verifies that insight from the perturbation approach can be used to produce a more desirable VSWR and a more favorable radiation pattern. Fig. 5.43 shows the three-dimensional total gain patterns for both loading cases. The patterns show that the modified loading positions produce more defined endfire lobes. Furthermore, Fig. 5.44 shows the ϕ, θ, and total gain patterns along the 292 degree cutplane. The plots show that loading at nodes 190 and 243 produces higher gain pattern lobes. This results from the reduced radiation in the plane orthogonal to the endfire

lobes. This is best seen from the 3D patterns in Fig. 5.43. Furthermore, a deeper null at broadside occurs for the node 190 and 243 positions due to the resulting lower G_θ cross polarization. Finally, Fig. 5.45 shows the VSWR over frequency for both load position cases. Comparing the traces verifies how the VSWR is significantly improved at and around 3 GHz. The VSWR was decreased from 29.6 to 1.75 at 3 GHz by modifying the load positions consistent with the perturbation approach insight. The comparison between the loading options shows that through proper load positioning improved VSWR performance and more favorable radiation properties can be obtained. The perturbation design approach was shown to be instrumental in determining these best load positions.

5.7 Discussion

In this chapter a new design paradigm based on the characteristic mode perturbation equations was applied to the development of spiral antenna loading schemes. Load position, type, and value were selected using the new approach that could transform the spiral's pattern from broadside to endfire. The first two design examples focused on obtaining mode 2 contributions to the excitable modes 1 and 3. Contributions from mode 2 to mode 1 occurred rapidly, in large part due to the small eigenvalue difference between the modes and the effect of the small difference in the eigencurrent contribution coefficient denominator. Contributions to mode 3 proved more difficult, in part due to the larger eigenvalue differences. Although more optimal mode contributions could be obtained with the tradeoff of more loads on the antenna, increasing the eigencurrent contribution magnitudes does not solve the underlying problem of large VSWR and high return loss.

The perturbation approach was applied to understand what factors were causing the high VSWR and low radiated power. The perturbation analysis showed that mode 3 contributions were primarily contributing to a decrease in the mode 1 eigencurrent magnitude at the feed location as loading perturbations were applied. By changing the load positions, the contributions from mode 3 could be suppressed which allowed the mode 1 eigencurrent magnitude at the feed to increase with applied loading instead of decreasing. The larger eigencurrent magnitude resulted in a lower input impedance and

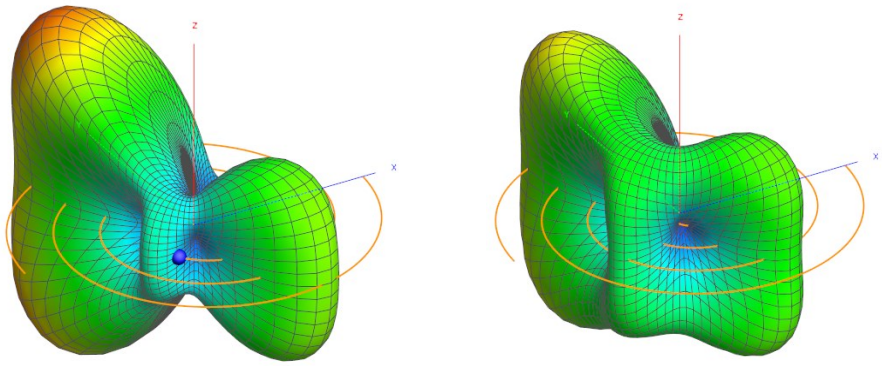

(a) (b)

Figure 5.43: Total gain pattern at 3 GHz of the two-turn spiral with ±j500 Ω loading applied at (a) nodes 190 and 243 and (b) nodes 203 and 230. Magnitude ranges from 0 (Blue) to 3 (Red).

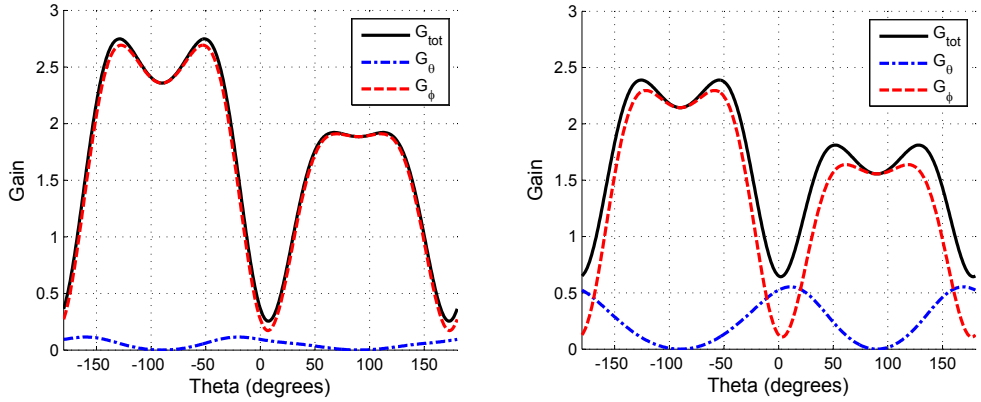

(a) (b)

Figure 5.44: Gain pattern components at 3 GHz ($\phi = 292$ degree cutplane) of the two-turn spiral with ±j500 Ω loading applied at (a) nodes 190 and 243 and (b) nodes 203 and 230.

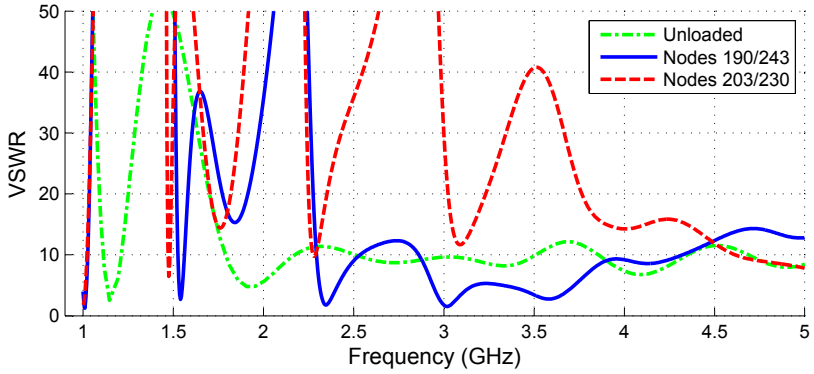

Figure 5.45: Comparison of the VSWR over frequency for the two-turn spiral with ±j500 Ω loading at either nodes 190 and 243 or 203 and 230.

a desirable VSWR at and around 3 GHz.

Because eigencurrents in general tend to vary slowly over frequency, in many cases the narrowband design approach can provide useful insight that holds true over a wider bandwidth. The spiral example focused on improving the VSWR at a target frequency of 3 GHz. However, a VSWR improvement was seen over a much wider frequency range as seen in Fig. 5.45. The load positions that suppressed the mode 3 contributions at 3 GHz tend to be near the same positions that suppress these contributions at neighboring frequencies. Fig. 5.45 shows that the insight at 3 GHz improved the VSWR performance approximately over a 2 GHz frequency range. Therefore, although the present design approach is narrowband in nature, we see that the insight holds true over a much wider bandwidth. This can be attributed to the eigencurrent distributions varying slowly over frequency.

The improved understanding of the factors responsible for the high VSWR through the use of the characteristic mode perturbation equations suggests an alternative overall design approach. First, we can obtain the eigencurrent contributions from mode 2 to mode 1. Then instead of trying to transform mode 3, eigencurrent contributions can be used to increase the mode 1 eigencurrent feed magnitude. This allows mode 1 to be much more strongly excited and radiate significantly more power than mode 3. Contributions from higher order modes that do not effectively radiate power can be used to increase the mode 1 feed current magnitude. The detrimental contributions from mode 3 can be suppressed through proper load placement suggested by the perturbation equations. The contributions from higher order modes increase the current at the feed which improves the spiral's impedance match and VSWR.

The perturbation approach developed in this work clearly indicated which mode contribution was most significantly decreasing the mode 1 eigencurrent feed magnitude as loading was increased. Traditional characteristic mode approaches do not reveal this information. Characteristic mode techniques traditionally focus on suppressing the characteristic modes themselves. Undesirable eigencurrent distributions on the antenna are suppressed with loading or through geometry modifications. However, the characteristic mode perturbation design method which is based on the perturbation equations is a fundamentally different approach. The approach focuses on analyzing the contributions of each characteristic mode to the transformation of a different

mode. Therefore, while traditional characteristic mode techniques may focus on suppressing the actual characteristic mode eigencurrent, the perturbation approach focuses on suppressing the undesired contribution of that mode to another mode. We saw that it was not mode 3 itself that was causing the VSWR issue, but its contribution to mode 1 as the loading perturbations were applied. The perturbation approach not only provided understanding of what was causing the VSWR issue, but it provided the insight needed to modify the design to solve the problem.

CHAPTER 6

ANTENNA EFFICIENCY ANALYSIS AND IMPROVEMENT USING THE PERTURBATION METHOD

The theory of characteristic modes provides a useful expansion for the surface currents of perfectly conducting metallic antennas. Characteristic modes in their commonly used formulation, however, do not account for losses. Ignoring losses is often a good approximation since most antennas are highly efficient and losses are negligible. However, losses can be significant for electrically small antennas, reconfigurable antennas, or antennas operating with a lossy structure nearby. Resistive loading is also sometimes used by practicing engineers to achieve a desired impedance match or bandwidth enhancement. In these cases the inclusion of loss in the characteristic mode analysis is necessary. In this chapter a modified characteristic mode formulation is used that includes ohmic losses. By including ohmic losses in the characteristic mode analysis, antenna efficiency can be found. Furthermore, an efficiency can be found for each individual characteristic mode that depends on the mode eigencurrent distribution with respect to the antenna loss mechanisms. In this chapter, the characteristic mode perturbation approach is applied to improve antenna efficiency using reactive loading. The approach is demonstrated on a lossy dipole antenna in the electrically small regime.

6.1 Characteristic Mode Formulation Including Loss

The characteristic mode weighted eigenvalue problem in its general form has a complex system matrix, complex eigenvectors, and corresponding complex eigenvalues as given in Section 2.2 by Eqn. 2.23 as

$$(Z + Z_L)(J_n) = \nu_n M(J_n). \tag{6.1}$$

By assuming a lossless structure and selecting the weight matrix M equal to R, the eigenvalue problem was simplified to that given by Eqn. 2.24. In the

lossless case the computed eigencurrents J_n and corresponding eigenvalues λ_n are real. The characteristic currents are orthogonal with respect to the impedance matrix and the characteristic fields form an orthogonal set over the sphere at infinity. However, when loss is included in the analysis, the characteristic mode expressions do not simplify as readily and compromises in the mode orthogonality properties must be made. The compromises were initially discussed by Harrington in [20] and were later accepted and used by Ethier in [15].

Different generalized eigenvalue problem formulations are available depending on the choice of weighting M. Each formulation maintains different orthogonality properties. First, if the weighting is chosen as $M = R + R_L$ where R_L is the real part of the load impedance matrix which contains the loss, the eigencurrents are real but the radiation patterns are not orthogonal. The eigencurrents satisfy the orthogonality relationship given by

$$\langle J_m^*, (R + R_L)J_n \rangle = \delta_{mn}. \tag{6.2}$$

Alternatively, if the weighting is chosen as $M = R$, the orthogonality of the radiation patterns is maintained yet the eigencurrents and eigenvalues become complex. The eigencurrents now satisfy the orthogonality relationship given by

$$\langle J_m^*, RJ_n \rangle = \delta_{mn}. \tag{6.3}$$

Using the second formulation with $M = R$ is particularly useful since in this formulation the mode efficiency can be directly related to the eigenvalue. This allows the eigenvalue perturbation expression to be used to understand the antenna efficiency behavior when loading is applied. To see how the eigenvalue and efficiency are related we first consider the loaded eigenvalue problem

$$(Z + Z_L)(J_n) = \nu_n R(J_n). \tag{6.4}$$

The inner product can be taken with the complex conjugate of the eigencurrent where the inner product is defined as $< X, Y >= x_1 y_1 + ... + x_n y_n$.

$$\langle J_n^*, (Z + Z_L)(J_n) \rangle = \nu_n \langle J_n^*, R(J_n) \rangle. \tag{6.5}$$

The equation can be rearranged to obtain an expression for the complex

mode eigenvalues. Furthermore, the Z and Z_L matrices can be expanded in terms of their real and imaginary parts to obtain

$$\nu_n = \frac{\langle J_n^*, (Z + Z_L)(J_n)\rangle}{\langle J_n^*, R(J_n)\rangle} \tag{6.6}$$

$$= \frac{\langle J_n^*, (R + R_L)(J_n)\rangle}{\langle J_n^*, R(J_n)\rangle} + j\frac{\langle J_n^*, (X + X_L)(J_n)\rangle}{\langle J_n^*, R(J_n)\rangle}. \tag{6.7}$$

The mode efficiency e_n can be recognized in the expression as the inverse of the real part of the complex eigenvalue which is given here as

$$e_n = \frac{1}{Re(\nu_n)} = \frac{\langle J_n^*, R(J_n)\rangle}{\langle J_n^*, (R + R_L)(J_n)\rangle} = \frac{P_{r,n}}{P_{r,n} + P_{L,n}}, \tag{6.8}$$

where $P_{r,n}$ is the power radiated by and $P_{L,n}$ is the power dissipated by mode n on the structure. Since the real part of a mode eigenvalue is directly related to the mode efficiency, the eigenvalue perturbation expression can be used to understand how loading affects the efficiency of each mode and the antenna.

6.2 Electrically Small Dipole Efficiency and Validation

The dipole from Section 2.3 will be investigated in terms of modal efficiency at a frequency of 900 MHz. At 900 MHz the dipole is electrically small with an electrical size ka value of 0.37. Here, k is the wavenumber and a is the radius of a sphere that circumscribes the dipole. The dipole is electrically small at this frequency so the dipole's efficiency will be noticeably lower than 100% when copper loss is included. Electrically small antennas tend to be dominated by a single characteristic mode. As a result, the electrically small dipole's total current is dominated by its first characteristic mode.

The dipole's modal efficiency calculated for each mode is shown in Fig. 6.1. The modal efficiency is calculated as the inverse of the real part of the characteristic mode eigenvalue. For loss calculations the dipole is assumed to be copper which has a surface resistance of 7.895 mΩ. The surface resistance is applied to each mesh node which results in a constant 7.895 mΩ value in each diagonal entry of the load resistance matrix R_L. From the figure, mode 1 has an efficiency of 95.7% and mode 2 has an efficiency of 14.72%. The higher order modes have very low efficiencies. Mode 2 has lower effi-

ciency than mode 1 since the mode doesn't radiate as effectively. Mode 2 requires a larger eigencurrent magnitude to radiate unit power which results in higher dissipated power and lower efficiency. For multimode antennas the total antenna efficiency is determined as a weighted sum of modal efficiencies dependent on the significance of each eigencurrent in the total antenna current. However, because the dipole's excited current will be dominated by the mode 1 eigencurrent, the mode 1 efficiency should be very close to the value for the total antenna. An efficiency of 94.3% was calculated using analytical efficiency expressions for a short dipole found in [37]. The computed mode 1 efficiency matches closely with the calculated value. The small difference can be attributed to the fact that the analytical expression approximates the antenna current as a triangular distribution. The analytical calculation validates the characteristic mode efficiency formulation.

The radiation efficiency of the higher order dipole modes are approximately zero. This is expected since these are reactive modes that store large net energy and do not radiate effectively. As a result, the modes have high power loss compared to radiated power. This can also be understood from a slightly different point of view. Typically each mode is normalized to radiate unit power. The higher order reactive modes require larger current magnitudes to radiate unit power. The large current magnitudes contribution to larger I^2R losses on the antenna leading to reduced radiation efficiency.

When a reactive load is applied to the antenna, the efficiency will depend on the Q of the reactive load and the resulting modified current distribution. Hansen used parametric studies to determine the best load locations for a monopole whip antenna [4]. Hansen characterized and plotted the efficiency tradeoff that occurs when changing the inductive load position and varying its value to maintain antenna resonance. When the load is placed further out on the antenna, lower loss occurs due to the lower current magnitude. However, a larger load value is needed to resonate the antenna. When the inductor Q is kept constant the inductor loss increases for larger reactance values and a tradeoff occurs. Hansen's plots characterize the tradeoff and establish an optimal load position of 0.4 the length of the antenna arms (Nodes 16 and 36). To verify the characteristic mode efficiency formulation with a finite Q reactive load, +j1030 Ω loads with Q values of 300 are used to resonate the dipole and are placed on each arm at the optimal load positions. Fig. 6.2 shows the modal efficiency for the applied loads. The computed mode

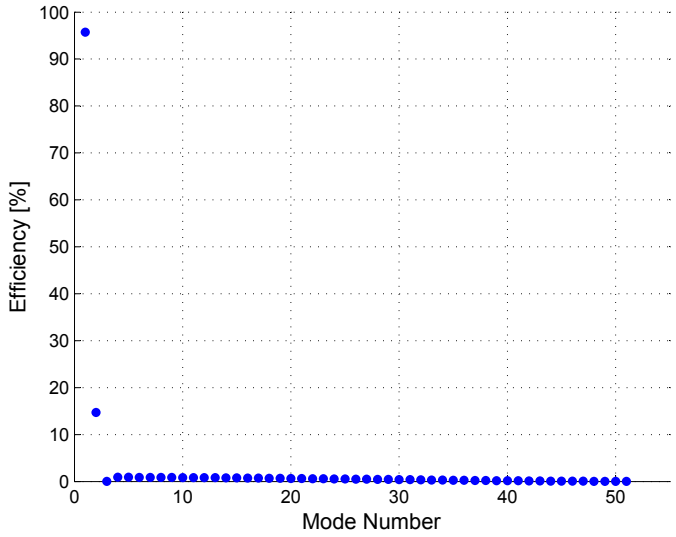

Figure 6.1: Modal efficiency for the copper dipole at 900 MHz.

1 efficiency result matches closely with the total antenna efficiency values computed by Hansen.

6.3 Eigenvalue Perturbation Equation in Terms of Complex Currents

When lossless antennas are analyzed using characteristic mode theory, the computed eigencurrents are real and the eigenpatterns are orthogonal. However, when loss is introduced on the antenna and the eigenvalue problem weighting is chosen as $M = R$, the real parts of the complex eigenvalue problem do not cancel and the computed eigencurrents and eigenvalues become complex. The perturbation equations were intentionally derived in Chapter 3 to handle the complex eigenvalue problem so the equations would apply to the lossy antenna case. The complex perturbation equations are repeated here from Section 3.4 as

$$d\nu_i = \frac{\langle dZ_L J_i, J_i \rangle}{\langle R J_i, J_i \rangle} \tag{6.9}$$

and

$$dJ_i = \sum_{j=1}^{N} \frac{\langle dZ_L J_i, J_j \rangle}{\langle R J_j, J_j \rangle (\lambda_i - \lambda_j)} J_j \quad i \neq j, \tag{6.10}$$

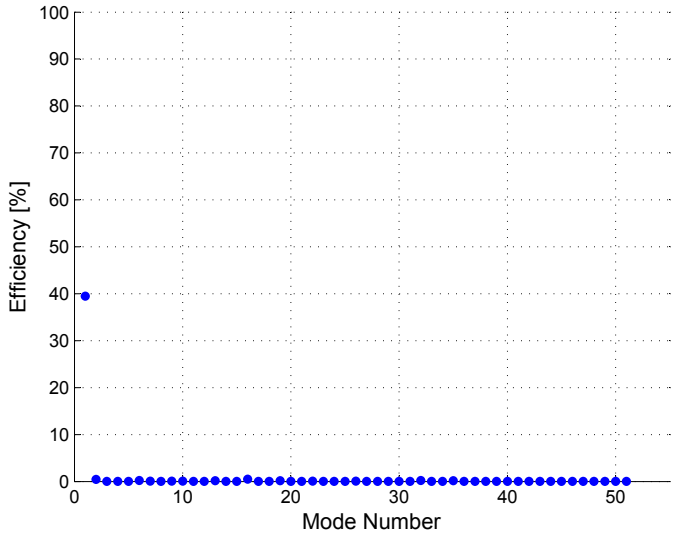

Figure 6.2: Modal efficiency for the copper dipole when +j1030 Ω loads (Q = 300) are places at 0.4 the length of each dipole arm (Nodes 16 and 36).

where they have been rewritten to reflect a different inner product definition of $\langle x, y\rangle = x_1 y_1 + ... + x_n y_n$ simply for interpretation convenience. Since the eigencurrents are now complex, the interpretations of the quantities previously mentioned change. For instance, the quantity $\langle RJ_i, J_i\rangle$ is no longer the real radiated power since no power factor is present in the quantity. The impedance load perturbation matrix in Eqn. 6.9 can be further expanded as

$$d\nu_i = \frac{\langle (dR_L + jdX_L)J_i), J_i\rangle}{\langle RJ_i, J_i\rangle}, \tag{6.11}$$

where dR_L is a matrix containing the resistance perturbations on the antenna.

Consider a lossless reactive load placed on the antenna ($dR_L = 0, dX_L \neq 0$). The purely imaginary reactance perturbation multiplies with the complex eigencurrent value resulting in a change in both the real and imaginary eigenvalue components. Because the mode efficiency is equal to the inverse of the real part of the eigenvalue, the perturbation equation shows that a purely reactive load can alter a mode's efficiency and the resulting total efficiency of the antenna. This suggests that we may be able to use reactive loading to improve the antenna efficiency. However, in practice all reactive loads will have finite loss, so the minimum Q of the load necessary to still achieve an efficiency improvement must be determined.

6.4 Improving the Efficiency when a Large Loss Mechanism is Present on the Antenna

Loss mechanisms are often introduced on an antenna either intentionally or unavoidably. This may include intentional resistive loading for bandwidth enhancement or unavoidable loss that comes with reactive loading or other components that facilitate reconfiguration. The characteristic mode perturbation approach provides a new perspective on managing antenna efficiency in designs. The antenna efficiency is tied closely to the current through the loss mechanism. Therefore, to improve efficiency the current through the loss mechanism must be reduced or the antenna radiated power must be enhanced without increasing the current through the loss.

The perturbation approach can often be used to manage antenna efficiency. However, the efficiency cannot be improved without affecting other antenna performance metrics to some extent. Loss that is intentionally introduced on an antenna typically serves a specific design purpose such as improving the bandwidth or the impedance match. The ability of an intentionally placed loss mechanism to affect antenna performance is closely related to the current through the loss. For instance, a resistor placed in an antenna total current null will not affect antenna performance properties such as bandwidth. Although the resistor would not harm the antenna efficiency, its introduction on the antenna would serve no purpose.

Loss also often comes as an undesired yet unavoidable effect from finite Q components and finite conductivity metal. Unintentional loss that comes from finite Q reactive components cannot be placed independently of the reactance. The reactance must be placed in finite current magnitude to achieve its desired affect which also results in unavoidable loss. Therefore, some loss must be tolerated when loading for complex antenna functionality. A tradeoff exists between loading effectiveness and antenna efficiency. The characteristic mode perturbation approach provides a useful method to manage this tradeoff more systematically.

Cases will be examined where a large resistance is placed on the dipole antenna in addition to the copper loss. Infinite Q reactive load perturbations will be introduced on the antenna and the change in the eigenvalue will be calculated using the eigenvalue perturbation equation. Because the efficiency is inversely proportional to the real part of the eigenvalue, the change in

the real part of the eigenvalue is examined to see how loading affects the antenna efficiency. A negative change in the eigenvalue means the efficiency is improved by the introduced reactive loading while a positive change in the eigenvalue means the efficiency was worsened.

We first look at the case where a 100 Ω resistance is places in the center of the dipole at node 26. Copper loss is also included. Fig. 6.3 shows the change in the real part of the mode 1 eigenvalue as reactive load perturbations are swept across the dipole. A +j1 Ω inductive load is first swept across the dipole followed by a −j1 Ω capacitive load. Interestingly, the real part of the eigenvalue change for the swept single inductor has a similar pattern to the mode 1 eigencurrent change when a single inductor is placed in the center of the antenna as previously seen in Fig. 4.6. Evident by the roughly three half-sine variations, Fig. 4.6 showed that the mode 1 eigencurrent change is dominated by the mode 3 eigencurrent contribution in addition to some higher order modes when loaded in the center. When the loading is such that the mode 3 eigencurrent contribution acts to increase the current through the resistance, the efficiency is reduced ($Re(d\nu) > 0$). On the other hand, when loading causes the mode 3 eigencurrent contribution to act to decrease the current through the resistance, the efficiency improves ($Re(d\nu) < 0$). The relationship seen between Fig. 6.3 and Fig. 4.6 shows that in this case the efficiency is tied heavily to the eigencurrent contribution from mode 3 to mode 1. As seen in Chapter 4, the amount mode 3 contributes to mode 1 is related to both the mode 1 and mode 3 eigencurrent magnitudes at the load location. As the load is moved along the dipole, the mode 3 eigencurrent contribution to mode 1 changes resulting in various current magnitudes through the resistance. Therefore, the plot that is swept out by the changing eigenvalue is directly related to the magnitude of the mode 3 eigencurrent and some higher order mode eigencurrents. Mode 3 contributions are essential to controlling the efficiency with reactive loading because the large loss was placed in the center of the dipole. Because mode 3 eigencurrent contributions have the largest effect on the current through the resistance, their contributions are the dominant influence on the antenna efficiency. However, the higher order modes also contribute to a rapid spatial change in current around the reactance location. The higher order mode contributions cause a large dip in the mode 1 eigencurrent at the reactance location. This contributes to the best location to improve efficiency being at the same node position and in

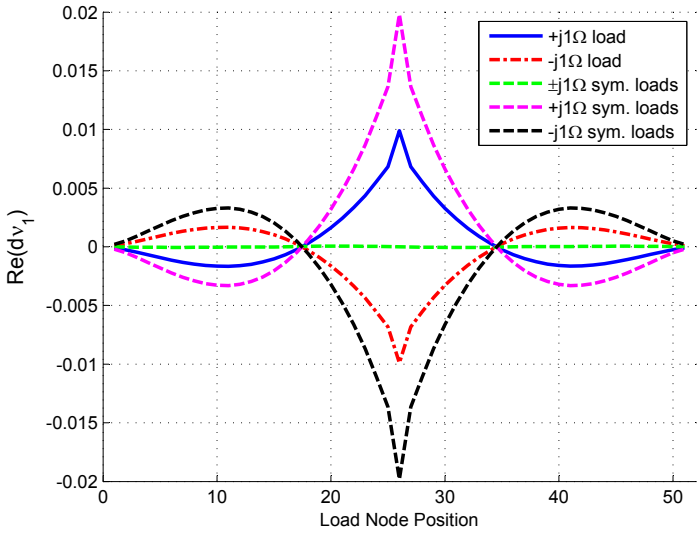

Figure 6.3: Change in the real part of the dipole mode 1 eigenvalue for different reactive loading combinations. The dipole has a 100 Ω resistance in the center (node 26) and copper conductivity.

series with the large loss resistance.

Fig. 6.3 also shows the eigenvalue behavior when reactive loads are symmetrically applied starting at the dipole ends and systematically moved toward the middle. Inductors, capacitors and opposite load types on each arm were investigated. When the same type of load is used on either arm, the eigenvalue change is simply doubled compared to a single reactance. However, when ±j1 Ω loading is used on the dipole, mode 3 to 1 eigencurrent contributions are suppressed along with the contributions from other modes with finite magnitude at the center resistor location. Instead, the ±j1 Ω loading produce a mode 2 to 1 contribution. Since mode 2 has a null at the dipole center, it can't change the current through the resistance, and we see essentially no change in the mode 1 efficiency. The only way the ±j1 Ω loads would be able to increase the efficiency is if the mode 2 eigencurrent contribution makes mode 1 radiate more power compared to the power lost in the resistor. Fig. 6.3 indicates that this is not the case and shows that the efficiency is best improved by working to decrease the current through the loss resistance. The eigencurrent perturbation equation provides a quantitative method to systematically manipulate the currents on the structure or to understand the limitations of current manipulation using reactive loading.

6.5 Minimum Load Q

The loaded dipole example shows that the efficiency can be improved using reactive loads that have infinite Q values. However, in practice all components have finite Q. We next consider the same dipole loading example and determine the minimum reactive load Q necessary to still achieve an efficiency increase. Fig. 6.4 plots the bound on the minimum Q for both an applied +j1 Ω single inductive load and a -j1 Ω single capacitive load as their positions on the dipole are varied. No efficiency improvement is possible when the change in the real part of the eigenvalue is already positive for the introduction of an infinite Q component. Positive eigenvalue change means that the introduction of the lossless component is decreasing the efficiency. Adding component loss will certainly only reduce the efficiency further. Therefore, the minimum component Q that still improves efficiency is only defined when the change in the eigenvalue is negative for infinite Q reactive loading.

When the real eigenvalue change is negative, the minimum Q is calculated, thereby increasing the reactive load's resistance until the real part of the eigenvalue change calculated using the eigenvalue perturbation equation changes from negative to zero. This component resistance value R_{max} serves to define the bound at which efficiency can still be improved and is used along with the reactive load perturbation value X_L to calculate the minimum Q

$$Q_{min} = \frac{|X_L|}{R_{max}}. \tag{6.12}$$

The minimum Q results are plotted in Fig. 6.4. As previously seen from Fig. 6.3, when the large resistance is in the center of the dipole, inductors must be placed near the ends of the dipole to improve the efficiency while capacitors must be placed closer to the center. Regardless of its Q, to improve antenna efficiency the type of loading must be changed depending on the load application position. Therefore, the minimum Q is only defined near the dipole ends for inductive loading and near the center for capacitive loading. The transition is seen in Fig. 6.4. The plot shows that the best position to place a capacitance is as close to the loss mechanism as possible. This reduces the current through the loss which improves the efficiency. Since a capacitance near the resistor most significantly decreases the current through the loss, the reactance can have a lower minimum Q.

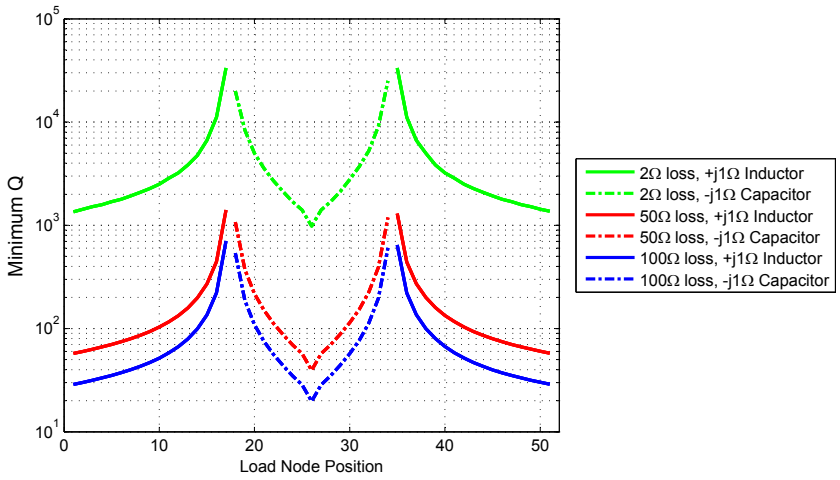

Figure 6.4: Minimum component Q necessary to produce an efficiency improvement using inductive or capacitive load perturbations. The dipole has copper conductivity and different resistance values in the center (node 26).

As expected, Fig. 6.4 indicates that for relatively large losses positioned in the center of the dipole, a mode 1 efficiency improvement can be obtained using components with practically obtainable Q values. However, for a 2 Ω resistance which could model the insertion loss of a switch or other reconfiguration component, efficiency improvement using reactive loading becomes impractical. It would be difficult and expensive to obtain reactive loads with large enough Q values to see a noticeable efficiency increase. Therefore, as one might expect, improving efficiency is not practical when the size of the undesired loss is on the same order of magnitude as the loss of the introduced reactive loading.

6.6 Discussion

In this chapter, antenna radiation efficiency analysis was performed using characteristic mode theory and the new perturbation approach. The I^2R power losses are heavily dependent on the current through the loss mechanism. Therefore, reducing the current through the loss can significantly improve antenna efficiency. Reactive loading can be used to modify the total current and the eigencurrents on the antenna structure. If the mag-

nitude of the significant eigencurrents at the load location can be reduced, the antenna efficiency will improve. However, the efficiency cannot be improved without affecting the antenna electrical performance to some extent, since reactive loading will alter the antenna current and resulting electrical properties. The characteristic mode perturbation approach provides a useful method to systematically tradeoff antenna efficiency and other antenna performance criteria.

This thesis focused on developing a characteristic mode perturbation approach that quantifies how reactive loading affects the characteristic mode eigencurrents. The approach provides a foundation to use reactive loading to systematically control the current through a loss resistance. The equations guide the application of reactive loading to enhance eigencurrent contributions to the excitable modes. Therefore, the approach provides a systematic method to increase or decrease the current through a particular loss resistance, thereby controlling the antenna efficiency. There is always a tradeoff between the antenna efficiency and the ability of the load to affect the antenna performance. The perturbation equations provide a means to understand and manage the tradeoff.

The perturbation equations provide insight into the best reactive load type and placement location to improve efficiency. Opportunities are always available to improve efficiency using infinite Q reactive loads. In practice, however, reactive loads have finite Q values and so will always introduce some loss. If the introduced reactive loads dissipate more power than what is saved by their introduction, then the use of reactive loading to improve efficiency is not practical. We showed that for large resistances on the antenna, efficiency improvements can be obtained using reactive loads with reasonable Q values. However, higher Q reactive loads are required as the loss decreases eventually making the technique impractical.

CHAPTER 7

CONCLUSION

Impedance loading is a useful mechanism to achieve current and future antenna functionality requirements. Antenna loading has the potential to modify antenna functionality or provide antenna reconfiguration for many canonical antenna topologies in a cost effective manner. However, the design of useful antenna reactive loading schemes is a challenging problem especially as the number of loads and antenna performance requirements increase. In this thesis, a new approach to antenna loading design was presented that extends beyond basic characteristic mode theory concepts. By applying eigenvalue perturbation theory to the loaded antenna characteristic mode problem, a quantitative understanding of how mode eigenvalues and eigencurrents transform with applied loading was obtained. The perturbation equations that were developed suggest a new design paradigm based on controlling the eigencurrent contributions between modes. The benefits of the approach were demonstrated with an Archimedean spiral pattern synthesis example. The complex electromagnetic interactions between the spiral arms are inherently taken into account in the characteristic mode based perturbation approach. Therefore, complicated modeling of spiral arm coupling was not required. The eigencurrent contribution perspective suggested by the perturbation approach provides a new perspective on designing with antenna loss and efficiency in mind. The perturbation expressions generalize to the complex characteristic mode eigenvalue problem providing insight to better understand the efficiency tradeoff and to better manage this tradeoff with loading. This work forms the foundation for a new design paradigm whose full potential as a design tool has yet to be discovered. Future efforts will reveal new applications and insights that have not yet been explored.

7.1 Contributions

This research has culminated in a number of contributions to both our understanding of characteristic mode theory and characteristic mode design techniques. This work:

- **Developed the first analytical equations that describe how characteristic modes transform with respect to reactive loading or frequency variation.**

  The change in characteristic modes with respect to reactive loading was previously only known qualitatively from experience. By applying eigenvalue perturbation theory to the loaded characteristic mode eigenvalue problem, analytical equations were developed that describe how modes change due to reactive loading or frequency variation. The equations are the first mathematical description of how characteristic mode eigenvalues and eigencurrents transform. The analytical expressions reveal the explicit factors that govern mode transformations.

- **Introduced a novel design paradigm based on the new perturbation equations in which loading is used to control eigencurrent contributions between modes.**

  The eigencurrent perturbation equation reveals that the change in a particular mode can be viewed as having contributions from each of the other modes. This insight suggests a new design approach in which we control the transformation of a mode by enhancing or suppressing the eigencurrent contributions from desirable or undesirable modes. The eigencurrent perturbation equation reveals how to position loading on the structure in order to enhance or suppress certain eigencurrent contributions. This allows a designer to synthesize useful eigencurrent distributions and patterns by obtaining eigencurrent contributions from modes with desirable properties.

- **Demonstrated the first application of characteristic mode theory to traveling wave spiral antenna analysis and design.**

  Characteristic modes have been applied in a number of ways to a variety of different structures. However, this work is the first application of characteristic mode theory to the traveling wave spiral antenna

topology. Furthermore, the new characteristic mode perturbation approach design techniques developed in this work were applied to an Archimedean spiral antenna. The spiral's center fed broadside pattern was transformed to an endfire pattern using only reactive loading. Desirable VSWR performance as loading increased was maintained using insight from the perturbation equations.

- **Showed that the new mode contribution perspective can reveal the causes and solutions to antenna issues that traditional characteristic mode theory techniques cannot reveal.**

  With the initial chosen spiral loading profile, significant VSWR degradation occurred at the frequency of interest as load value magnitudes were increased. An application of the perturbation equations to the loaded antenna revealed the source of the VSWR degradation and a solution. The perturbation approach revealed that it was a particular mode contribution that was causing the VSWR degradation as loading increased. The developed equations show how to modify the load positions to suppress the offending mode contributions. Traditional examination of the total characteristic mode currents does not reveal the source of the problem or a solution as the new approach does. The new approach can be viewed as a design guide for antenna impedance matching.

- **Established the difference between total eigencurrents and eigencurrent contributions.**

  Traditional characteristic mode analysis looks at the eigencurrent magnitudes present on an antenna structure. The traditional characteristic mode design approach focuses on suppressing undesired modes. This thesis exposes a limitation of traditional characteristic mode analysis and design. Many modes may not be excited in the final total antenna current. However, as the antenna is loaded these modes may contribute to the change in a mode that is excited. Therefore, this work established that we also need to consider the effect of mode contributions in addition to the traditional characteristic mode approach of analyzing just the total excited eigencurrents. This new understanding allowed the improvement of spiral antenna VSWR by suppressing

the contributions of an undesirable mode to a desired mode as loading was increased.

- **Revealed that higher order modes can contribute to the change in lower order excitable modes.**

  Higher order modes are typically ignored in traditional characteristic mode analysis. These modes have large eigenvalues, which makes them difficult to excite on the antenna structure. This work demonstrated that although higher order modes may not be easily excitable, they can contribute to the change in lower order excitable modes. The higher order modes were shown to be responsible for the rapid spatial change in current of lower order modes near load positions. Although these higher order modes are not excited on the structure, they contribute strongly to the change in the excited lower order modes as loading is increased. This research reveals the cause of the eigencurrent transformations for the first time, since traditional characteristic mode techniques do not reveal how eigencurrents transform.

- **Used the perturbation approach to manage the antenna efficiency tradeoff.**

  High current through loss mechanisms leads to significant dissipated power and reduced antenna efficiency. Efficiency can often be managed using the perturbation approach. The method can be used to systematically place reactive loading to manipulate the current through the loss thereby altering the antenna efficiency. Insight into the minimum reactive load Q needed to still achieve efficiency improvement was developed.

7.2 Future Work

The research presented in this thesis developed a new design paradigm based on a rigorous mathematical foundation. Examples were presented to reveal the capabilities of the new technique and its applicability to complicated antenna design problems. The current work forms a foundation for future avenues of research.

- **Combine perturbation equations with an optimization algorithm.**

  The research in this thesis focused on understanding how the eigencurrents transform and explored some different design processes to obtain desired antenna functionality. The increase in loading was performed manually and the characteristic modes were analyzed after each load increment was added to the antenna. This process would ideally be automated. An optimization algorithm could be applied with the perturbation equations to automate the design process. The perturbation equations would provide the foundation for a better optimization goal function that would provide more insight and understanding within the optimization routine.

- **Use the perturbation equations to quantify characteristic mode coupling.**

  The eigenvalues of two different characteristic modes often become equal at certain frequencies or when certain loading combinations are applied. Around the eigenvalue crossing, the modes are degenerate and the behavior of the modes can be described as mode coupling. The eigenvalues are no longer distinct so the eigencurrent perturbation equation has a singularity at the degeneracy. The perturbation equations predict that near the degeneracy, the changing eigencurrents will receive extremely large eigencurrent contributions from each other. Therefore, the current distributions of the changing and contributing modes swap. This behavior can physically be described by mode coupling. The perturbation equations mathematically describe the coupling behavior. Further investigation is needed to characterize the mode coupling using the perturbation equations.

- **Include the effect of frequency variation on the characteristic modes in the loading analysis.**

  This thesis focused on understanding the change in the characteristic modes with respect to a lumped load perturbation at a single frequency. However, the perturbation equation formulation characterizes the effect of any changes in the reactance matrix on the characteristic modes. A change in the reactance matrix also results from a frequency vari-

ation. By combining frequency and load perturbations, the frequency dependence of a loaded structure can be characterized. This approach could have applications to trap dipoles. The approach may help determine the best trap locations and component values and could be useful specifically when the trap is operating away from resonance. An admittance formulation could also be explored to characterize the effect of shunt load elements on the antenna.

- **Use the perturbation equations for mode tracking.**

  Significant attention has been applied to tracking modes over wide frequency ranges. When mode eigenvalues cross, the labeling of the modes when ordered in terms of eigenvalue magnitude will change. An algorithm is needed to track the modes through eigenvalue crossings. However, current tracking algorithms based on eigencurrent correlation are not always robust. The perturbation equations provide an ideal foundation for a new tracking method. The change in the eigenvalue and eigenvectors can be calculated using the perturbation equations with the reactance matrix perturbation due to frequency variation. The quantities are then added on to the previous calculated eigenvalues and eigenvectors. This process can be repeated over wide frequency ranges. Mode tracking is implicit when calculating the characteristic modes over frequency using the perturbation approach. Unlike other approaches, a correlation between eigencurrents at two different frequency steps is not relied upon to track the modes. Instead, the modes are updated at each frequency step and are never relabeled. Therefore, the perturbation method provides a much more robust approach for mode tracking.

- **Apply the perturbation approach to mutually coupled structures.**

  The research presented in this thesis focused on the effect of discrete lumped loading on the characteristic modes. However, a mutually coupled structure also produces a load matrix in the method of moments formulation. Therefore, the perturbation approach can be applied without modification to characterize the effect of mutual coupling on the characteristic modes of a structure. This approach could potentially

lead to insight for characterizing and reducing mutual coupling in antenna arrays or in cosite interference situations.

APPENDIX A

THE CHARACTERISTIC MODE PERTURBATION APPROACH AND THE NETWORK COMPENSATION THEOREM

The characteristic mode perturbation approach shares similarities with the compensation theorem used in network analysis and boundary value electromagnetic problems. The network compensation theorem provides a method to calculate the effect of small circuit value changes on the rest of the network. For instance, if an impedance is changed in one branch of a circuit network, the changes in the currents of the other branches can be determined using the theorem. The compensation theorem is a fundamental principle in network analysis and has been used by Judd and Chirlian to prove Thevenin's and Norton's theorems [38]. Furthermore, Geselowitz used the compensation theorem to derive the scattering parameters of a network [39]. In addition to network analysis, the compensation theorem has been applied to electromagnetic problems. Monteath applied the theorem to determine the effect of an external surface impedance such as earth ground on the input impedance of an antenna [40]. Following Monteath's work, Mittra extended the approach to the vector case [41].

In this section, the characteristic mode perturbation approach is related to the compensation theorem. The network compensation theorem is first presented and is then for the first time applied to the characteristic mode problem. The novel application of the compensation theorem provides useful insight and an alternative view to better understand the perturbation approach and the meaning of the perturbation expressions.

A.1 Network Compensation Theorem

Any impedance in a branch of a linear bilateral electrical network can be replaced by a voltage source with the same value as the voltage drop through the impedance. If a network branch is perturbed by adding or subtracting

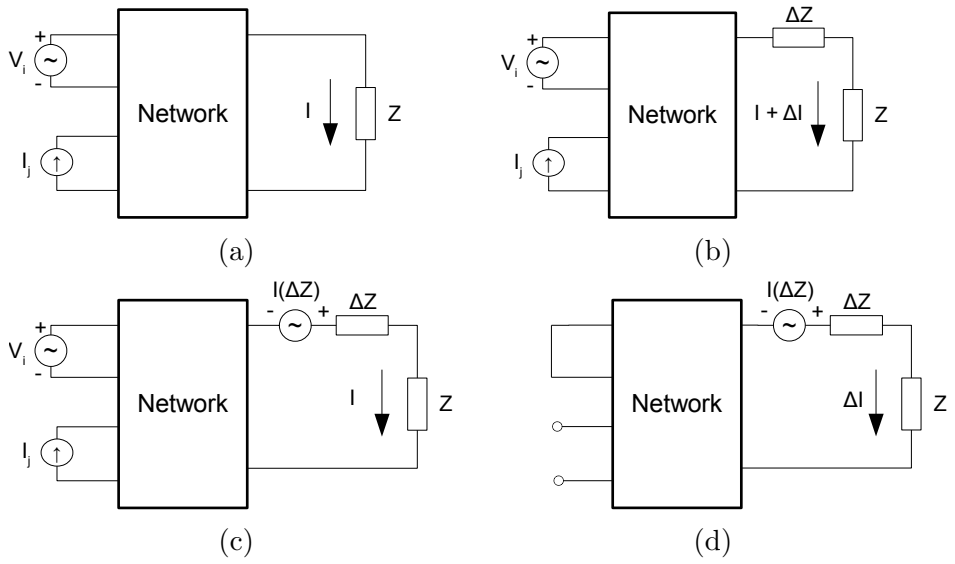

Figure A.1: A linear bilateral network undergoing an impedance change. (a) Original network, (b) adding an impedance to a single branch, (c) voltage source compensation for the introduced impedance, and (d) current change using the compensation theorem.

an impedance, the change in the current in all the other branches is equal to the current produced by a compensating voltage source acting in series with the modified branch.

To clarify this concept, consider the linear bilateral network shown in Fig. A.1a. The voltage and current sources feed a network composed of multiple branches. If an impedance is added to a single branch, it will result in a current change in all the branches as shown in Fig. A.1b. The effect of the added impedance on the network can be eliminated by adding a compensating voltage source in series with the impedance as shown in Fig. A.1c. The voltage source would have a value equal to the voltage drop across the impedance ($I\Delta Z$). The compensation theorem states that the current change in each network branch due to the added impedance is equal to the current response in each branch from the insertion of a compensating voltage source in series with the perturbed branch [38]. The original sources are replaced by their internal impedance values. Application of the compensation theorem is illustrated in Fig. A.1d.

The change in each branch current is found by calculating the current in each branch excited by the compensating source. The calculated results characterize the effect of the introduced impedance on the network. The current

changes calculated using the compensation theorem are exact regardless of the magnitude of the introduced impedance. However, the tradeoff is that the approach does require prior knowledge of the current through the introduced impedance before an appropriate compensating source value can be determined.

A.2 Compensation Theorem Application to Antennas

Insight into useful antenna loading schemes can be obtained using characteristic mode theory along with a detailed understanding of the effect of loading on the characteristic modes. The characteristic mode perturbation approach developed in this thesis characterizes the effect of a small load impedance on the mode eigencurrents and eigenvalues of an antenna. The approach provides a detailed understanding of how modes transform when loading is placed on the antenna structure and results in significant insight for the design of loaded antennas. The compensation theorem can also be applied to the characteristic mode antenna problem by viewing an antenna structure as a network. The compensation theorem provides an alternative method to determine the change in the excited mode currents when a load is introduced onto the antenna structure. Novel expressions describing the antenna current changes due to an introduced impedance are derived as follows.

Consider the antenna shown in Fig. A.2a. A voltage source is attached at the antenna terminals resulting in a current distribution on the antenna structure J_{tot}. The introduction of an impedance on the antenna will produce a change in the total antenna current ΔJ as shown in Fig. A.2b. The antenna can be viewed from a network perspective in which the source and load connected to antenna terminals form branches of the overall antenna network. When the antenna structure is viewed in this manner, the compensation theorem can be readily applied to determine the effect of the load impedance on the antenna currents.

As illustrated in Fig. A.2c, the change in the antenna current due to the introduced impedance can be determined by solving for the currents on the antenna structure when a compensating voltage source is placed in series with the introduced impedance and the original excitation source is replaced by its internal impedance. The value of the compensating voltage source

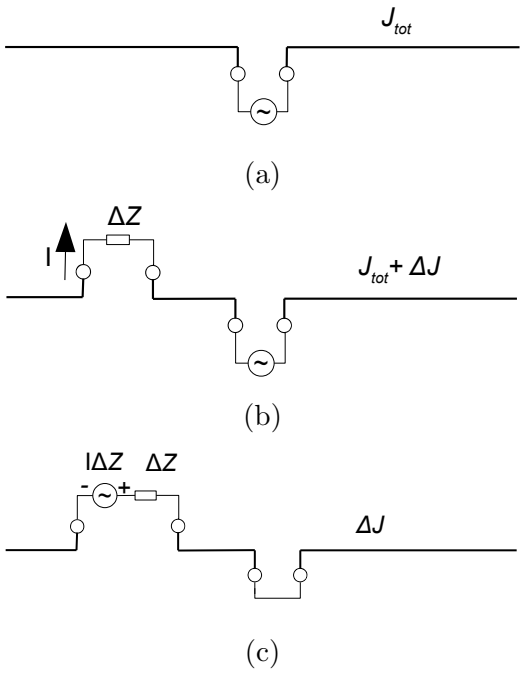

Figure A.2: Application of the compensation theorem to an antenna. (a) Excited antenna, (b) excited antenna with an introduced impedance load, and (c) current change computation setup including the compensation source.

is equal to the voltage drop across the introduced impedance ($I\Delta Z$) where I is the current through the load and ΔZ is the value of the introduced impedance. The change in antenna current is then determined by solving for the currents on the antenna structure excited by the compensating voltage source in series with the impedance.

The series combination of the compensating voltage source and introduced impedance are represented in the method of moments formulation as

$$\mathbf{V_{comp}} = [\mathbf{Z} + \mathbf{\Delta Z}]\mathbf{\Delta J}, \tag{A.1}$$

where $\mathbf{V_{comp}}$ is a vector containing the compensating voltage source, $\mathbf{Z}$ is the unloaded system matrix, $\mathbf{\Delta Z}$ is a matrix containing the introduced impedance, and $\mathbf{\Delta J}$ is a vector of the current change along the antenna. Solving Eqn. A.1 for $\mathbf{\Delta J}$ gives the exact current change along the antenna due to the introduced impedance. The calculated current change is exact and is not an approximation.

A.3 Compensation Theorem Application to Antenna Characteristic Modes

Section A.2 showed how the compensation theorem can be applied to calculate the change in the total currents on an antenna structure. Furthermore, it is useful to characterize how the introduced impedance affects the currents on a modal basis. In this section, the compensation theorem is applied to antenna characteristic modes to provide insight into how the excited characteristic modes change when loading is applied to the structure.

As introduced in Chapter 2, the total currents on an antenna can be decomposed using the characteristic mode basis set as

$$\mathbf{J_{tot}} = \sum_n \frac{\langle \mathbf{J_n}, \mathbf{E^i} \rangle}{1 + j\lambda_n} \mathbf{J_n}. \tag{A.2}$$

Here $\mathbf{E^i}$ is the electric field introduced by the excitation voltage source. The total current through the load in Fig. A.2b can be decomposed in terms of the characteristic mode currents at the load terminal as

$$I_{tot,load} = \sum_n \frac{\langle \mathbf{J_{n,loaded}}, \mathbf{E^i} \rangle}{1 + j\lambda_{n,loaded}} I_{n,load}, \tag{A.3}$$

where $I_{tot,load}$ is the scalar value of the total current through the load on the antenna and $I_{n,load}$ is the particular characteristic mode eigencurrent value through the load from a network characteristic mode perspective [42]. The eigencurrents here, $\mathbf{J_{n,loaded}}$ and $I_{n,load}$, are those calculated from the loaded characteristic mode eigenvalue problem given by expression 2.24.

As illustrated in Fig. A.2c, the compensation theorem can be applied by including in series with the impedance a compensating voltage source that is equal in value to the voltage drop through the impedance on the antenna $I_{tot,load}\Delta Z$. The original voltage source is replaced with its internal impedance value, a short. The change in the total current in terms of the characteristic modes is given as

$$\mathbf{\Delta J_{tot,loaded}} = \sum_n \frac{\langle \mathbf{J_{n,loaded}}, \mathbf{V_{comp}} \rangle}{1 + j\lambda_{n,loaded}} \mathbf{J_{n,loaded}}, \tag{A.4}$$

where $\mathbf{V_{comp}}$ is a vector containing the value of the compensating voltage

source in a position in the vector corresponding to its location on the antenna structure

$$\mathbf{V_{comp}} = \begin{bmatrix} \vdots \\ I_{tot,load}\Delta Z \\ \vdots \end{bmatrix}. \tag{A.5}$$

The change in a particular mode eigencurrent can be viewed as having a contribution from each of the other eigencurrents. This insight was gained from the perturbation approach derived in Chap. 3. Similarly, for the compensation theorem derivation approach the contribution of a particular mode q to the change in a mode p eigencurrent $\mathbf{\Delta J_{p,loaded}}$ can be found as

$$\mathbf{\Delta J_{p,loaded}} = \frac{\langle \mathbf{J_{p,loaded}}, \mathbf{V_{q,comp}} \rangle}{1 + j\lambda_{p,loaded}} \mathbf{J_{p,loaded}}, \tag{A.6}$$

where

$$\mathbf{V_{q,comp}} = \begin{bmatrix} \vdots \\ I_{q,load}\Delta Z \\ \vdots \end{bmatrix} \tag{A.7}$$

and $I_{q,load}$ is the value of the q^{th} eigencurrent through the load.

A.4 Discussion

The novel application of the compensation theorem to the characteristic mode antenna problem provides an alternative viewpoint to better understand the characteristic mode perturbation expressions derived using eigenvalue perturbation theory. The compensation theorem provides a method to calculate the change in each excited characteristic mode eigencurrent when an impedance is introduced on the antenna structure. A compensation theorem approach provides validation of the insight gained from the perturbation expressions.

Application of the compensation theorem to antenna problems allows the change in the excited eigencurrents to be calculated exactly regardless of the size of the introduced impedances. Unlike the perturbation expressions, the compensation theorem derived expressions are not approximations. However, this comes at a significant tradeoff. Application of the compensation theo-

rem calculates the change in the excited mode eigencurrents by determining the amount each mode is excited by a compensating voltage source. In order to determine the magnitude of the compensating voltage source, the mode currents through the introduced impedance must be known. Determination of the mode current through the load requires the solution of the loaded characteristic mode problem given by Eqn. 2.24. Furthermore, the compensating voltage source acts on the loaded characteristic modes once again requiring a solution of the loaded eigencurrents. In contrast, the perturbation approach expressions do not require solution of the loaded characteristic mode problem. This is a significant benefit. Since the perturbation approach does not require the solution of the loaded eigenvalue problem, a priori knowledge of the load locations is not required. As a result, the perturbation expressions can be used to provide useful design insight for optimal load placement. The compensation theorem approach, although exact, would require knowledge of the load locations and would not be as useful for load placement problems.

Although the compensation theorem approach provides a means to calculate the change in the excited eigencurrents exactly, there is an additional drawback compared to the perturbation approach formulation. A direct application of the compensation theorem requires an initial excitation specified in the antenna structure. Although this is useful when analyzing excited antenna mode currents, the beneficial feed-independent nature of characteristic modes is not maintained. In contrast, because the perturbation expressions look at the changes in the unexcited eigencurrents, the expressions are feed independent. Feed independence is extremely beneficial for many characteristic mode design problems where the best excitation position is initially unknown.

The compensation theorem approach provides useful insight to aid in the understanding of the perturbation expressions. Application of the compensation theorem to the antenna problem showed that an impedance load on the antenna can be viewed as a voltage source. The changes in the mode eigencurrents are found to be the eigencurrents excited by the impedance's compensating voltage source. As a result, the effects of the load on the antenna current can be found in terms of how the compensating voltage source in series with the impedance at the load location excites the loaded characteristic modes. For instance, if a load is placed in a particular mode eigencurrent null, the load's compensating voltage source cannot excite that mode. As a

result, the mode cannot contribute to the change in the antenna current. On the other hand, if the load is placed in a mode eigencurrent maxima, the load's compensating voltage source can better excite the mode. This leads to the particular contributing mode having a larger contribution to the antenna current change. The same behavior was seen when analyzing the perturbation approach expressions. The compensation theorem approach provides an alternative method and understanding to arrive at this conclusion.

The application of the compensation theorem verifies that the change in a particular mode eigencurrent depends on the interaction of the load with both the changing and contributing mode currents. Eqn. A.6 shows that the magnitude of the compensating voltage source is determined by the contributing mode. The excitation of the changing mode by the compensating source is determined by the changing mode current magnitude and distribution. Therefore, the compensation theorem shows that the change in a particular mode eigencurrent is determined by the interaction of the load with both the changing and contributing mode currents. This insight was initially gained by analyzing the perturbation approach expressions and is validated by the compensation theorem.

The compensation theorem provides an alternative approach for determining the effect of an introduced load on the excited characteristic modes of an antenna. The approach validates much of the insight gained from analyzing the perturbation expressions derived using eigenvalue perturbation theory. The compensation theorem suggests that the introduced impedance loads are often best viewed as sources themselves, which provides a useful perspective on how loading affects the total antenna currents and the characteristic modes.

APPENDIX B

PERTURBATION EQUATION PROPERTIES AND DESIGN METRICS

The perturbation equations provide the foundation for a new characteristic mode design paradigm in which the loading design process is viewed from a mode contribution perspective. The perturbation equations have a number of properties that are useful to consider when using the expressions for antenna loading design. Furthermore, useful metrics based on the perturbation equations can be developed to aid the design process. In this section, some useful properties of the equations are detailed and metrics are derived that find use in the perturbation approach design method. First, the effect of a load perturbation on a mode's power is derived from a mode contribution perspective. The derivation provides a useful metric that can be used to evaluate loading alternatives during the design process. Then a simple expression to calculate the power radiated by each excited characteristic mode is derived. Furthermore, a reaction property is described that states that a contributing mode receives an equal contribution from the changing mode it is contributing to. The reaction property is important to consider throughout the perturbation method design process. Finally, a technique to modify the characteristic mode currents without changing the eigenvalues is detailed. The expressions derived in this appendix are typically plotted to guide the perturbation approach design process.

B.1 Load Perturbation Effect on Mode Power

The power radiated by each eigencurrent is important to consider when designing a loading scheme to achieve a desired radiation pattern. Eigencurrents can have large current magnitudes but may not radiate significant power. These mode current distributions tend to store large net energy but do not radiate significantly. These reactive modes can contribute signifi-

cant current magnitude to another mode but will have minimal effect on the mode's radiated power. As a result, these reactive mode contributions will not cause changes in another mode's radiation pattern. When obtaining mode contributions to shape a radiation pattern, a metric is needed that characterizes the effect of a particular mode contribution on another mode's radiation pattern. Eigencurrent contribution magnitude alone does not provide this information. Instead, a radiated power contribution metric is derived here to address this need. The derived metric is used extensively to guide the perturbation approach design process.

A load perturbation produces a change in each mode eigencurrent. The perturbation expressions reveal that the change in a mode current can be decomposed in terms of each of the other characteristic mode eigencurrents. Because each mode contributes to an eigencurrent's change, a particular mode's radiated fields will be a linear combination of the fields originating from the original current and the fields radiated by each eigencurrent change contribution. In order to understand the impact of each eigencurrent contribution on a mode's radiation pattern, the radiated power contributed by each particular eigencurrent can be considered. Modes that contribute more radiated power will have a larger effect on the radiation pattern of a changing mode than modes that contribute less radiated power. Although some mode contributions have large current magnitudes, the larger magnitude current contribution does not necessarily produce a larger effect on the radiation pattern. Some high current modes may not radiate effectively resulting in minimal impact on the changing mode's eigenpattern.

Here we derive the radiated power of a perturbed eigencurrent mode. The derivation shows that the radiated power is the sum of the power radiated by the original unloaded eigencurrent and the power radiated by each mode contribution. The derivation begins as follows. The change in a particular characteristic mode eigencurrent is governed by the eigencurrent perturbation equation and was given previously in Eqn. 5.1 as

$$dJ_i = \sum_{j=1}^{N} dJ_{i,j} = \sum_{j=1}^{N} \frac{\langle dX_L J_i, J_j \rangle}{\langle RJ_j, J_j \rangle (\lambda_i - \lambda_j)} J_j \quad i \neq j. \tag{B.1}$$

The new loaded, perturbed mode i eigencurrent is the combination of the unloaded eigencurrent and the eigencurrent change in terms of the contributions

from the other modes

$$J_{i,pert} = J_i + \sum_{j=1}^{N} dJ_{i,j} = J_i + \Delta J_i, \tag{B.2}$$

where ΔJ_i represents the sum of the eigencurrent contributions to mode i from each of the other modes. The total power radiated by the unloaded eigencurrent i is given as

$$P_{rad,i} =< J_i^*, RJ_i >, \tag{B.3}$$

where * indicates the complex conjugate. The power radiated by the perturbed eigencurrent is given and simplified as

$$\begin{aligned} P_{rad,i,pert} &=< J_{i,pert}^*, RJ_{i,pert} > \\ &=< (J_i + \Delta J_i)^*, R((J_i + \Delta J_i) > \\ &=< J_i^*, RJ_i > + < J_i^*, R\Delta J_i > \\ &\qquad + < \Delta J_i^*, RJ_i > + < \Delta J_i^*, R\Delta J_i > . \end{aligned} \tag{B.4}$$

The quantity ΔJ_i is composed of a contribution from each of the other modes except J_i. Since each of the modes are R-orthogonal with respect to eigencurrent i, the center two terms always evaluate to zero leaving

$$P_{rad,i,pert} =< J_i^*, RJ_i > + < \Delta J_i^*, R\Delta J_i > . \tag{B.5}$$

The second term consists of the self and cross terms between each of the other mode eigencurrents. Again, the cross terms cancel due to the characteristic mode orthogonality property leaving only the self-terms. Expression B.5 then becomes

$$P_{rad,i,pert} =< J_i^*, RJ_i > + \sum_j < dJ_{i,j}^*, RdJ_{i,j} > . \tag{B.6}$$

The first term is the real power radiated by unloaded mode i. The second term is the power radiated by each of the eigencurrent contributions to mode i.

Although the expression seems to suggest that more power will be radiated with each load perturbation, it is important to remember that the eigencurrents are not physical quantities until they have been excited. After all,

eigencurrents are often scaled to radiate unit power. The perturbed eigencurrents can also be scaled to radiate arbitrary power. However, what the expression does reveal is which mode contribution will radiate the most power as part of the perturbed eigencurrent after the perturbed mode has been excited. As a result, comparing each mode power contribution indicates which contribution to the changing unloaded mode is responsible for the largest power change. This reflects in the mode's radiation pattern and tells which contributing mode now radiates the largest portion of the total mode power as part of the new perturbed mode. Regardless of the perturbed eigencurrent scaling, the fraction of the power radiated by a contributing mode n $P_{i,n}$ with respect to the total perturbed eigencurrent power is the same

$$\frac{P_{i,n}}{P_{rad,i,pert}} = \frac{< dJ_{i,n}^*, RdJ_{i,n} >}{< J_i^*, RJ_i > + \sum_j < dJ_{i,j}^*, RdJ_{i,j} >}. \tag{B.7}$$

This means that the fraction quantity is also the same when considering the actual excited mode power. Because the contributions are excited as part of the changing perturbed mode, the unperturbed and contribution currents that make up the perturbed eigencurrent both experience the same modal weight coefficient and the fraction quantity is maintained. Therefore, comparing the power contribution quantity $< dJ_{i,n}^*, RdJ_{i,n} >$ provides a useful metric to determine which mode contribution will have the most significant effect on the excited radiation pattern. By analyzing a plot of the power contribution quantities from each mode, designers can determine which modes are affecting a particular mode's radiated power and resultant radiation pattern. The power contribution quantity is used during the antenna loading design process to determine which modes are contributing most significantly to the change in a mode pattern for a particular loading arrangement.

B.2 Calculating Mode Radiated Power

Characteristic modes are solved independent of a feed, and each characteristic current basis is typically normalized to radiate unit power. When a feed is placed in the antenna structure, however, each characteristic mode will be excited with a different modal weight coefficient dependent on the feed location and magnitude. As a result, each excited characteristic mode will

radiate a different amount of power. When considering the total antenna radiation performance, it is useful to consider how much power each mode is contributing to the antenna's total radiated power. Certain modes that radiate effectively can be regarded as strong radiating modes and are critical to the antenna radiation performance. Focus should be placed on modifying or controlling these strong radiating modes in order to control the antenna pattern or other antenna radiation characteristics.

The total radiated power can be decomposed in terms of the characteristic modes mathematically as follows. First, the characteristic currents J_n are assumed to have been scaled to radiate unit power as is typically done during their calculation. An excited characteristic current from Eqn. 2.17 is given as

$$J_{n,excited} = \frac{\langle J_n, E^i \rangle}{1 + j\lambda_n} J_n = |A_n| e^{j\alpha_n} J_n \tag{B.8}$$

where $|A_n|$ is the magnitude of and α_n is the angle of the complex modal weight coefficient. The real power radiated by a mode current was given by Eqn. 2.16. Therefore, the power radiated by an excited characteristic current simplifies as

$$\begin{aligned} P_{n,excited} &= \langle (|A_n| e^{j\alpha_n} J_n)^*, R(|A_n| e^{j\alpha_n} J_n) \rangle \\ &= |A_n|^2 < J_n^*, RJ_n > \\ &= |A_n|^2, \end{aligned}$$

where * indicates the complex conjugate and where each characteristic mode is normalized to radiate unit power $< J_n^*, RJ_n >= 1$. Therefore, the magnitude of the modal weight coefficient squared gives the real power radiated by a particular excited mode when the eigencurrents have been scaled to radiate unit power. The total power radiated by an antenna can therefore be viewed in terms of the contribution from each characteristic mode.

B.3 Reaction Property

Careful inspection of the eigencurrent perturbation equation shows that for every contribution to a changing mode from a contributing mode there is an equal yet negative contribution from the changing mode back to the con-

tributing mode. To show this property we can consider the contributions from mode j to mode i and also the contribution from mode i to mode j. The eigencurrent contributions are given as

$$dJ_{i,j} = \frac{\langle dX_L J_i, J_j \rangle}{(\lambda_i - \lambda_j)} J_j = a_{i,j} J_j \tag{B.9}$$

and

$$dJ_{j,i} = \frac{\langle dX_L J_j, J_i \rangle}{(\lambda_j - \lambda_i)} J_i = a_{j,i} J_i, \tag{B.10}$$

where $a_{i,j}$ and $a_{j,i}$ are the mode contribution coefficients of the mode j to i and mode i to j contributions, respectively. As is typically done in characteristic mode design, the eigencurrents here have been assumed to be normalized to radiate unit power. The load perturbation matrix dX_L is a real symmetric linear operator so the numerators of both mode contribution coefficients are equivalent. Furthermore, the eigenvalue differences in the denominators are equal magnitude but are the negative of one another. Therefore, the mode contribution coefficients end up being the same magnitude but are the negative of one another

$$a_{i,j} = -a_{j,i}. \tag{B.11}$$

Although the peak magnitude of the contributing currents may be different, the radiated power contributed is the same. We can show that the radiated power contributed is the same by first considering the power contributed from mode j to mode i, then applying Eqn. B.11 as follows:

$$\begin{aligned} P_{i,j} &= < a_{i,j} J_j, R a_{i,j} J_j > \\ &= a_{i,j}^2 < J_j, R J_j > \\ &= a_{i,j}^2 \end{aligned}$$

using Eqn. B.11 in Eqn. B.12, where $< J_j, R J_j >= 1$ from the chosen normalization. Next, consider the power contributed from mode i to mode j

$$\begin{aligned} P_{j,i} &= < a_{j,i} J_j, R a_{j,i} J_j > \\ &= a_{j,i}^2 < J_j, R J_j > \\ &= a_{j,i}^2. \end{aligned}$$

Using Eqn. B.11 along with Eqns. B.12 and B.12 it can be seen that the

power contributions are equal

$$P_{i,j} = a_{i,j}^2 = (-a_{j,i})^2 = P_{j,i}. \tag{B.12}$$

The analysis shows that when considering a contribution to a particular mode, there is an equal power contribution from the changing mode back to the particular contributing mode. Therefore, one can't obtain a contribution from a mode without also receiving an equal power reaction from the changing mode back to the contributing mode. Eventually as loading is increased the changing and contributing modes will begin to share similar current distributions and radiation properties.

B.4 Changing a Mode Eigencurrent While Maintaining its Eigenvalue

A characteristic mode eigenvalue indicates the type of energy stored by the mode. Furthermore, the eigenvalue governs the phase difference between an eigencurrent and its associated radiated field. Therefore, it is important to understand how loading is affecting each mode's eigenvalue. The eigenvalue perturbation equation repeated here as

$$d\lambda_i = \frac{\langle dX_L J_i, J_i \rangle}{\langle R J_i, J_i \rangle} \tag{B.13}$$

provides insight into how reactive loading affects the mode eigenvalues. The equation reveals that a single load will always produce an eigenvalue change when placed away from an eigencurrent null. However, closer inspection of the equation shows that two loads can be used to keep the eigenvalue from changing. Consider an inductive and capacitive load perturbation. When placed on the antenna at locations with the same eigencurrent magnitude and phase, the total eigenvalue perturbation from the two loads will cancel as demonstrated by expanding the numerator of the equation

$$\langle dX_L J_i, J_i \rangle = (+|X_L^m|)(|J_i^m|^2) + (-|X_L^q|)(|J_i^q|^2) = 0, \tag{B.14}$$

where p and q are positions on the antenna with the same eigencurrent magnitude and phase. This concept can be used to keep the eigenvalue constant while still altering the eigencurrent distributions. The change in a mode eigenvalue for a small perturbation depends only on the load's interaction with the particular mode's eigencurrent distribution. The change in the mode's eigencurrent, however, depends on the interaction of the load with both the changing and contributing modes. Therefore, through proper choice of load type and placement, a mode eigenvalue can be maintained constant while the mode eigencurrent distribution can be altered.

Consider the eigencurrents of the spiral antenna given in Fig. 5.11. When two load perturbations, an inductor and a capacitor, are symmetrically placed on the opposite unloaded spiral arms, the loads each experience the same mode 2 current magnitude. The opposite sign reactances result in no eigenvalue change. However, the mode 2 eigencurrent will still receive a contribution from odd modes such as mode 1. Therefore, the mode 2 eigencurrent is changed while the eigenvalue is kept constant.

This observation is useful for characteristic mode design. For instance, a resonated characteristic mode ($\lambda = 0$) can be kept resonant while altering the eigencurrent distribution. This allows the mode eigencurrent and resulting field eigenpattern to be changed while maintaining mode resonance. Alternatively, when a mode is not resonant, an excited mode will have a phase difference between the eigencurrent and its radiated field. The mode eigenvalues can be manipulated to change the excited phase of each mode's radiated field. Changing the phase of each radiated field will alter how eigenpatterns combine to produce the total pattern of a multimode antenna. Understanding how to maintain the eigenvalue while altering the mode eigenpattern gives designers an additional degree of freedom in the characteristic mode design process. Designers can maintain a mode's eigenpattern excitation phase while altering the mode eigencurrent and resulting eigenpattern. This allows the designer to vary the antenna's total radiation pattern more systematically.

REFERENCES

[1] R. C. Hansen, *Electrically Small, Superdirective, and Superconducting Antennas*. Hoboken, NJ: John Wiley and Sons, 2006.

[2] H. Pues and A. Van de Capelle, "Accurate transmission-line model for the rectangular microstrip antenna," *IEE Proc.*, vol. 131, no. 6, pp. 334–340, Dec. 1984.

[3] Y. T. Lo, D. Soloman, and W. F. Richards, "Theory and experiment on microstrip antennas," *IEEE Trans. Antennas and Propag.*, vol. 27, no. 2, pp. 137–145, March 1979.

[4] R. C. Hansen, "Optimum inductive loading of short whip antennas," *IEEE Trans. Veh. Technol.*, vol. 24, no. 2, pp. 21–29, May 1975.

[5] K. A. Obeidat, B. D. Raines, R. G. Rojas, and B. T. Strojny, "Design of frequency reconfigurable antennas using the theory of network characteristic modes," *IEEE Trans. Antennas and Propag.*, vol. 58, no. 10, pp. 3106–3113, Oct. 2010.

[6] B. A. Kramer, C. Chen, and J. L. Volakis, "Optimization of an inductively loaded log-spiral antenna," in *Proc. Int. Symp. on Antennas and Propag.*, Honolulu, HI, 2007, pp. 2993–2996.

[7] M. Cabedo-Fabres, "Systematic design of antennas using the theory of characteristic modes," Ph.D. dissertation, Univ. Politecnica de Valencia, Spain, 2007.

[8] R. J. Garbacz and R. H. Turpin, "A generalized expansion for radiated and scattered fields," *IEEE Trans. Antennas and Propag.*, vol. 19, no. 3, pp. 348–358, May 1971.

[9] R. F. Harrington and J. R. Mautz, "Theory of characteristic modes for conducting bodies," *IEEE Trans. Antennas and Propag.*, vol. 19, no. 5, pp. 622–628, Sept. 1971.

[10] R. F. Harrington and J. R. Mautz, "Characteristic modes for dielectric and magnetic bodies," *IEEE Trans. Antennas and Propag.*, vol. 20, no. 2, pp. 194–198, March 1972.

[11] E. H. Newman, "Small antenna location synthesis using characteristic modes," *IEEE Trans. Antennas and Propag.*, vol. 27, no. 4, pp. 530–531, July 1979.

[12] R. J. Garbacz and D. M. Pozar, "Antenna shape synthesis using characteristic modes," *IEEE Trans. Antennas and Propag.*, vol. 30, no. 3, pp. 340–350, May 1982.

[13] B. A. Austin and K. P. Murray, "The application of characteristic-mode techniques to vehicle-mounted NVIS antennas," *IEEE Antennas and Propag. Mag.*, vol. 40, no. 1, pp. 7–21, Feb. 1998.

[14] M. C. Fabres, E. Antonino-Daviu, A. Valero-Nogueira, and M. F. Bataller, "The theory of characteristic modes revisited: a contribution to the design of antennas for modern applications," *IEEE Antennas and Propag. Mag.*, vol. 49, no. 5, pp. 52–68, Oct. 2007.

[15] J. Ethier, "Antenna shape synthesis using characteristic mode concepts," Ph.D. dissertation, Univ. of Ottawa, Ottawa, ON, 2012.

[16] J. J. Adams and J. T. Bernhard, "A modal approach to tuning and bandwidth enhancement of an electrically small antenna," *IEEE Trans. Antennas and Propag.*, vol. 59, no. 4, pp. 1085–1092, April 2011.

[17] G. Gampala and C. J. Reddy, "Compact LTE antenna design using the theory of characteristic modes for smart phone applications," in *USNC-URSI Radio Science Meeting*, Lake Buena Vista, FL, July 2013, p. 11.

[18] N. Inagaki and R. J. Garbacz, "Eigenfunctions of composite Hermitian operators with application to discrete and continuous radiating systems," *IEEE Trans. Antennas and Propag.*, vol. 30, no. 4, pp. 571–575, July 1982.

[19] R. F. Harrington and J. R. Mautz, "Computation of characteristic modes for conducting bodies," *IEEE Trans. Antennas and Propag.*, vol. 19, no. 5, pp. 629–639, Sept. 1971.

[20] R. F. Harrington and J. R. Mautz, "Control of radar scattering by reactive loading," *IEEE Trans. Antennas and Propag.*, vol. 20, no. 4, pp. 446–454, July 1972.

[21] D. K. Faddeev and V. N. Faddeeva, *Computational Methods of Linear Algebra*. San Francisco, CA: W. H. Freeman and Company, 1963.

[22] A. O. Yee and R. J. Garbacz, "Self- and mutual-admittances of wire antennas in terms of characteristic modes," *IEEE Trans. Antennas and Propag.*, vol. 21, no. 6, pp. 868–871, Nov. 1973.

[23] E. A. Elghannai and R. G. Rojas, "Oriented design of dual USB wireless application antenna using the theory of characteristic modes," in *Proc. Antenna Appl. Symp.*, Monticello, IL, Sep. 2013, pp. 99–109.

[24] E. M. Turner, "Spiral slot antenna," U.S. Patent 2 863 145, Dec. 2, 1958.

[25] V. H. Rumsey, "Frequency independent antennas," in *IRE National Convention Record*, New York, NY, March 1966, pp. 114–118.

[26] B. Cheo, V. H. Rumsey, and W. Welch, "A solution to the frequency-independent antenna problem," *IRE Trans. Antennas and Propag.*, vol. 9, no. 6, pp. 527–534, Feb. 1961.

[27] R. Sivan-Sussman, "Various modes of the equiangular spiral antenna," *IEEE Trans. Antennas and Propag.*, vol. 11, no. 5, pp. 533–539, Sep. 1963.

[28] J. A. Kaiser, "The Archimedean two-wire spiral antenna," *IRE Trans. Antennas and Propag.*, vol. 8, no. 3, pp. 312–323, May 1960.

[29] R. Bawer and J. J. Wolfe, "The spiral antenna," in *IRE National Convention Record*, New York, NY, 1966, pp. 84–95.

[30] D. S. Filipovic and J. L. Volakis, "Novel slot spiral antenna designs for dual-band/multiband operation," *IEEE Trans. Antennas and Propag.*, vol. 51, no. 3, pp. 430–440, 2003.

[31] M. Lee, B. A. Kramer, C. Chen, and J. L. Volakis, "Distributed lumped loads and lossy transmission line model for wideband spiral antenna miniaturization and characterization," *IEEE Trans. Antennas and Propag.*, vol. 55, no. 10, pp. 2671–2678, Oct. 2007.

[32] Z. Zhang and J. T. Bernhard, "Two-arm Archimedean spiral with filter-based reactive loading," in *Proc. Int. Symp. on Antennas and Propag.*, Albuquerque, NM, 2006, pp. 3677–3680.

[33] L. Gong, K. Y. Chan, and R. Ramer, "A reconfigurable spiral antenna with wide beam coverage," in *Proc. Int. Symp. on Antennas and Propag.*, Orlando, FL, 2013, pp. 206–207.

[34] P. Mookiah, D. Piazza, and K. R. Dandekar, "Reconfigurable spiral antenna array for pattern diversity in wideband MIMO communication systems," in *Proc. Int. Symp. on Antennas and Propag.*, San Diego, CA, 2008, pp. 1–4.

[35] F. D. Dahalan et al., "Frequency-reconfigurable Archimedean spiral antenna," *IEEE Antennas Wireless Propag. Lett.*, vol. 12, pp. 1504–1507, Nov. 2013.

[36] M. J. Radway, "Mode theory of multi-armed spiral antennas and its application to electronic warfare antennas," Ph.D. dissertation, Univ. of Colorado, Boulder, May 2011.

[37] W. L. Stutzman and G. A. Thiele, *Antenna theory and design*, 2nd ed. Hoboken, NJ: John Wiley and Sons, 1998.

[38] F. F. Judd and P. M. Chirlian, "The application of the compensation theorem in the proof of Thevenin's and Norton's theorems," *IEEE Trans. Educ.*, vol. 13, no. 2, pp. 87–88, Aug. 1970.

[39] D. B. Geselowitz, "Application of the compensation theorem in the development of the scattering parameters," *IEEE Trans. Educ.*, vol. 14, no. 2, pp. 71–72, May 1971.

[40] G. D. Monteath, "Application of the compensation theorem to certain radiation and propagation problems," *Proc. IEE*, vol. 98, no. 1, pp. 23–30, 1951.

[41] R. Mittra, "A vector form of compensation theorem and its application to boundary-value problems," *Appl. Sci. Res.*, vol. 11, no. 1-2, pp. 26–42, Feb. 1964.

[42] J. R. Mautz and R. F. Harrington, "Modal analysis of loaded n-port scatterers," *IEEE Trans. Antennas and Propag.*, vol. 21, no. 2, pp. 188–199, March 1973.